FUNCTIONAL ANALYSIS OF THE CENTROSOMAL PROTEIN PCMD-1 AND THE ESTABLISHMENT OF A SYSTEM FOR TESTING CENTROSOME INHERITANCE IN *C. ELEGANS*

Dissertation zur Erlangung des Doktorgrades der Naturwissenschaften
Doctor rerum naturalium (Dr. rer. nat.) an der Fakultät für Biologie der
Ludwig-Maximilians-Universität München

Anna Christina Erpf

München 2019

FUNCTIONAL ANALYSIS OF THE CENTROSOMAL PROTEIN PCMD-1 AND THE ESTABLISHMENT OF A SYSTEM FOR TESTING CENTROSOME INHERITANCE IN *C. ELEGANS*

vorgelegt von
Anna Christina Erpf
München, den 14. Oktober 2019

DECLARATION

Eidestattliche Versicherung

ich versichere hiermit an Eides statt, dass die vorgelegte Dissertation von mir selbstständig und ohne unerlaubte Hilfe angefertigt ist.

Toronto, Kanada, den 3.10.2019 　　　Anna C. Erpf
....
(Unterschrift)

Erklärung

Hiermit erkläre ich,

☒　dass die Dissertation nicht ganz oder in wesentlichen Teilen einer anderen Prüfungskommission vorgelegt worden ist.

☒　dass ich mich anderweitig einer Doktorprüfung ohne Erfolg nicht unterzogen habe.

☐　~~dass ich mich mit Erfolg der Doktorprüfung im Hauptfach~~ .... ~~und in den Nebenfächern~~ .... ~~bei der Fakultät für~~ .... ~~der~~ .... ~~unterzogen habe.~~
(Hochschule/Universität)

☐　~~dass ich ohne Erfolg versucht habe, eine Dissertation einzureichen oder mich der Doktorprüfung zu unterziehen.~~

Toronto, Kanada, den 3.10.2019 　　　Anna C. Erpf
....
(Unterschrift)

Publications originating from this thesis / Publicationen die aus dieser Arbeit entstanden sind

Anna Christina Erpf, Lisa Stenzel, Nadin Memar, Mariam Osepashvili, Martina Antoniolli, Ralf Schnabel, Barbara Conradt, Tamara Mikeladze-Dvali. PCMD-1 organizes centrosome matrix assembly in *C. elegans*. **Veröffentlicht im Journal Current Biology am 11. April 2019 / Published in the journal Current Biology on April 11th 2019.**

Contributions / Mitwirkungen

Tamara Mikeladze-Dvali, Lisa Stenzel, Mariam Osepashvili, Martina Antoniolli, Robert Wiesheu, Annabel Kirgis, Tsotne Chitiashvili, Eman Abu Khmail and Mariam Museridze have in part contributed to this work. Their contributions are indicated in the text or in the figure legends. / Tamara Mikeladze-Dvali, Lisa Stenzel, Mariam Osepashvili, Martina Antoniolli, Robert Wiesheu, Annabel Kirgis, Tsotne Chitiashvili, Eman Abu Khmail und Mariam Museridze haben teilweise an dieser Arbeit mitgewirkt. An gegebener Stelle ist ihr Mitwirken im Text oder in den Bildunterschriften gekennzeichnet.

ACKNOWLEDGEMENTS

I want to express my gratitude to my Ph.D. advisor Dr. Tamara Mikeladze-Dvali, for her support and guidance throughout my Ph.D. study. Thank you, Tamara, for opening up this wonderful and truly beautiful world of centrosome biology to me. Further, I would like to thank Prof. Barbara Conradt for taking over the responsibility to be my dissertation adviser. Thanks to both of you for giving me the opportunity to work on this study.

Further, I want to thank Prof. Gislene Pereira, Dr. Anne-Kathrin Classen, Prof. Angelika Böttger, and Dr. Esther Zanin, for their insightful comments and encouragement as my Thesis Advisory Committee. And to my Defense Committee, thank you for your time and feedback on this work.

My sincere thanks also go to Dr. Hartmann Harz, Dr. Stephane Rollande, and Dr. Nadin Memar for their valuable support. Your advice has been a great help during these years. I further want to thank Francisca Rosa-Mendes, former coordinator of the LSM graduate school, and Mo Liegl for their help.

My special thanks to all the members of the Zanin, Conradt, Lambie, and Wagner groups for their stimulating discussions. It has been a great working experience.

I want to thank my fellow labmates for all the joyful coffee breaks, movie nights, dinners, and fun times together. It's been so wonderful to get to know you all and to have shared this important time with you.

Last but not least, I want to thank my family, especially my parents, Sabine, and Dr. Rüdiger Erpf, for supporting me throughout writing this thesis and my life in general. Thank you, Mom, for teaching me that 'if it doesn't kill you, it makes you stronger', and for your great support in all my important life decisions. And thank you, Dad, for being an inspiration, spiritually, morally and intellectually for all my life.

CONTENTS

CONTENTS

LIST OF FIGURES

LIST OF TABLES

ABBREVIATIONS

ABBREVIATIONS

General abbreviations

IFT	intraflagellar transport
IL neuron	neurons of the inner labial sensilla
MTOC	microtubule-organizing center
NEBD	nuclear envelope breakdown
NGM	Nematode Growth Media
PCM	pericentriolar material
PNEB	pronuclear envelope breakdown
PNM	pronuclear meeting
PNMi	pronuclear migration

Gene and protein abbreviations

gene	protein	full name
aakg-1	AAKG-1	AMP-Activated protein Kinase Gamma subunit
agr	AGR	agrin
air	AIR	Aurora/Ipl1 Related kinase
ana	Ana	anastral spindle
apkc	aPKC	atypical protein kinase C-like
asl	Asl	asterless
cdk	CDK	cyclin-dependent kinase
cdk5rap2	CDK5RAP	CDK5 regulatory subunit associated protein
cegrip	CeGrip	*C. elegans* gamma-tubulin interacting protein
cep	Cep	centrosomal protein
cg4733	CG4733	B"/PR72 subunit of protein phosphatase 2A (PP2A) regulatory B unit
clec	CLEC	c-type lectin
cnn	Cnn	centrosomin
cpap	CPAP	centrosomal P4.1-associated protein
cya	CYA	cyclin A
cyb	CYB	cyclin B

cyd	CYD	cyclin D
cye	CYE	cyclin E
dao	DAO	dauer or aging adult overexpression
dendra2	Dendra2	green-to-red photoswitchable fluorescent protein
dex	DEX	dendrite extension defective
dlg	DLG	drosophila disc large homolog
dyf	DYF	abnormal dye filling
fbxa	FBX	F-box A protein
fkb	FKB	FK506-Binding protein family
flp	FLP	FMRF-like peptide
fog	FOG	feminization of germline
gcp	GCP	gamma complex associated protein
gfp	GFP	green fluorescent protein
grip	Grip	gamma-ring complex protein
hmr	HMR	hammerhead embryonic lethal
kif	KIF	kinesin famili member
klp	KLP	kinesin-like protein
lin	LIN	abnormal cell lineage
mai	MAI	mitochondrial ATPase inhibitor family
mCherry	mCherry	red fluorescent protein
mei	MEI	eiotic spindle formation protein
mex	MEX	muscle excess
mKate2	mKate2	red fluorescent protein
mng	mNG	mNeonGreen, bright green fluorescent protein
nedd	NEDD	neural precursor cell expressed developmentally down-regulated
nek	NEK	NIMA related kinase
par	PAR	partitioning-defective
pbd	PBD	polo-box domain
pcmd	PCMD	pericentriolar matrix deficient
pie	PIE	pharynx and intestine in excess
pkc	PKC	protein kinase C-like
plg	PLG	copulatory plug formation
plk	PLK	polo-like kinase
plp	Plp	pericentrin-like protein

polo	Polo	protein phosphotransferase (spindle-pole-dependent).
ppp2r3c	PPP2R3C	protein phosphatase 2 regulatory subunit B"gamma
rsa	RSA	regulator of spindle assembly
sas	SAS	spindle assembly-defective
sax	SAX	sensory axon guidance
sgfp	sGFP	superfolder GFP
spd	SPD	spindle-defective protein
sse	SSE	*Drosophila* separase
stil	STIL	SCL/TAL1 interrupting locus protein
sur	SUR	suppressor of activated let-60 Ras
tac/tacc	TAC/TACC	transforming acid coiled-coil-containing protein
tbb	TBB	β-tubulin
tbg	TBG	tubulin gamma chain
tpx	TPX	targeting protein for xenopus Klp
tpxl	TPXL	TPX2-like protein
tub	Tub	tubulin
tubg	TUBG	tubulin gamma chain
uba	UBA	UBA (human ubiquitin) related
unc	UNC	uncoordinated
xmap	XMAP	xenopus microtubule-associated protein
zyg	ZYG	zygote-defective
--	γ-TuRC	γ-tubulin ring complex

PROTEIN HOMOLOGY

C. elegans	D. melanogaster	H. sapiens
AIR-1	Aurora A	Aurora A
AIR-2	Aurora B	Aurora B
CDK-1	Cdk-1	CDK1
CDK-2	Cdk-2	hsCDK2
CDK-4	Cdk-4	hsCDK4
CeGrip-1	Grip91	GCP3
CeGrip-2	Grip84	GCP2
CYA-1/2	cyclin A	cyclin A
CYB-1/3	cyclin B	cyclin B
CYD-1	cyclin D	cyclin D
CYE-1	cyclin E	cyclin E
DEX-1	Ndg	SNED1
DYF-7	-	-
FBXA-171	-	-
KLP-11	Klp64D	KIF3A
KLP-7	Klp10A	KIF2C
MEI-1	-	KATNA1, KATNAL1
MEI-2	-	-
PAR-1	Par-1	hsPAR1a/b/c
PAR-2	-	-
PAR-3	Bazooka	ASIP
PAR-4	dLKB1	LKB1/STK11
PAR-5	14-3-3ε	14-3-3β
PAR-6	Par-6	hsPAR6α/β/γ
PCMD-1 *	Plp	pericentrin
PKC-3	aPKC	aPKCλ/ζ
PLK-1	Polo	PLK1
PP2A	PP2A	PP2A
RSA-1	CG4733	PPP2R3C
RSA-2	-	-
SAS-4	Sas-4	CPAP

SAS-5	Ana2	STIL
SAS-6	Sas-6	hsSAS6
SAS-7 *	Ana1	Cep295
Separase/SEP-1	SSE	Separase
SPD-2	Spd-2	Cep192
SPD-5 *	Cnn	CDK5RAP2
SUR-6	Twins	-
TAC-1	D-TACC	TACC1/2/3
TBG-1	γ-tubulin/Tub37C	γ-tubulin/TUBG1
TPXL-1	Tpx-2	TPX2
ZYG-1	Plk-4	PLK4
ZYG-9	Msps	XMAP215
-	Asl	Cep152
-	cyclin A	cyclin A
-	Cep135	Cep135
-	-	NEK9
-	-	NEDD-1

*functional homologue

- unknown

SUMMARY

Summary

Centrioles possess a unique dual function within the cell, where they are required for centrosome and cilia formation. The non-membrane-bound organelles recruit pericentriolar material (PCM) and serve as the major microtubule-organizing centers during cell division. In non-mitotic cells, centrioles can dock to the cell membrane and template cilia outgrowth. The nematode *C. elegans* has emerged as an important model organism in the field of centrosome biology. Due to a relatively small set of centrosomal proteins, it plays a vital role in elucidating the assembly pathways of the structure. The core centriole assembly pathway was initially identified in the worm. Further, studies of the nematode PCM assembly factors give valuable insights into the principle mechanisms of PCM formation. However, factors that link centriole and PCM assembly have not been identified in *C. elegans* to date.

In the first part of this study, I characterize the newly identified protein pericentriolar matrix deficient 1 (PCMD-1), which is required for bipolar spindle formation in the *C. elegans* one-cell embryo. I provide evidence, that PCMD-1 links microtubule nucleation activity to the centrosome, and fills in the gap between centriole and PCM assembly in worms. PCMD-1 targets the *C. elegans* centrosome matrix spindle-defective protein 5 (SPD-5) to non-mitotic centrosomes. The spindle-defective protein 2 (SPD-2) was previously found to recruit the PLK-1 kinase to mitotic centrosomes. This study shows that SPD-2 also targets PLK-1 to centrosomes in non-mitotic cells. Together PCMD-1 and SPD-2 implement PCM core formation in non-mitotic cells and ensure robust PCM expansion upon mitosis. PCMD-1, SPD-5, SPD-2, and PLK-1 form a centrosome module that is conserved across species.

Sensory neurons are the only cell type that possesses cilia and, thus, require centrioles postmitotically in *C. elegans*. Ciliary transition zones were found to mediate dendrite tip attachment in phasmid and amphid neurons. In these neurons, dendritic tip attachment to an extracellular matrix is required for successful dendrite elongation in a process termed retrograde dendrite extension.

In the second part of this study, I show that also the inner labial 1 (IL1) neurons form their dendrites by retrograde extension. Unexpectedly, dendrite tip attachment occurs before the asymmetric division of the IL1 neuroblast into the IL1 neuron and its dying sister cell. In mammalian cell culture, older mother centrosomes are more competent to form primary cilia. If this finding applies to *C. elegans*, the older mother centrosome might be inherited by the IL1 neuron during IL1 neuroblast division. To date, it is not possible to distinguish the older mother from the younger daughter centrosome in *C. elegans*, since specific markers are

unknown. I established an assay that allows tracking age-related centrosome inheritance in *C. elegans*. Further, the partitioning-defective protein 6 (PAR-6) is required for *C. elegans* amphid dendrite attachment. Whether the partitioning-defective protein 3 (PAR-3) and 6 play a role in centriole positioning during dendritic tip attachment remains to be examined.

GRAPHICAL SUMMARY
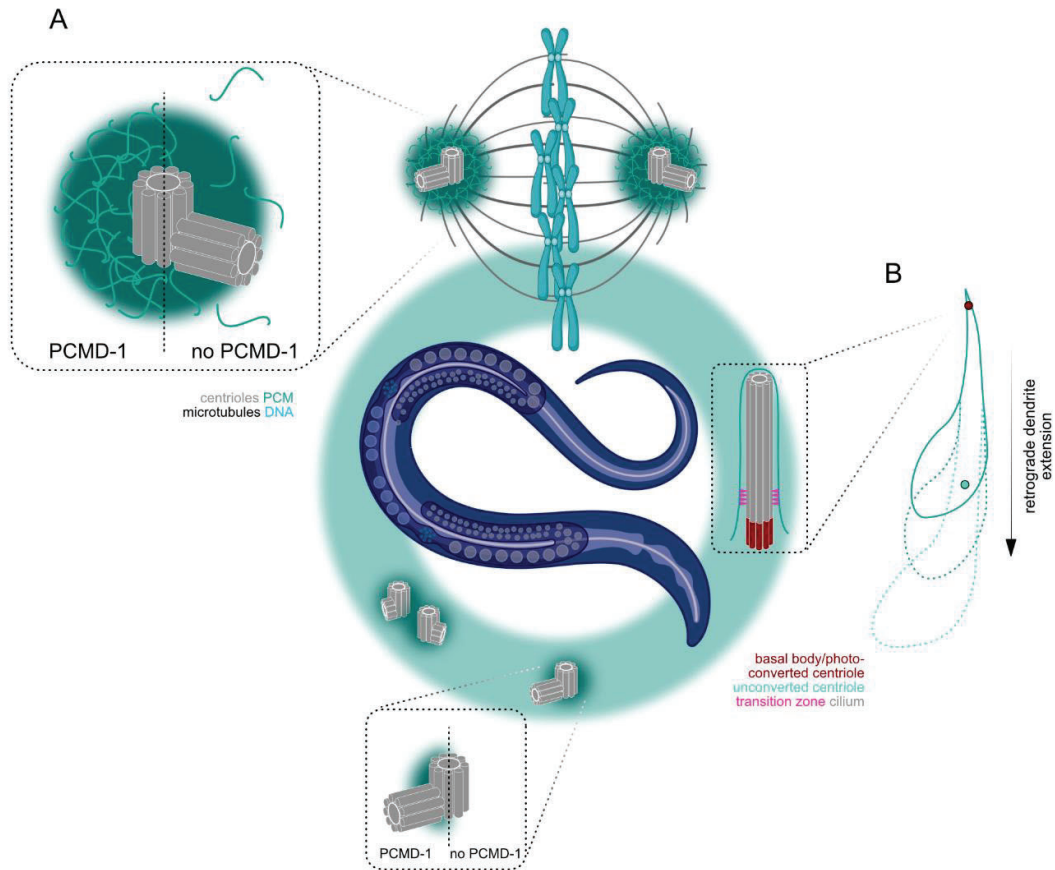
Graphical summary: (A) PCMD-1 facilitates PCM core formation and subsequent mitotic PCM expansion in *C. elegans*. The protein specifically links the centrosome matrix to centrioles. (B) Centrosomes have an inherent age difference and are inherited non-randomly, correlating with cell fate decisions, in several model systems. Centrosome age might play a role in successful dendrite tip attachment during retrograde dendrite elongation of *C. elegans* sensory neurons. *This graphical summary was partially created using bioRENDER* (https://biorender.com/).

ZUSAMMENFASSUNG

Zentriolen besitzen eine einzigartige Doppelfunktion in der Zelle, wo sie für die Bildung von Zentrosomen und Zilien benötigt werden. Die Organellen, die nicht durch eine Membran begrenzt sind, rekrutieren perizentrioläres Material (PZM) und organisieren während der Zellteilung die Mikrotubuli. In nicht-mitotischen Zellen können Zentriolen an die Zellmembran andocken und initiieren als Basalkörper die Zilienbildung. Aufgrund einer relativ kleinen Anzahl von zentrosomalen Proteinen, hat sich *C. elegans* zu einem wichtigen Modellorganismus im Gebiet der Zentrosomenbiologie entwickelt. Der Signalweg für den Aufbau von Zentriolen wurde als erstes im Wurm beschrieben. Darüber hinaus liefern Untersuchungen der PZM-Proteine in Nematoden wertvolle Einblicke in Aufbau und Function der PZM. In *C. elegans* ist bisher jedoch nicht klar, welche Faktoren die PZM an das Zentriol binden.

Im ersten Teil dieser Studie charakterisiere ich das neu identifizierte Protein Pericentriolar matrix deficient 1 (PCMD-1), das in *C. elegans* für die Bildung einer bipolaren Spindel im einzelligen Embryo erforderlich ist. Ich zeige auf, dass PCMD-1 die Mikrotubulibildung am Zentrosom vermittelt und damit die Lücke zwischen Zentriol- und PZM-Assemblierung in Würmern schließt. PCMD-1 rekrutiert das *C. elegans* Zentrosommatrixprotein Spindle-defective 5 (SPD-5) zu Zentrosomen. Es wurde bereits beschrieben, dass das Spindle-defective protein 2 (SPD-2) die Polo-like-Kinase 1 (PLK-1) zu mitotischen Zentrosomen rekrutiert. In dieser Studie zeige ich, dass SPD-2 PLK-1 auch zu Zentrosomen in nicht mitotischen Zellen lokalisiert. Damit initiieren PCMD-1 und SPD-2 gemeinsam die Bildung der PZM-Matrix in nicht mitotischen Zellen und gewährleisten eine robuste Expansion der PZM während der Mitose. PCMD-1, SPD-5, SPD-2 und PLK-1 sind zusammen Teil eines evolutionär konservierten Moduls, das dem Aufbau der Zentrosom Matrix dient.

In *C. elegans* sind sensorische Neuronen der einzige Zelltyp, der Zilien besitzt und daher Zentriolen auch postmitotisch benötigt. Es wurde beschrieben, dass die ziliare Übergangszone die Verankerung der Dendritenspitzen in Phasmid- und Amphid-Neuronen gewährleistet. Für ein erfolgreiches Auswachsen der Dendriten, welches hier durch retrograde Verlängerung geschieht, ist die Verankerung der Dendritenspitzen an eine extrazelluläre Matrix erforderlich.

Im zweiten Teil dieser Studie zeige ich, dass auch die Inner labial 1 (IL1)-Neuronen ihre Dendriten retrograd verlängern. Ungewöhnlicherweise kommt es bereits vor der asymmetrischen Teilung des IL1-Neuroblasten, in das IL1-Neuron und seine apoptotische Schwesterzelle, zur Verankerung der Dendritenspitzen. In Zellekultur wurde gezeigt, dass Zellen mit älteren Zentrosomen früher primäre Zilien formen können, als die Schwesterzellen mit jüngeren Zentrosomen. Wenn dieser Befund auch auf *C. elegans* zutrifft, könnte das ältere Zentrosom während der Teilung des IL1-Neuroblasten an das IL1-Neuron vererbt werden. In *C. elegans* ist es bisher nicht möglich, das ältere von dem jüngeren Zentrosom zu unterscheiden, da spezifische Marker nicht beschrieben sind. Ich habe eine Methode etabliert, die ermöglicht die Vererbung des älteren Zentrosoms zu verfolgen. Ferner ist das Protein Partitioning-defective 6 (PAR-6) für die Bildung von Amphid-Dendriten in *C. elegans* erforderlich. Ob die Proteine Partitioning-defective 3 (PAR-3) und -6 eine Rolle bei der Positionierung von Zentrosomen in Dendriten spielen, muss noch untersucht werden.

INTRODUCTION

INTRODUCTION

1.1.   The centrosome and its cellular function

1.1.1.   The evolution of the centrosomal structure and its biological relevance

Centrosomes are non-membrane-bound organelles that serve as the major microtubule-organizing centers (MTOCs) in metazoans and various other eukaryotic lineages (Carvalho-Santos *et al.*, 2011; Azimzadeh, 2014; Loncarek and Bettencourt-Dias, 2018). The structure is built of a pair of barrel-shaped, microtubule-based centrioles, each displaying a nine-fold symmetry, which is embedded in the pericentriolar material (PCM), a proteinaceous matrix and its downstream factors that are required for microtubule nucleation and regulation (Figure 1B). The organelle is highly dynamic throughout the cell cycle (Figure 1A). Moreover, the dynamics of the centrosome are strictly coupled to the progression of the cell cycle. For example, centrosomes duplicate when the replication of the DNA takes place (with some rare exceptions). PCM levels are highest during mitosis, were centrosome function is required to organize the bipolar spindle for the separation of the genetic material and cell content (Figure 1A; Nigg and Stearns, 2014). Furthermore, centrioles possess a unique dual function and are, in addition to their role in organizing centrosome assembly, required to template the outgrowth of cilia and flagella, which usually are resorbed before mitotic entry (Figure 1A; Plotnikova, Pugacheva and Golemis, 2009; Hu *et al.*, 2015).

Phylogenetic studies suggest that centriole comprising centrosomes were present in the last common ancestor of eukaryotes, which is substantiated through the exceptionally conserved structure of the organelle (Carvalho-Santos *et al.*, 2011; Gräf, 2018). Cilia and flagella originally evolved as important structures for locomotion, and have further been shown to exhibit sensory function (Bloodgood, 2010; Carvalho-Santos *et al.*, 2011). In some early sessile or amoeboid eukaryotes, centrioles were most likely nonessential, and thus the structure was lost in the course of evolution (Carvalho-Santos *et al.*, 2011; Gräf, 2018). Higher plants, most fungi, and amoebas lack centrosomal structures (Loncarek and Bettencourt-Dias, 2018). Curiously enough, one of the earliest reports of centrosomes dates back to 1894, where the Japanese botanist Sakugoro Hirase described 'attractive spheres' in the pollen of *Ginkgo biloba* (Hirase, 1894). During late spermatogenesis centrioles arise *de novo* in lower plants with motile gametes, such as ginkgo (Vaughn and Harper, 1998; Renzaglia and Garbary, 2001; Vaughn and Renzaglia, 2006; Loncarek and Bettencourt-Dias,

2018), emphasizing the ancestral character of the centriole and the theory that centrioles originally developed to template locomotive cilia and flagella (Carvalho-Santos *et al.*, 2011; Gräf, 2018). Consequently, centriolar function as part of the MTOC evolved most likely secondarily in some eukaryote lineages (Carvalho-Santos *et al.*, 2011). In recent years increasing evidence suggests that centrosomes act as signaling centers, allowing proteins to interact at high concentrations to coordinate multiple cellular functions (Arquint, Gabryjonczyk and Nigg, 2014; Conduit, Wainman and Raff, 2015).
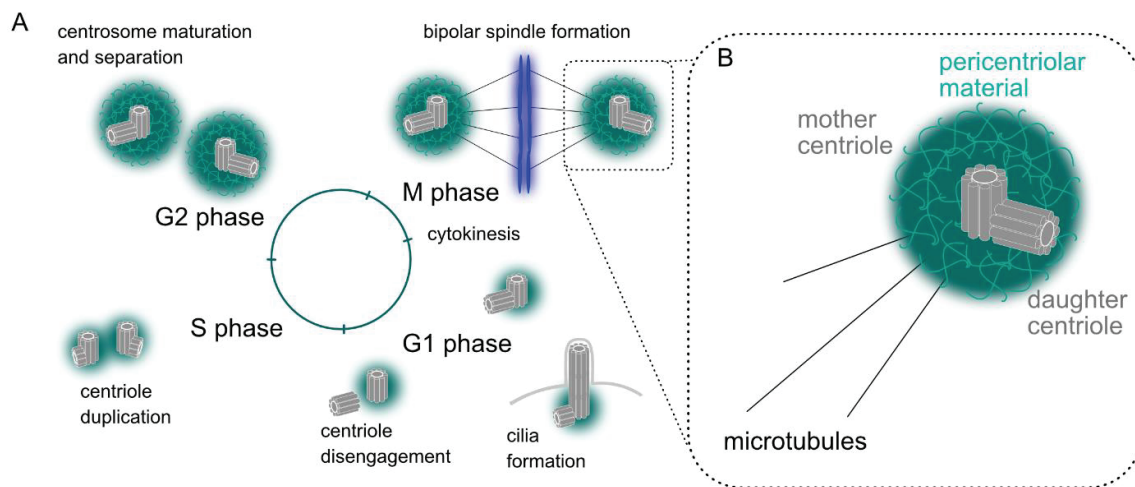
Figure 1: **Centrosome formation and duplication**. (A) Centrosome duplication is tightly linked to the cell cycle. After cell division, each daughter cell inherits one centriole pair. The more mature centriole can dock to the cell membrane and form a cilium in Gap 1 (G1) phase. Towards the synthesis (S) phase, the centriolar pair disengages. During S phase, one daughter centriole starts to assemble on each of the parental centrioles. Centrosomes move apart once they accumulate PCM in Gap 2 (G2) phase. The fully matured centrosomes disengage as the cell enters the mitotic (M) phase and organize the bipolar spindle for the next cell division. (B) New centrioles always form at the proximal site of a mature parental centriole. Thus, the centrioles of one centrosome have an intrinsic age difference. They are referred to as mother and daughter centrioles. The centrosomes recruit PCM for microtubule nucleation and bipolar spindle formation.

1.1.2. Centrosomes in cell division and development

Over a century ago, the centrosome was described independently by Edouard Van Beneden and Theodor Boveri (VanBeneden, 1887; Boveri, 1887; reviewed in: Scheer, 2014). The authors recognized the centrosome as a permanent organelle of the cell, which self-replicates and is passed on to the next generation of cells (VanBeneden, 1887; Boveri, 1887; reviewed in: Scheer, 2014). At that time, Boveri already concluded that the centrosome mediates the nuclear and cellular division (Boveri, 1887). He further found that an excess of centrosomes led to spindles with multiple poles and proposed that tumor formation is linked to the presence of supernumerary centrosomes (Boveri, 1914; reviewed in: Scheer, 2014).

Centrosome aberrations and malfunctions have been linked to genome instability, cancer, microcephaly and primordial dwarfism (Lingle *et al.*, 1998, 2001; Pihan *et al.*, 1998; Basto *et al.*, 2008; Castellanos and Dominguez, 2008; Thornton and Woods, 2009; Megraw, Sharkey and Nowakowski, 2011; Vitre and Cleveland, 2012; Barbelanne and Tsang, 2014; Chavali *et al.*, 2014). Overduplication of centrosomes is common in cancer cells, which may lead to multipolar spindles and thus, errors in cell division that cause genomic instability. The same holds true for cytokinesis failure, which can entail multipolar spindle formation in the following cell cycle if centrosomes undergo regular duplication (Figure 2A). The affected cell polarity and migration can result in cancer metastasis (Godinho and Pellman, 2014). Multipolar spindle formation can, however, also be caused by premature centriole disengagement or PCM fragmentation (Maiato and Logarinho, 2014). In the case of premature centriole disengagement, multiple poles can be formed by centrosomes containing only a single centriole (Figure 2B). When it comes to PCM fragmentation, acentriolar PCM accumulations form due to the loss of PCM integrity (Figure 2C). Further, mutations in PCM proteins are linked to primordial dwarfism and microcephaly (Chavali *et al.*, 2014). However, it is not clear why aberrations in PCM formation lead to these growth defects. For example, primordial dwarfism is caused by a decrease in cell numbers in affected individuals. This could be the result of an increased number of cells undergoing cell death or a reduction in cell proliferation. Impaired PCM expansion might lead to mitotic catastrophe and cell-death (Fry *et al.*, 2017). Alternatively, cell cycle progression might be compromised as a result of cell cycle checkpoint activation caused by PCM aberrations (Klingseisen and Jackson, 2011; Arquint, Gabryjonczyk and Nigg, 2014; Fry *et al.*, 2017). In microcephaly patients, growth defects are restricted to the brain. As described for primordial dwarfism, this could be due to increased cell death or a reduction in cell proliferation. However, neuronal progenitor cells are

specifically affected, leading to the exhaustion of the progenitor pool (O'Neill *et al.*, 2018). The centrosome is a complex organelle, and its assembly and function have to be tightly regulated. Even though centrosomes were discovered more than a century ago and substantial progress in understanding the structure was made in the last decades, many open questions remain (Bornens and Gönczy, 2014).
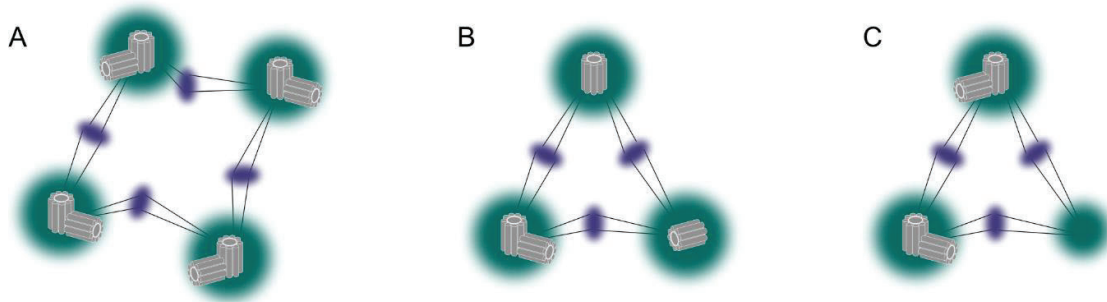
Figure 2: **Multipolar spindle formation during mitosis**. (A) Overduplication of centrosomes and incomplete cytokinesis can cause multipolar spindle formation in the next cell cycle. (B) Single centrioles can recruit PCM and form centrosomes. Thus, if centrioles separate prematurely, multiple centrosomes can form and give rise to a multipolar spindle during mitosis. (C) Instable PCM formation can lead to PCM fragmentation and the assembly of a multipolar spindle.

1.1.3. Asymmetric centrosome inheritance and cilia formation

Antoni van Leeuwenhoek, a Dutch scientist, and father of microbiology, was the first one to describe cilia when he discovered protozoa and their locomotive cilia under a self-made microscope in 1674 (Van Leeuwenhoek, 1677). Most vertebrate cells possess cilia. Abnormal formation or function of cilia can lead to severe illnesses, such as retinal degradation, kidney or congenital fibrocystic liver disease, encephalic anomalies, dwarfism, diabetes and obesity (Waters and Beales, 2011). Illnesses deriving from ciliary defects are also referred to as ciliopathies and can be caused by defective core centriole proteins that lead to aberrations in cilia formation. As mentioned previously, centrioles are required to template cilia outgrowth. The centrosomal pair of centrioles always contains an older mother and a

younger daughter centriole due to the intrinsic asymmetry during their duplication: The daughter or pro-centriole always assembles at the proximal site of a parental centriole (Figure 1). Mother versus daughter centrioles are compositionally and structurally distinct, meaning that specific proteins are exclusively associated with the mature mother centriole, whereas others are daughter centriole specific (Dormoy, Tormanen and Sütterlin, 2013; Tormanen and Su, 2013; Loncarek and Bettencourt-Dias, 2018). Further, particular structures associated only with the mother centriole, namely the distal appendages, mediate membrane docking of the mother centriole as an initial step of cilia formation. Thus, cilia always emanate from the mother centriole. When the centriolar pair splits after entering a next cell cycle and a new round of duplication starts, the resulting centrosomes contain mother centrioles of different ages (Figure 1A). The centrosome that contains the older (grand-)mother centriole is referred to as mother centrosome. The centrosome with the younger mother centriole is the daughter centrosome. In 2001, Pereira *et al*. found that in budding yeast, *Saccharomyces cerevisiae*, the newly emerged daughter cell inherits the older of the two spindle pole bodies (the yeast functional equivalents to centrosomes) (Pereira *et al.*, 2001). Similar mechanisms have been found in animals, linking centrosome asymmetry and cell fate: In *Drosophila melanogaster (D. melanogaster)* male germline stem cells, the older centrosome remains in the self-renewing stem cell. The younger centrosome is inherited by the differentiating daughter cell (Yamashita *et al.*, 2007). Also, *D. melanogaster* larval neuroblasts undergo asymmetric cell division and produce one renewed neuroblast, as well as one ganglion mother cell, which divides again before terminal differentiation. However, in this system, it is the younger daughter centrosome which is inherited by the neuroblast, whereas the older centrosome is passed on to the ganglion mother cell (Conduit *et al.*, 2010; Januschke *et al.*, 2011). Interestingly, Anderson *et al*., 2009 discovered that in symmetrically dividing stable cell lines, the cell inheriting the older mother centrosome could grow a primary cilium first, and further, responds to Sonic hedgehog signaling earlier than the sister cell that inherited the younger centrosome (Anderson and Stearns, 2009). Cultures of mouse neuroepithelial cells show the same asymmetry in cilia growth and their response to sonic hedgehog signaling (Piotrowska-Nitsche and Caspary, 2012). Taken together, these findings suggest that in asymmetrically dividing cells the inherent asymmetry of centrosomes can be exploited to support the determination of daughter cell fates.

1.2. *C. elegans* as a model organism to study centrosome biology

1.2.1. The model organism *C. elegans*

In the late 1950s, Dougherty and Calhoun proposed that nematodes could be of great value in genetic research due to their eutely (Dougherty and Grant Calhoun, 1948). Each individual of a eutelic species undergoes the same differentiation process, resulting in an invariant cell lineage between animals. Sydney Brenner proposed *Caenorhabditis elegans* (*C. elegans)* as a model system in 1963 and aimed to establish its complete cell lineage. A decade later, Brenner presented his results (Brenner, 1974). Since then, *C. elegans* developed into a widely used model system. Sulston *et al*. eventually published the entire cell lineage of *C. elegans* in 1983 (Sulston and Schierenberg, 1983). The worms are microscopic (~ 1mm) and easy to culture in Petri dishes filled with agar and spread with a bacterial lawn of *E. coli* as a food source. They reproduce quickly, and at 20 °C, it takes only three days for the worms to develop from egg to the fully mature adult. There are two sexes, hermaphrodites (XX) and males (Xo). Hermaphrodites can self-reproduce. Typically, there is only a very low frequency of males occurring in a wild-type population with about 1 male in 500 (Hodgkin, Horvitz and Brenner, 1979; Zarkower, 2006). Due to limited production of sperm, self-inseminated hermaphrodites lay up to 300 fertilized eggs, whereas male inseminated hermaphrodites can produce up to 1400 fertilized eggs (reviewed in: Singson, 2001). The worms are transparent throughout their life cycle. Accordingly, microscopy can be performed easily at all life stages. Moreover, the eggs are large in size (~50 μm length x 30 μm diameter), and their mitotic divisions are highly stereotypic (Oegema, 2006). Thus, their development can be followed and investigated using differential interference contrast (DIC) microscopy. *C. elegans* hermaphrodites and males possess 959 and 1031 somatic cells, respectively, with about a third of the cells developing into neurons (*WormAtlas*, Altun *et al.*, 2002-2019). The complete *C. elegans* genome was published in 1998 and was the first complete metazoan genome available at the time (Equence *et al.*, 1998). It comprises ~100 million base pairs (103 022 290 bp, WBcel235 *wormbase*) with 20,222 coding genes and 61,109 gene transcripts. The haploid *C. elegans* genome includes six chromosomes, chromosome I-V, and one sex chromosome X, plus the mitochondrial genome (*wormbase*). Judged by their genomic sequences, 38 % of the *C. elegans* genes are predicted to have orthologues in mammals (Shaye and Greenwald, 2011). Other resources report that 60 to 80 % of the human genes have on orthologue in *C. elegans* (Lai *et al.*, 2000; Kaletta and Hengartner, 2006).

1.2.2. The *C. elegans* life cycle

At 20 °C, it will take approximately 11 hours from fertilization until hatching of the eggs (Figure 3). The worm enters the L1 larval stage, followed by the three larval stages L2-L4. The larvae remain in the L1 stage for about 16 hours. The remaining larval stages are each about 12 hours long. The transition from one to another larval stage is marked by a short period of a lethargy or sleep-like state, referred to as lethargus, which is followed by a molting (Raizen *et al.*, 2008). If environmental conditions are unfavorable, worms can enter a dormancy stage after the L2 larval stage. This stage is also referred to as the dauer larval stage and allows the worms to survive for up to 4 months without food or at high temperatures (Golden and Riddle, 1984). If the shortcomings are remedied, the larva in dauer stage can enter L4 stage and continue their development. At 20 °C, the worms live for about two weeks, and the reproductive phase lasts for six days (Figure 3; Klass, 1977). Importantly, developmental timing and cell cycle progression of *C. elegans* vary depending on the temperature (Byerly, Cassada and Russel, 1976; Begasse *et al.*, 2015). Standard maintenance temperatures of *C. elegans* in the laboratory range from 12 °C to 25 °C (Corsi, Wightman and Chalfie, 2015).
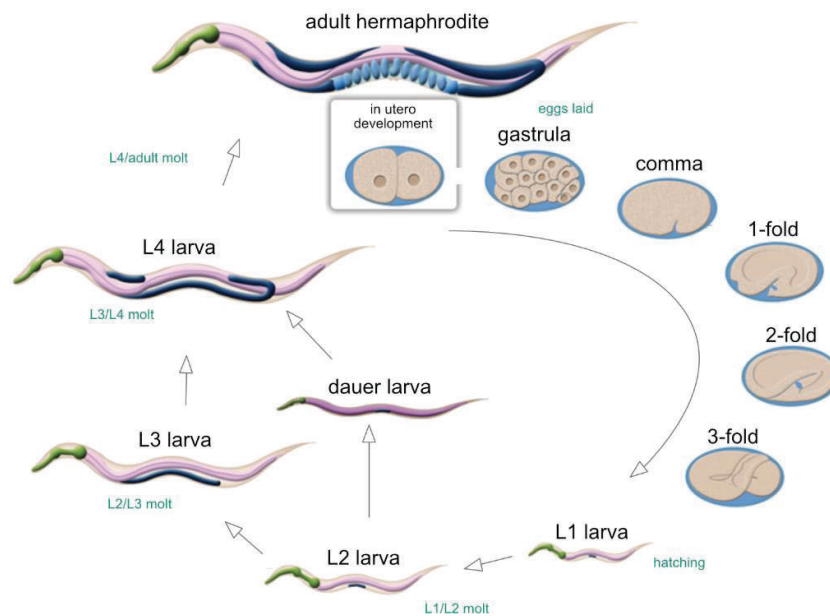
Figure 3: **The *C. elegans* life cycle**. Eggs are laid when they reach the gastrula stage and develop ex utero until they hatch. They undergo four larval stages until they reach adulthood.

Worms can enter the so-called dauer larval stage if environmental conditions are unfavorable. Adapted from *WormAtlas* (https://www.wormatlas.org/hermaphrodite/introduction/mainframe .htm).

1.2.3. *C. elegans* as a model to study cell division

1.2.3.1. The *C. elegans* one-cell embryo

The *C. elegans* one-cell embryo was studied extensively as a model for cell division. The invariant nature of *C. elegans* cell divisions enables us to analyze precisely the phenotypes of molecular aberrations. Due to silencing of the DNA damage response in early *C. elegans* embryos and the poor spindle assembly checkpoint response, embryo development progresses even in animals with severe spindle formation, chromosome segregation and centrosome assembly errors (Encalada *et al.*, 2005; Holway *et al.*, 2006; Oegema, 2006; Galli *et al.*, 2016). Before fertilization takes place, oocytes remain arrested in the meiotic prophase. Oocytes lack centrioles, which are actively removed from the oocyte during oogenesis (Mikeladze-dvali *et al.*, 2012). Upon fertilization, the sperm introduces a pair of centrioles and defines the posterior side of the embryo (Figure 4A; Rose and Gönczy, 2014). After that, the two female meiotic divisions are completed by an acentriolar spindle, located at the anterior side of the embryo, which leads to the extrusion of two polar bodies (Figure 4A; Albertson and Thomson, 1993). The sperm-derived centrioles, which are associated with the male pronucleus, duplicate immediately after fertilization. They start accumulating PCM and, while microtubule nucleation activity and pulling forces increase, centrosomes separate (Figure 4B; Gönczy *et al.*, 1999; Cabral *et al.*, 2013). The microtubules, emanating from the centrosomes, associate with the paternal pronucleus and capture the female pronucleus. Subsequently, the opposing parental nuclei start to migrate towards each other. The process is termed pronuclear migration (PNMi, Figure 4B). During the pronuclear meeting (PNM), centrosomes are positioned at each side of the contact area of the nuclei. Nuclei and centrosomes are then moving to the approximate center of the embryo, and, as the mitotic spindle is forming, it aligns with the anterior-posterior axis of the embryo (Figure 4C). Pronuclear envelope breakdown (PNEB) occurs (Figure 4D) and chromosomes align in the metaphase plate as centrosomes form the mitotic spindle (Figure 4E). In late anaphase chromosomes are progressively pulled towards the opposite poles of the mitotic spindle. The

individual centrioles of a centrosome disengage at this stage and are distinguishable in confocal micrographs (Figure 4F).

The first division of the *C. elegans* zygote is asymmetric, giving rise to a bigger anterior cell, the AB cell, and a smaller posterior cell referred to as P_1 cell (Figure 4G; Sulston and Schierenberg, 1983). The partitioning defective (PAR) proteins are required for establishing the anterior-posterior (AP) polarity in the one-cell embryo and ensure robust cytokinesis during the asymmetric cell division (Kemphues *et al.*, 1988; Rose and Kemphues, 1998; Jordan *et al.*, 2016). The PDZ domain containing proteins PAR-3[ASIP, Bazooka] and PAR-6[hsPAR6, Par-6] are found in complex with the atypical protein kinase C (PKC-3[aPKCλ/ζ, aPKC]) (Tabuse *et al.*, 1998; Hung and Kemphues, 1999). The protein complex is referred to as anterior PAR complex and is present throughout the cortex after fertilization, but gets restricted to the anterior half of the embryo shortly after the centrosome is juxtaposed to the cortex (Cuenca *et al.*, 2003; Munro, Nance and Priess, 2004). The Ring-finger protein PAR-2 and the kinase PAR-1[hsPar1, Par-1] occupy the posterior half of the embryo. The redistribution of the anterior and posterior PAR complexes was shown to be concomitant with the contraction of the actomyosin network in the zygote shortly after fertilization (Munro, Nance and Priess, 2004). The kinase PAR-4[LKB1, dLKB1] and the 14-3-3 protein PAR-5[14-3-3β, 14-3-3ε] are present at the cortex and in the cytoplasm (Watts *et al.*, 2000; Morton *et al.*, 2002). Aberrations in PAR protein function can lead to altered symmetry and fate of daughter cells, misorientation of the mitotic spindle, and failure of cell cycle progression (Kemphues *et al.*, 1988). Furthermore, PAR proteins undertake various other functional roles later in development, such as gastrulation associated apicobasal asymmetry establishment, apical centrosome localization in the intestine or neuronal dendrite extension in *C. elegans* (Nance, Munro and Priess, 2003; Feldman and Priess, 2012; Fan *et al.*, 2019). In other species, PAR proteins have also been linked to primary cilium assembly and centrosome orientation during asymmetric cell division (Sfakianos *et al.*, 2007; Inaba, Venkei and Yamashita, 2015).
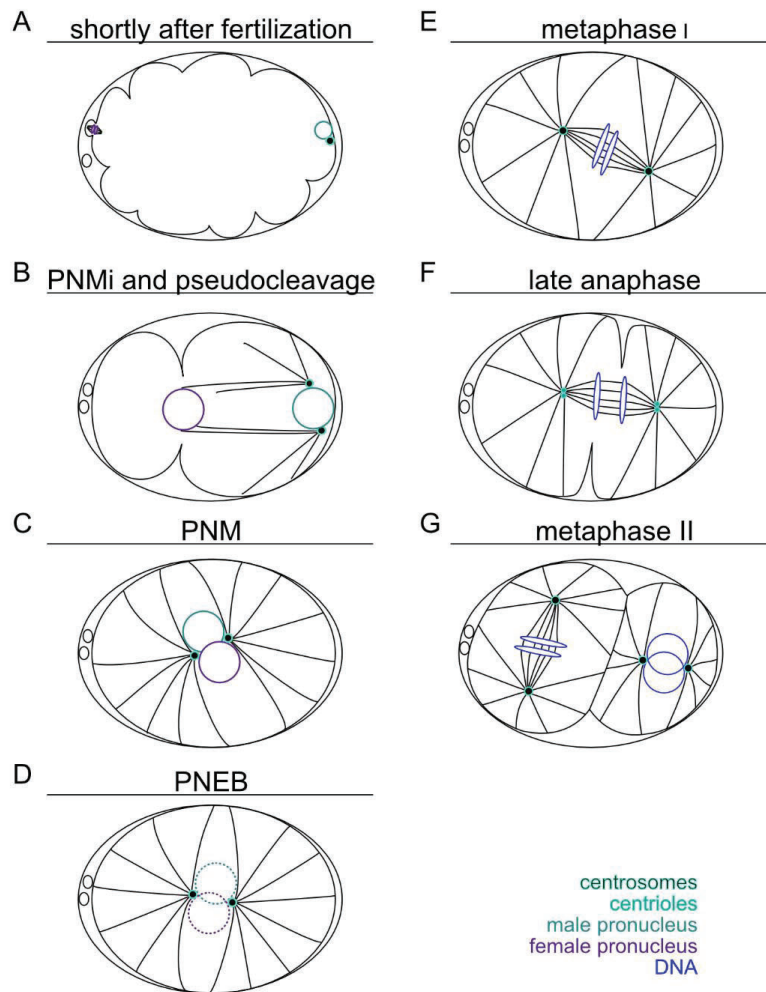
Figure 4: **Developmental stages of the *C. elegans* one-cell embryo**. Adapted from Greenstein (2005). (A) Upon fertilization, the sperm introduces the paternal DNA and a centrosome to the zygote. The entry side of the sperm determines the posterior of the embryo (here on the right). In worms, both meiotic divisions are completed after fertilization. Two polar bodies are extruded at the anterior side of the embryo (here on the left). Fertilization occurs ~750 sec[*] before the pronuclear envelope breaks down (PNEB). (B) The duplicated centrosomes nucleate microtubules, which capture the female pronucleus and facilitate pronuclear migration (PNMi). The pseudocleavage furrow occurs. PNMi occurs ~470 sec[*] before PNEB. (C) Pronuclear meeting (PNM) occurs ~120 sec[*] before PNEB. (D) PNEB is used as the relative reference point and is set as time point 0 sec[*]. (E) Chromosome alignment in metaphase I occurs ~160 sec[*] after PNEB. (F) In late anaphase, the two centrioles of a centrosome disengage and are distinguishable in confocal micrographs. Anaphase occurs ~240 sec[*] after PNEB. (G) The anterior cell is slightly ahead of the posterior cell in its progression through the cell cycle. [*]Developmental timing at 20 °C.

1.2.3.2. *C. elegans* sensory neurons as a model for asymmetric cell division

In vertebrates, the majority of cells possess cilia. On the contrary, sensory neurons are the only ciliated cell type in *C. elegans* (Ward *et al.*, 1975; Perkins *et al.*, 1986). There are 60 sensory neurons in the adult hermaphrodite, implicated in various processes such as chemo-, osmo-, machano- and thermosensation, as well as dauer stage transition and regulation of longevity (Inglis *et al.*, 2007). Males have 52 additional sensory neurons, which are mainly located in their tail rays and are required for male mating (Sulston, Albertson and Thomson, 1980; Peden and Barr, 2005). Thus, sensory neurons are the only cell type in the worm that require centrioles post mitotically to form cilia. Many sensory neurons are derived from asymmetric divisions by size and by fate. In these lineages sister cells of neurons either undergo programmed cell death or acquire a fate, which does not require cilium formation (Sulston and Schierenberg, 1983). Thus, asymmetric cell divisions, which give rise to a ciliated neuron and a cell of different fate, are particularly attractive to study the inherent differences between mother and daughter centrosomes and their inheritance. One example is the inner labial sensilla 1 (IL1) neuron lineage, where the IL1 neuroblast gives rise to the ciliated mechanosensory IL1 neuron and its dying sister cell. Aberrations in IL1 neuron function disrupts the aversive head-withdrawal reflex of worms touched on the dorsal or ventral sides of their nose (J. Kaplan and H.R. Horvitz, unpubl., *WormAtlas*).

1.3.   Centrosome and cilia formation

1.3.1. Centrosome regulation throughout the cell cycle

The somatic cell cycle typically consists of the Gap1 (G1) phase for cell growth, the synthesis (S) phase for DNA replication, the Gap2 (G2) phase as preparation for mitosis, and the mitotic (M) phase, in which the cell divides into the two daughter cells (Figure 1A). After fertilization, zygotes undergo a series of rapid cleavages, without increasing the overall cell mass of the embryo. These early cell cycles generally lack the G1 and G2 phases. The cyclin-dependent kinase (Cdk)/cyclin complexes and other kinases, including the Polo and Aurora kinases, were identified as important regulators of the cell cycle. In mice, Cdk1$^{\text{CDK1, Cdk-1, CDK-1}}$ and its regulatory subunits cyclin A$^{\text{cyclin A, cyclin A, CYA-1/2}}$ and cyclin B$^{\text{cyclin B, cyclin B, CYB-1/3}}$ are the only Cdk/cyclins required for viability (Murphy *et al.*, 1997; Geng *et al.*, 2003; Kozar *et al.*, 2004; Santamaría *et al.*, 2007; Kalaszczynska *et al.*, 2009). In addition, Cdk2$^{\text{hsCDK2, CDK-2}}$/cyclin E$^{\text{cyclin E, CYE-1}}$ are essential in flies (Lehner and O'Farrell, 1990; Knoblich and Lehner, 1993; Knoblich *et al.*, 1994). Furthermore, Cdk4$^{\text{hsCDK4, CDK-3}}$/cyclin D$^{\text{cyclin D, CYD-1}}$ are required for cell growth in flies (Emmerich *et al.*, 2004). In *C. elegans,* the CDK-1$^{\text{CDK1, Cdk-1}}$/CYB-1/3$^{\text{cyclin B, cyclin B}}$, CDK-2$^{\text{hsCDK2, Cdk-2}}$/CYE-1$^{\text{cyclin E, cyclin E}}$, and the CDK-4$^{\text{hsCDK4, Cdk-4}}$/CYD-1$^{\text{cyclin D, cyclin D}}$ complexes are all required for survival (Boxem, Srinivasan and Van Den Heuvel, 1999; Cowan and Hyman, 2006).

Moreover, the polo-like kinases (PLKs) are important for mitotic progression. All PLKs carry a Polo-box domain (PBD) at their carboxy-terminal end (N-terminus). The domain serves as a binding pocket for phosphorylated sites in the target substrates (Elia *et al.*, 2003). The phosphorylation at these sites is often mediated by CDKs, which thereby govern the specific and targeted recruitment of the PLKs. The PLK1 kinase in mammals, and its homologues Polo and PLK-1 in *D. melanogaster* and *C. elegans*, respectively, are critical regulators of mitosis and cytokinesis (Kumagai and Dunphy, 1996; Watanabe *et al.*, 2004; Inoue and Sagata, 2005). The Aurora A$^{\text{Aurora A, AIR-1}}$ and B$^{\text{Aurora B, AIR-2}}$ kinases phosphorylate PLK1$^{\text{Plk-1, PLK-1}}$ to activate the kinase (Archambault and Glover, 2009). Centrosome duplication is strictly coupled to the cell cycle (Figure 1A), and the kinases CDK1$^{\text{Cdk-1, CDK-1}}$, PLK1$^{\text{Polo, PLK-1}}$, PLK4$^{\text{Plk-4, ZYG-1}}$, and Aurora A $^{\text{Aurora A, AIR-1}}$ were found to be important regulators of centrosome duplication and function. When the tight connection of the centriolar pair is released at the mitotic exit, the centrioles stay in close proximity. In vertebrates, PLK1$^{\text{Polo, PLK-1}}$ and the cysteine protease Separase$^{\text{SSE, SEP-1}}$ were found to play an important

role in regulating centriole disengagement (Tsou *et al.*, 2009). In human cells, the PCM protein pericentrin[Plp] is cleaved by Separase[SSE, SEP-1] and, subsequently, it is downregulated at centrosomes in late mitosis. Furthermore, this cleavage of pericentrin[Plp] is regulated by PLK1 (Kim *et al.*, 2015). In *C. elegans*, depletion of SEP-1[Separase, SSE] impairs separation of sperm-derived centrioles after fertilization, and duplication is impaired (Cabral *et al.* 2013). However, centrioles disengage normally in the following cell cycles. In worms, SEP-1[Separase, SSE] might specifically regulate disengagement in a context where PCM levels at centrioles are low, and thus, cytoskeletal forces and pericentriolar material disassembly cannot drive centriole separation (Cabral *et al.* 2013).

In S phase, a procentriole is assembled at the proximal side of the parental centriole. The cartwheel structure of the younger centriole is removed in a CDK1[Cdk-1, CDK-1] dependent manner, further unlocking the block of reduplication (Arquint and Nigg, 2016; Kim *et al.*, 2016). Centriole duplication is governed by Polo-like kinase 4 (PLK4/Plk-4) activity in human and *D. melanogaster* and its homologue Zygote-defective 1 (ZYG-1) in *C. elegans* (Bettencourt-Dias *et al.*, 2005; Habedanck *et al.*, 2005; O'Connell *et al.*, 2001; see below for more details).

Next, the centrosomes fully disengage as the cell enters mitosis to organize the bipolar spindle (Figure 1A, Nigg and Stearns, 2014). The centrosome associated amount of PCM changes over the cell cycle. Whereas in interphase, especially S phase, PCM association is minor, the centrosomes undergo a maturation process towards mitosis by recruiting PCM, and thus, increase microtubule nucleation capacity for bipolar spindle assembly (Figure 1). This spacial and functional expansion of the PCM is regulated by the PLK1[Polo, PLK-1], and Aurora A[Aurora A, AIR-1] kinases (V Joukov, Walter and De Nicolo, 2014). A conserved set of scaffolding proteins, namely Pericentrin/Pericentrin-like protein (Plp) and centrosomal protein of 152 kDa (Cep152)/Asterless (Asl) in human and flies, as well as Cep192/Spindle-defective protein 2 (Spd-2)/SPD-2 and CDK5 regulatory subunit associated protein 2 (CDK5RAP2)/D-Centrosomin (Cnn)/SPD-5 in human, flies and worms, have been identified as components of the so-called centromatrix, a scaffolding structure onto which downstream regulators of centrosome function are loaded (For more details see below; Gosti-Testu *et al.*, 1986; Doxsey *et al.*, 1994; Bonaccorsi, Giansanti and Gatti, 1998; Vaizel-Ohayon and Schejter, 1999; Hamill *et al.*, 2002; Andersen, Wilkinson and Mayor, 2003; Pelletier *et al.*, 2004; Varmark *et al.*, 2007). Moreover, the ability of a daughter centriole to recruit PCM is further required for centriole duplication in the next cell cycle (Izquierdo *et al.*, 2014; Fu *et al.*, 2016; Tsuchiya *et al.*, 2016). This process is called centriole to centrosome conversion and was shown to be

regulated by CDK1[Cdk-1, CDK-1] and PLK1[Polo, PLK-1] (Wang *et al.*, 2011; Novak *et al.*, 2016). Furthermore, the younger centrosome has to undergo mitosis to acquire its competence for ciliogenesis. Thereby, the younger mother centriole acquires appendage structures at its distal end, which are needed for basal body function and to template ciliary growth. The process is regulated in a Plk-1[Polo, PLK-1] dependent manner (Kong *et al.*, 2014).

As cells exit mitosis, also PCM levels decline (Figure 1A). Work in *C. elegans* has shown that two independent mechanisms ensure regulated PCM disassembly: The Protein phosphatase 2A (PP2A) and its regulatory subunit Suppressor of activated let-60 Ras (SUR-6) have been shown to dephosphorylate the centrosome matrix protein SPD-5[CDK5RAP2, Cnn] and potentially also other PCM components (Enos *et al.*, 2018). This ultimately leads to the disassembly of the PCM. Additionally, microtubule pulling forces, directed towards the cortex, help to dissipate the PCM (Enos *et al.*, 2018).

1.3.2. The centriole assembly pathway

Centrioles are barrel-shaped structures that are arranged in a pairwise manner perpendicular to one another (Figure 1B). Their underlying architecture shows a nine-fold symmetry of singlet, doublet, or triplet microtubule arrays (Gönczy, 2012). In humans, triplet microtubules are arranged around a central cartwheel in a nine-fold manner. Centrioles are 450 nm long and 250 nm wide (Gönczy, 2012). On their distal end, they carry distal and subdistal appendages, which are essential for membrane docking and microtubule anchorage, respectively (reviewed in Hoyer-Fender, 2010). In *C. elegans* centrioles consist of a central tube. Only recently, this central tube was found to resemble the cartwheel structure described in other organisms, including humans (Sugioka *et al.*, 2017). The cartwheel structure is surrounded by nine singlet microtubules in worms (Gönczy, 2012). They are 150 nm long and 100 nm in diameter (Toole *et al.*, 2003; Pelletier *et al.*, 2006). In human and *D. melanogaster*, the primary regulator of centriole duplication is the PLK4/Plk-4[ZYG-1] kinase (Bettencourt-Dias *et al.*, 2005; Habedanck *et al.*, 2005). In humans, PLK4[Plk-4, ZYG-1] is recruited to centrosomes through Cep152[Asl] and Cep192[Spd-2, SPD-2] (Kim *et al.*, 2013; Sonnen *et al.*, 2013). The kinase is activated through binding to the SCL/TAL1 interrupting locus protein (STIL[Ana2, SAS-5]) (Arquint *et al.*, 2015; Moyer *et al.*, 2015). STIL[Ana2, SAS-5] is then phosphorylated by PLK4[Plk-4, ZYG-1], and Spindle assembly abnormal protein 6 (hsSAS6[Sas-6, SAS-6]) is recruited for cartwheel assembly (Kratz *et al.*, 2015; Moyer *et al.*, 2015). PLK4[Plk-4, ZYG-1], STIL[Ana2, SAS-5], and human

hsSAS6[Sas-6, SAS-6] get restricted to the region where daughter centrioles form via an unknown mechanism (Sonnen *et al.*, 2012; Kim *et al.*, 2013; Ohta *et al.*, 2014). Cep135[Cep135] then links hsSAS6[Sas-6, SAS-6] to the Centrosomal p4.1-associated protein (CPAP[Sas-4, SAS-4]) and the microtubules of the microtubule triplets (Lin *et al.*, 2013). CPAP[Sas-4, SAS-4] further regulates the elongation of the microtubules (Tang *et al.*, 2009; Sharma *et al.*, 2016; Zheng *et al.*, 2016). This core centriole duplication pathway was first discovered in *C. elegans* (Figure 5). The homologue of Cep192 in worms, namely SPD-2[Cep192, Spd-2], acts most upstream of the centriole duplication pathway and recruits the kinase ZYG-1[PLK4, Plk-4] to initiate centriole duplication in *C. elegans* (O'Connell *et al.*, 2001; Kemp *et al.*, 2004; Pelletier *et al.*, 2004). The coiled-coil protein SAS-6[hsSAS6, Sas-6] directly interacts with ZYG-1[PLK4, Plk-4], and is phosphorylated by the kinase (Kitagawa *et al.*, 2009; Lettman *et al.*, 2013). The SAS-5[STIL, Ana2]/SAS-6[hsSAS6, Sas-6] complex is thereby targeted to the centrosome (Lettman *et al.*, 2013), where it is required for central tube formation (Dammermann *et al.*, 2004; Delattre *et al.*, 2004; Leidel *et al.*, 2005). Next, the coiled-coil protein SAS-4[CPAP, Sas-4] is stably incorporated into the centriole wall and is required for the assembly of the singlet microtubules onto the newly forming centriole (Kirkham *et al.*, 2003; Leidel and Gönczy, 2003). SAS-7, a recently identified coiled-coil protein, is essential for the formation of the so-called paddle wheel structures at *C. elegans* centrioles (Chang *et al.*, 2016; Saurya *et al.*, 2016; Sugioka *et al.*, 2017). SAS-7 is a potential homologue of CEP295/Anastral spindle 1 (Ana1), which are required for centriole elongation in human and *D. melanogaster*, respectively. The protein recruits what will be referred to as the centriolar fraction of SPD-2[Cep192, Spd-2]. SPD-2[Cep192, Spd-2] has a dual function in centriole and PCM assembly (Sugioka *et al.*, 2017).

Figure 5: **The *C. elegans* centriole assembly pathway**. In *C. elegans* SPD-2[Cep192, Spd-2], ZYG-1[PLK4, Plk-4], SAS-5[STIL, Ana2] and SAS-6[hsSAS6, Sas-6] are required for cartwheel formation. Nine singlet microtubules are then arranged symmetrically around the cartwheel in a SAS-4[CPAP, Sas-4] dependent manner. SAS-7[Cep295, Ana1] is needed for paddlewheel assembly and the capability to template the formation of a new daughter centriole (O'Connell *et al.*, 2001; Kirkham *et al.*, 2003; Leidel and Gönczy, 2003; Delattre *et al.*, 2004; Kemp *et al.*, 2004; Pelletier *et al.*, 2004; Leidel *et al.*, 2005; Sugioka *et al.*, 2017).

1.3.3. Pericentriolar material (PCM) formation

The PCM facilitates the microtubule nucleation capacity of the centrosome. In interphase cells, a thin layer of PCM, from now on referred to as PCM core, assembles around centrioles. In flies, Plp organizes around centrioles in a nine-fold symmetry, and with its carboxy-terminus located at the outer centriole wall, it stretches outwards, spanning the interphase PCM core (Mennella *et al.*, 2012). Similar observations were made for its human homologue pericentrin (Lawo *et al.*, 2012). Moreover, Plp$^{\text{Pericentrin}}$ is required for the localization of several interphase PCM proteins in fly cells (Mennella *et al.*, 2012). To date, no worm homologue of pericentrin$^{\text{Plp}}$ has been identified. As mentioned previously, centrosome maturation is regulated by the PLK1$^{\text{Polo, PLK-1}}$ and Aurora A$^{\text{Aurora A, AIR-1}}$ kinases (V Joukov, Walter and De Nicolo, 2014). PLK1$^{\text{Polo, PLK-1}}$ phosphorylates pericentrin$^{\text{Plp}}$ in vertebrate cells, driving the recruitment of downstream PCM proteins (Lee and Rhee, 2011). Together with CDK5RAP2$^{\text{Cnn, SPD-5}}$, pericentrin$^{\text{Plp}}$ facilitates the recruitment of the γ-tubulin ring complexes (γ-TuRCs), which are required for the outgrowth of centrosomal microtubules (Zimmerman *et al.*, 2004; Fong *et al.*, 2008). Further, PLK1$^{\text{Polo, PLK-1}}$ phosphorylates the NIMA related kinase 9 (NEK9), which itself phosphorylates Neural precursor cell expressed developmentally down-regulated 1 (NEDD-1) (Sdelci *et al.*, 2012). The NEDD-1 mitotic phosphorylation is modulated by Cep192$^{\text{Spd-2, SPD-2}}$, and required for γ -TuRC recruitment (Gomez-Ferreria *et al.*, 2012). Cep192$^{\text{Spd-2, SPD-2}}$, CDK5RAP2$^{\text{Cnn, SPD-5}}$, and Pericentrin$^{\text{Plp}}$ can interact with the PLK1$^{\text{Polo, PLK-1}}$ or Aurora A$^{\text{Aurora A, AIR-1}}$ kinases, or both (Haren, Stearns and Lüders, 2009; Lee and Rhee, 2011; Vladimir Joukov, Walter and De Nicolo, 2014). Moreover, Cep192$^{\text{Spd-2, SPD-2}}$ activates Aurora A$^{\text{Aurora A, AIR-1}}$ kinase, thereby regulating the reciprocal activation of Aurora A$^{\text{Aurora A, AIR-1}}$ and PLK1$^{\text{Polo, PLK-1}}$ (Meng *et al.*, 2015).

In addition to the microtubule nucleation activity, PCM also functions to prevent premature splitting of centrioles. Pericentrin$^{\text{Plp}}$ and CDK5RAP2$^{\text{Cnn, SPD-5}}$ were shown to play an important role in centriole engagement and centrosome cohesion (Graser, Stierhof and Nigg, 2007; Barrera *et al.*, 2010; Lee and Rhee, 2012; Pagan *et al.*, 2015).

In *C. elegans* the conserved centrosome module, consisting of SPD-5$^{\text{CDK5RAP2, Cnn}}$, SPD-2$^{\text{Cep192, Spd-2}}$ (the PCM fraction), and PLK-1$^{\text{PLK1, Polo}}$, is required to form the PCM matrix (Figure 6, Hamill *et al.*, 2002; Kemp *et al.*, 2004; Pelletier *et al.*, 2004; Decker *et al.*, 2011; Woodruff *et al.*, 2014). SPD-5$^{\text{CDK5RAP2, Cnn}}$ is the main centrosome matrix protein in worms and has the potential to self-assemble into matrix-like structures *in vitro* (Woodruff *et al.*, 2015). The Polo kinase PLK-1$^{\text{PLK1, Polo}}$ phosphorylates SPD-5$^{\text{CDK5RAP2, Cnn}}$ upon mitotic entry

to trigger PCM expansion *in vivo* (Wueseke *et al.*, 2016). Moreover, the centrosomal protein SPD-2[Cep192, Spd-2] is needed for SPD-5[CDK5RAP2, Cnn] matrix expansion, and further, determines centrosome size (Kemp *et al.*, 2004; Pelletier *et al.*, 2004; Decker *et al.*, 2011). While SPD-5[CDK5RAP2, Cnn] was reported to not display cytoplasmic exchange in metaphase arrested embryos, as it is expected for a scaffold protein, SPD-2[Cep192, Spd-2] exchanges with the cytoplasmic pool, suggesting a more regulatory role of the protein (Laos, Cabral and Dammermann, 2015). *In vitro*, PLK-1[PLK1, Polo] and SPD-2[Cep192, Spd-2] accelerate SPD-5[CDK5RAP2, Cnn] self-assembly (Woodruff *et al.*, 2015). Examples for downstream PCM factors include the Aurora A kinase homologue Aurora/Ipl1 Related kinase (AIR-1), which localizes to the PCM and microtubules and is required for centrosome maturation and spindle assembly (Schumacher *et al.*, 1998; Hannak *et al.*, 2001), or the *C. elegans* γ-tubulin homologue tubulin gamma chain 1 (TBG-1). The gamma-tubulin interacting protein 1 and 2 (CeGrip-1/2[GCP3/2, Grip91/84]) are needed interdependently for the recruitment of TBG-1[TUBG1, Tub37C] to centrosomes (Hannak *et al.*, 2002). In TBG-1[TUBG1, Tub37C] and AIR-1[Aurora A, Aurora A] deficient embryos spindle formation is disrupted. The two asters of the spindle collapse after nuclear envelope breakdown (NEBD), leading to the formation of a monopolar spindle (Bobinnec, Fukuda and Nishida, 2000; Strome *et al.*, 2001; Hannak *et al.*, 2002). TBG-1[TUBG1, Tub37C] and AIR-1[Aurora A, Aurora A] can localize independently to centrosomes and play distinct roles in astral microtubule assembly. If both factors are downregulated simultaneously, astral microtubules are not forming. However, some microtubules are still nucleated at the center of the cell and in the cytoplasm (Motegi *et al.*, 2006). A similar phenotype is observed in SPD-5[CDK5RAP2, Cnn] deficient *C. elegans* embryos, where TBG-1[TUBG1, Tub37C] and AIR-1[Aurora A, Aurora A] fail to localize to centrosomes (Hamill *et al.*, 2002; Motegi *et al.*, 2006). TPX2-like protein 1 (TPXL-1), the homologue of Targeting Protein for Xenopus Klp2 (TPX2), localizes AIR-1[Aurora A, Aurora A] to spindle microtubules and also activates the kinase (Özlü *et al.*, 2005; Mangal *et al.*, 2018). This facilitates AIR-1[Aurora A, Aurora A] dependent phosphorylation of downstream substrates required for microtubule stability, since the mitotic spindle collapses in TPXL-1[TPX2, Tpx-2] deficient embryos, similar to the phenotype observed in the absence of AIR-1[Aurora A, Aurora A] (Özlü *et al.*, 2005). Target of AIR-1[Aurora A, Aurora A] phosphorylation might be the transforming acid coiled-coil-containing protein 1 (TAC-1), a homologue of the human and *D. melanogaster* TACC proteins. TAC-1[TACC1/2/3, TACC] forms a complex with the Xenopus microtubule-associated protein of 215 kDa (XMAP215) homologue Zygote-defective protein 9 (ZYG-9). The factors are interdependent for their localization and require TBG-1[TUBG1, Tub37C] and AIR-1[Aurora A, Aurora A] for their recruitment to the centrosome. The TAC-1[TACC1/2/3,

[TACC] and ZYG-9[XMAP215, Msps] complex is required for microtubule stabilization (Matthews *et al.*, 1998; Bot *et al.*, 2003; Srayko *et al.*, 2003; Bellanger *et al.*, 2007). Upstream of TPXL-1[TPX2, Tpx-2], the regulator of spindle assembly (RSA) protein phosphatase complex, which comprises RSA-1[PPP2R3C, CG4733] and RSA-2, is specifically required for microtubule outgrowth from centrosomes and spindle microtubule stability during mitosis. The RSA2 protein physically interacts with SPD-5[CDK5RAP2, Cnn] (Schlaitz *et al.*, 2007; Boxem *et al.*, 2008). The RSA complex facilitates proper targeting of TPXL-1[TPX2, Tpx-2] to centrosomes, and downregulates microtubule depolymerase Kinesin-like protein 7 (KLP-7[KIF2C, Klp10A]) (Schlaitz *et al.*, 2007). Mutations in either of the two subunits lead to reduced microtubule nucleation and the collapse of centrosomes into chromatin after NEBD in *C. elegans* one-cell embryos (Schlaitz *et al.*, 2007).

However, microtubule nucleation activity is not necessarily restricted to centrosomes. For example, during female meiosis, the meiotic spindle formation protein 1 and 2 (MEI-1[KATNA1/L1]/MEI-2) katanin complex assembles acentrosomal spindles (Clark-Maguire and Mains, 1994; Srayko *et al.*, 2000). Microtubules can nucleate from non-centrosomal MTOCs, including chromatin. However, in a mitotic environment, the chromatin-based pathways of microtubule nucleation are not effective enough to organize a robust bipolar spindle (Heald *et al.*, 1996; Hamill *et al.*, 2002; Srayko *et al.*, 2005; Hayward and Wakefield, 2014).

Figure 6: **The PCM assembly module in *C. elegans*.** A conserved module is required for centrosome assembly across species. In *C. elegans* SPD-5[CDK5RAP2, Cnn] and SPD-2[Cep192, Spd-2] have been reported to be interdependent for their localization to the PCM. SPD-5[CDK5RAP2, Cnn] is the PCM matrix protein, which is phosphorylated by PLK-1[PLK1, Polo] for PCM matrix expansion upon mitotic entry. Following PCM matrix establishment, downstream factors for microtubule nucleation and stabilization are recruited to the PCM (Hamill *et al.*, 2002; Pelletier *et al.*, 2004; Decker *et al.*, 2011; Wueseke *et al.*, 2016).

1.3.4. Cilia formation

Two subtypes of cilia exist - motile and immotile, or primary cilia. A cilium generally nucleates from a basal body, a centriole-derived structure. Cilia function comprises motility, generation of fluid flow, the sensation of environmental cues, and developmental signaling. As previously mentioned, sensory neurons are the only cell type with cilia in worms. In *C. elegans*, centrioles possess singlet microtubules in the early embryo. However, basal bodies display doublet microtubules in a subset of cells developing into sensory neurons by the time the embryo reaches the embryonic comma stage (Nechipurenko and Sengupta, 2017; Serwas *et al.*, 2017). Cilia are segmented in the ciliary base, the transition zone, the proximal, and the distal segment (Figure 7). As described for other organisms, the *C. elegans* transition zone is linked to the ciliary membrane by typical y-shaped microtubule-cilia membrane connectors (y-links) and also contains a central cylinder (Perkins *et al.*, 1986; Schouteden *et al.*, 2015; Serwas *et al.*, 2017). Moreover, there are outer doublet microtubules arranged in a nine-fold symmetry, which are the extended basal body microtubules, and inner singlet microtubules that vary in number. These microtubules elongate into the axoneme (Serwas *et al.*, 2017). In *C. elegans*, centrioles are required to initiate cilia outgrowth, but the structure degenerates rapidly thereafter (Serwas *et al.*, 2017). In the two-fold stage, basal bodies of amphid neurons have docked to the cell membrane at the side where the future cilium grows out. Transition zone structures start forming, and intraflagellar transport (IFT) proteins are recruited for the elongation of the cilium. At this time, the centriolar cartwheel is lost from the basal body (Serwas *et al.*, 2017). In these neurons, the transition zone is fully formed in the L1 larval stage, and basal bodies are fully degenerated (Serwas *et al.*, 2017). When the worm reaches the L4 larval stage, the elongation of the axoneme is completed (Serwas *et al.*, 2017). The cilia of *C. elegans* are considered as primary or sensory cilia according to their 9+0 structure and immobility (Bae and Barr, 2008). *C. elegans* is thus a valuable model system to study ciliopathies.
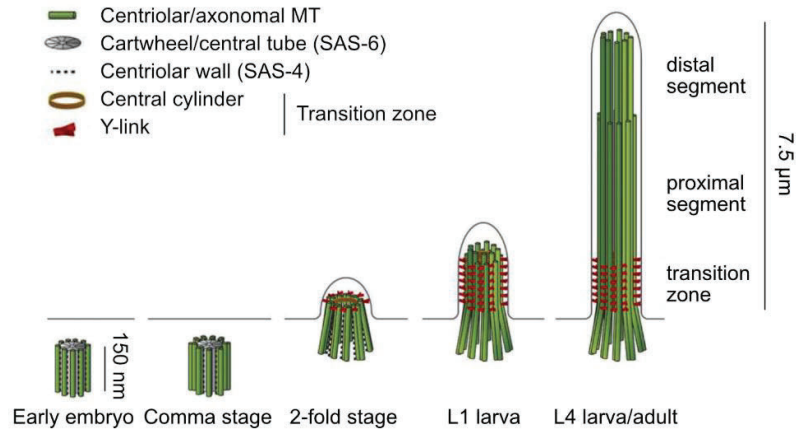
Figure 7: **Cilia formation in *C. elegans* amphid neurons**. Figure adapted from Serwas *et al.* (2017). In the early embryo, centrioles organize the mitotic spindle. Here, singlet microtubules are attached to centrioles in a 9-fold manner. In embryonic comma stage, in preparation for basal body conversion, centrioles can possess doublet microtubules. In ciliated neurons, basal bodies have docked to the cell membrane, and transition zone formation is initiated at the embryonic 2-fold stage. At this time, cartwheels are lost from the structure. In L1 larvae the transition zone is fully formed, and centrioles degenerated. By the L4 larval stage, also the axoneme is fully developed.

1.4. Aims of the study

The centrosome was discovered more than a hundred years ago. However, only in the late 20th century, when molecular studies became applicable, research lead to a deeper understanding of the function of the structure and its importance in human health and disease. Similarly, cilia, which were first described even earlier, in the 17th century, are now linked to several human conditions, referred to as ciliopathies. Despite the importance of the structures and significant discoveries in the field, many open questions remain.

C. elegans has proven itself as a powerful model system for the discovery of novel proteins and the dissection of their function. A limited set of factors, required for centriole and centrosome assembly, were identified in the worm. The *t3421* mutant allele was isolated in a genetic screen for temperature-sensitive embryonic mutants, conducted in the laboratory of R. Schnabel. At restrictive temperature, the allele shows defects that suggest aberrations in centrosome function. In this study, I aim to determine which gene is affected in the *t3421* mutant and to unveil its molecular function.

Centrosomes within a cell are of inherently different ages. In several systems, centrosomes can be inherited non-randomly in an age-dependent manner. Research suggests that this bias can have functional relevance, especially in the maintenance of a stem cell progenitor pool. The invariant cell lineage of *C. elegans* provides an excellent basis to study asymmetric centrosome inheritance. I aim to establish the IL1 sensory neuron lineage as a model to study asymmetric centrosome inheritance and its functional relevance. Therefore, I aim to develop a system in the worm to distinguish age-related centrosome function.

MATERIAL AND METHODS

MATERIAL AND METHODS

2.1. Worm maintenance and experimental protocols

All *C. elegans* strains were maintained on OP50 *Escherichia coli* (*E. coli*) seeded nematode growth media (NGM) plates at 15 or 20 °C as described by Brenner, 1974 (Brenner, 1974). The alleles used in this study are listed in Table 1. As wild-type strain, the N2 *C. elegans* wild isolate from Bristol was used. The *pcmd-1(t3421)* mutant strain, a kind gift from the laboratory of Professor Ralph Schnabel, was backcrossed into the wild-type. All strains homozygous for *pcmd-1(t3421)* were maintained at 15 °C. Unless stated otherwise, L4 stage homozygous mutant worms and appropriate controls were shifted to restrictive temperature (25 °C) for 16-20 h for experiments.

Table 1: **Alleles** used in this study are listed. Alleles are divided into (a) mutation alleles used in this study, (b) single copy insertion alleles generated for this study, (c) transgenes and extrachromosomal arrays used in this study.

(a)

Allele	affected gene	LG	Reference
t3421	*pcmd-1(c17d12.7)*	I	this study
syb975	*pcmd-1(c17d12.7)*	I	this study (SunyBiotech, http://www.sunybiotech.com/)
or293	*spd-2*	I	O'Rourke *et al.*, 2011
or213	*spd-5*	I	Hamill *et al.*, 2002
e907	*dpy-5*	I	Thacker *et al.*, 2006
n566	*lin-11*	I	Ferguson and Horvitz, 1985
m1	*unc-101*	I	Lee *et al.*, 1994
ed3	*unc-119*	III	Davis *et al.*, 2009
e1489	*him-8*	IV	Phillips *et al.*, 2005
q71	*fog-2*	V	Katju *et al.*, 2008

(b)

Allele	Transgene	LG	Plasmid	Reference
mikSi1	*psas-4:dendra2::sas-4:sas-4*	II	TMD29	this study
mikSi6	*pmai-2:gfp::pcmd-1:mai-2*	II	TMD49	this study
mikSi7	*pmai-2:gfp::pcmd-1(t3421):mai-2*	II	TMD51	this study
mikSi8	*pmai-2:pcmd-1(t3421)::gfp:mai-2*	II	TMD52	this study
mikSi9	*pmai-2:pcmd-1::gfp:mai-2*	II	TMD50	this study
mikSi3	*pagr-1:mkate2:unc-54*	IV	TMD41	this study
mikSi4	*pmex-5:mkate2::tac-1:unc54*	IV	TMD34	this study
mikSi5	*pmex-5:mkate2::pcmd-1(c17d12.7):tbb2*	IV	TMD48	this study
mikSi10	*psas-4:mkate2::sas-4:sas-4*	IV	TMD74	this study
syb370	*gfp::pcmd-1*	I	PHX370	this study (SunyBiotech)

(c)

Allele	Transgene	LG	Reference
transgenes			
itSi202	*pspd-2::gfp::spd-5+ unc-119(+)*	II	A. Dammermann
it18	*[plk-1::sgfp]::loxp*	III	CGC, Martino *et al.*, 2017
ttTi5605	Mos transposon insertion	II	Frøkjær-Jensen *et al.*, 2008
oxTi177	*pCFJ687 unc-18(+)*	IV	Frøkjær-Jensen *et al.*, 2014
bcSi1	*pmex-5:gfp::tac-1*	II	Chakraborty *et al.*, 2015
vieSiIs18	*psas-4:gfp::sas-4:sas-4*	II	A. Dammermann
itIs44	*ppie-1:mcherry::ph*	V	CGC
itIs69	*ppie-1:mcherry-TEV-Stag::spd-2*	IV	A. Dammermann
xnIs312	*ppar-6::par-6::mcherry + unc-119(+)*	--	Armenti *et al.* 2014
estSi121	*Pmex-5:tpxl-1::mNeonGreen:tbb-2*	III	Mangal *et al.*, 2018
kdIs66	*agr-1:gfp*	--	Hrus *et al.*, 2007
xnIs3	*ppar-6:par-6::gfp + unc-119(+)*	--	CGC
itIs38	*ppie-1:gfp::ph(plc1delta1) + unc-119(+)*	--	CGC
zuIs20	*pjn271:par-3::par-3::zf1::gfp+unc-119(+)*	--	gift from J. Nance

xnIs96	*pJN455(hmr-1p::hmr-1::GFP::unc-54 3'UTR) + unc-119(+)* --		CGC, Achilleos *et al.*, 2010
itIs64	*ppie-1:mcherry-TEV-Stag::sas-4*	--	A. Dammermann
itIs37	*ppie-1:mcherry::h2b:pie-1 + unc119(+)*	IV	CGC

extrachromosomal arrays

sEx15005	*prCesY111B2A.8:gfp + pCeh361*	--	McKay *et al.*, 2003

2.2.   Cloning and allele generation

All clonings were performed using the sequence and ligation independent cloning (SLIC) method (Jeong *et al.*, 2012). Plasmids were integrated into the genome as single-copies by employing the universal MosSCI integration method (Frøkjær-Jensen *et al.*, 2014) using germline microinjection as described by Mello *et al.* (1991) (Mello and Kramer, 1991).

2.2.1. Cloning and single-copy integration of the photo-convertible *dendra::sas-4* construct

To generate the TMD23 plasmid, the *sas-4* endogenous protein sequence was amplified from genomic DNA and cloned into the linearised standard pBluescript II KS(+) (pBSK II KS(+)) cloning vector using the TM168 and TM169 primers. The Dendra2 fluorophore coding sequence was then cloned into the plasmid in frame upstream of the *sas-4* coding sequence using the TM316, TM317, TM180, and TM178 primers to generate the TMD23b plasmid. The *dendra::sas-4* sequence was then subcloned into the pCFJ350 MosSCI vector containing the *sas-4* regulatory regions amplified from the DAM170 vector (a kind gift from A. Dammermann). The TM169, TM179, TM356, TM357 primers were used for this cloning step, generating the TMD29 plasmid. Subsequently, a single copy of the TMD29 plasmid was integrated into the *C. elegans* genome. The EG6699 [*ttTi5605; unc-119(ed3)*] strain was injected for targeted MosSCI integration on linkage group II (LGII) to create the *mikSi1* allele.

2.2.2. Cloning and single-copy integration of the *pcmd-1* constructs fused to *gfp*

The pBC1483 plasmid (a kind gift from B. Conradt) comprises the *gfp*::*h2b* coding sequence, flanked by the *mai-2* regulatory regions. The *h2b* coding region was deleted using the TM549 and TM550 primers, generating the TMD53 plasmid (Table 2, Table 3). The *pcmd-1* cDNA was then cloned into the TMD53 plasmid to create either an N-terminal (TMD49) or C-terminal (TMD50) *gfp* fusion construct by using the TM555-TM558 or the TM551-TM554 primers, respectively (Table 2, Table 3). With the TM559 and TM560 primers, the *pcmd-1(t3421)* single nucleotide exchange was introduced into the *pcmd-1*

coding region to generate the TMD51 and TMD52 constructs (Table 2, Table 3). Single-copies of the TMD49-TMD52 plasmids were integrated into the *C. elegans* genome. The EG6699 [*ttTi5605; unc-119(ed3)*] strain was injected for targeted MosSCI integration on LGII to create the *mikSi6*, *mikSi9*, *mikSi7* and *mikSi8* alleles (Table 1).

2.2.3. Cloning and single-copy integration of the *pcmd-1* construct fused to *mkate2* fluorophore

The *mkate2* fluorophore sequence (a kind gift from E. Zanin) and the *pcmd-1* cDNA coding sequence were cloned into the TMD19 plasmid, thereby deleting the *dendra::sas-4* sequence in TMD19, to generate the TMD47 plasmid (Table 2). The fluorophore and the *pcmd-1* coding region are separated by a small linker sequence. The EZ629, EZ632 (a kind gift of E. Zanin) and TM455-458 primers were used for the cloning step (Table 3). The fused *mkate2*::*pcmd-1* cDNA coding sequence, flanked by the *mex-5* 5'- and *tbb-2* 3'-UTRs was then sub-cloned into the pCFJ350 plasmid to generate the TMD48 plasmid. A single copy of the TMD48 plasmid was integrated into the *C. elegans* genome. The EG8081 [*unc-119(ed3); oxTi177*] strain was injected for targeted MosSCI integration on LGIV to create the *mikSi5* allele.

2.2.4. Single-copy insertions of the *mkate::h2b* and *mkate::tac-1* constructs

A single-copy insertion of the TMD34 plasmid was integrated into the *C. elegans* genome (Table 2). The EG8081 [*unc-119(ed3); oxTi177*] strain was injected for targeted MosSCI integration on LGIV to create the *mikSi4* allele (Table 1).

2.2.5. Cloning and single-copy insertion of the *mkate::sas-4* construct

The *mkate* fluorophore and the reencoded *sas-4* coding sequences amplified from the DAM170 plasmid (gift from A. Dammermann) were cloned into the pBSK II KS(+) vector to generate the TMD55 plasmid (Table 2). The TM169, TM378-381, and TM512 primers were used for this cloning (Table 3). The *mkate* and *sas-4*$_{reenc}$ coding sequences are separated by a

liker sequence also present in the DAM170 plasmid. The *mkate* and part of the *sas-4*$_{reenc}$ coding sequence was subcloned into the DAM170 plasmid, thereby exchanging the GFP fluorophore, to create the TMD74 plasmid (Table 2). The TM172, TM173, TM362 and TM363 primers were used for this cloning step (Table 3). A single copy of the TMD74 plasmid was integrated into the *C. elegans* genome. The EG6699 [*ttTi5605; unc-119(ed3)*] strain was injected for targeted MosSCI integration on LGII to create the *mikSi10* allele (Table 1).

2.2.6. Cloning and single-copy integration of the *pagr-1:mkate2* construct

The *agr-1* promoter was amplified from wild-type genomic DNA and cloned, together with the *mkate2* fluorophore coding sequence and the *unc54* 3'-UTR, into the pCFJ350 vector. The TM322, TM323, TM350, TM351, TM354, TM355, TM366 and TM367 primers were used for this 4-piece assembly cloning step, generating the TMD28 plasmid (Table2, Table 3). A single-copy of the TMD28 plasmid was integrated into the *C. elegans* genome. The EG8081 [*unc-119(ed3); oxTi177*] strain was injected for targeted MosSCI integration on LGIV to create the *mikSi3* allele (Table 1).

Table 2: **Plasmids** used in this study are listed. (a) TMD plasmids generated for this study. (b) other TMD plasmids. (c) External plasmids.

Name	Description	Backbone	Map
(a)			
TMD23	*sas-4*$_{endog}$	pBSK II KS(+)	
TMD23b	*dendra2:: sas-4*$_{endog}$	pBSK II KS(+)	
TMD28	*pagr-1:mkate2*	pCFJ350	pm28
TMD29	*psas-4:dendra2::sas-4*$_{endog.}$*:sas-4*	pCFJ350	pm29
TMD47	*mkate2::linker::pcmd-1*	pBSK II KS(+)	
TMD48*	*pmex-5:mkate2::linker::pcmd-1:tbb2*	pCFJ350	pm48
TMD49	*pmai-2:gfp::pcmd-1:mai-2*	pCFJ350	pm49
TMD50	*pmai-2:pcmd-1::gfp:mai-2*	pCFJ350	pm50

TMD51	*pmai-2:gfp::pcmd-1(t3421):mai-2*	pCFJ350	pm51
TMD52	*pmai-2:pcmd-1(t3421)::gfp:mai-2*	pCFJ350	pm52
TMD53	*pmai-2:gfp:mai-2*	pCFJ350	
TMD55	*mkate2::link::sas-4$_{reenc}$*	pBSK II KS(+)	

* plasmid TMD48 was cloned together with Robert Wiesheu.

(b)

TMD19[§]	*mex-5:dendra2::sas-4$_{cDNA}$:: tbb2*	pBSK II KS(+)	
TMD34[$]	*pmex-5:mkate2::tac-1:tbb2*	pCFJ350	pm34
TMD74[&]	*psas-4:mkate2::linker::sas-4$_{reenc}$:sas-4*	pCFJ350	pm74

[§] Cloned by Tsotne Chitiashvili, [$] cloned by Eman Abu Khmail, [&] cloned by Lisa Stenzel and Mariam Museridze

(c)

| DAM170 | *psas-4:gfp::sas-4$_{reenc}$:sas-4* | pCFJ151 |
| pBC1483 | *pmai-2:gfp::h2b:mai-2* | pCFJ350 |

Table 3: **Primers** used for the clonings are listed. Primers are divided into (a) designed for this study and (b) received from external resources.

Name	Primer sequence

(a)

TM168	CCTTCAGATGGCTTCCGATGAAAATATCGG
TM169	GGGGTTGGAATTTCTCATTTTTTCCACTGG
TM172	CATTTTTATACTTTAAAGCATCATCAGACAA
TM173	GATGCTTTAAAGTATAAAAATGCAGCTGCCG
TM178	GTCAAGCATGGATGGCTTCCGATGAAAATAT
TM179	AAAAATGAGAAATTCCAACCCCTTTATTTTAACTTGTGG
TM180	TCGGAAGCCATCCATGCTTGACTTGGTAGAG
TM316	GTGGCCTTCAGATGAACCTTATTAAGGAAGA
TM317	ATAAGGTTCATCTGAAGGCCACTAGTTCTAG
TM322	CCGTACGTCTCCTTAAGAAGATACCGTTTTT

TM323   ATCTTCTTAAGGAGACGTACGGTGCGCGCGA

TM350   TGAGACTTCACATGTCCGAGCTCATCAAGGA

TM351   AGCTCGGACATGTGAAGTCTCATGTCGACAT

TM_354   ATAACTGTTTGGAGGAATTCCTGCAGGATAT

TM_355   AGGAATTCCTCCAAACAGTTATGTTTGGTAT

TM_356   TCAGCCTTCAGATGAACCTTATTAAGGAAGA

TM_357   ATAAGGTTCATCTGAAGGCTGAAAAGGTTTT

TM362   TCAGCCTTCAGATGTCCGAGCTCATCAAGGAG

TM363   AGCTCGGACATCTGAAGGCTGAAAAGGTTTT

TM366   TCGGACACCGTTAGCTGTATGTTTCGAATGATAC

TM367   GAAACATACAGCTAACGGTGTCCGAGCTTGGATG

TM378   GTGGCCTTCAGATGTCCGAGCTCATCAAGGA

TM379   AGCTCGGACATCTGAAGGCCACTAGTTCTAG

TM380   TCCCCCGGGCAACGGTGTCCGAGCTTGGATG

TM381   TCGGACACCGTTGCCCGGGGGATCGGTGGAG

TM455   GTGGAGGTACTGAGGTGGAATACGACGAGGGA

TM456   GGATCTTGCATTTAGTCTTTAAAAAGTGCAT

TM457   TTAAAGACTAAATGCAAGATCCTTTCAAGCA

TM458   TATTCCACCTCAGTACCTCCACCTCCACGGT

TM512   GGAAAAAATGAGAAATTCCAACCCCATCAAG

TM549   AACTATACAAATAATTTGCAGTACAAGAACGCG

TM550   ACTGCAAATTATTTGTATAGTTCATCCATGCC

TM551   CAATTTTCAGAATGGAGGTGGAATACGACGAG

TM552   TCCACCTCCATTCTGAAAATTGAGTGAATTAG

TM553   AAAGACGGAGGTGGAGGTACTAGTAAAGGAGAAGAACTTTTCACTGG

TM554   TTTACTAGTACCTCCACCTCCGTCTTTAAAAAGTGCATTATGAATAA

TM555   AAAGGAGGTGGAGGTACTGAGGTGGAATACGACGAGGG

TM556   CTCAGTACCTCCACCTCCTTTGTATAGTTCATCCATGCC

TM557   CTTTTTAAAGACTAATTTGCAGTACAAGAACGCG

TM558   ACTGCAAATTAGTCTTTAAAAAGTGCATTATGAAT

TM559   ATTTATGTTAGATTTCGCCGAAAAAGAGCGA

TM560   TTCGGCGAAATCTAACATAAATCCAGTCTTTG

(b)

EZ629   TCAGACAGAGAATGTCCGAGCTCATCAAGGAG

EZ632   AGCTCGGACATTCTCTGTCTGAAACATTCAATTG

2.3. Mapping, rescue experiments, and homology analysis

2.3.1. Mapping the *t3421* allele

To identify the mutation underlying the *t3421* mutant phenotype, the strain, originally received from the laboratory of Professor Ralph Schnabel, was backcrossed to the N2 wild-type strain twice and sent to the *C. elegans* Knockout Facility in Vancouver B.C. Canada for whole-genome sequencing (WGS). Subsequently, SNP mapping was performed as described in (Wicks *et al.*, 2001). The CB4856 *C. elegans* wild isolate from Hawaii was used for further backcrossing of the *pcmd-1(t3421)* mutant in the course of SNP mapping. Further, a strain carrying the visual markers *lin-11(n566)* and *unc-101(m1)* was generated to define a narrow mapping region carrying contemplable mutations (Figure 10A). The SNP mapping was performed by M. Osepashvili and T. Mikeladze-Dvali. The *lin-11(n566)* and *unc-101(m1)* visual markers were crossed to the *pcmd-1(t3421)* mutant with T. Mikeladze-Dvali.

2.3.2. Rescue experiments

To determine whether the *t3421* mutant phenotype is caused by a mutation in a protein coding gene within the mapped region between the *lin-11(n566)* and *unc-101(m1)* visual markers, rescue experiments of embryonic lethality were performed. Since the *pcmd-1* (*c17d12.7*) gene was the most promising candidate, the *mikSi5 [pmex-5:mkate2::pcmd-1:tbb2]* allele was generated. Details on the cloning and strain generation are described above. The resulting strain was crossed to the *pcmd-1(t3421)* mutant. The strain, homozygous for the *pcmd-1(t3421)* mutation and homozygous for *mikSi5 [pmex-5:mkate2::pcmd-1:tbb2]*, was tested for embryonic lethality at restrictive temperature (25 °C, parental animals shifted at L4 stage). Furthermore, additional alleles, *mikSi6 [pmai-2:gfp::pcmd-1:mai-2]*, *mikSi7 [pmai-2:gfp::pcmd-1(t3421):mai-2]*, *mikSi9 [pmai-2:pcmd-1::gfp:mai-2]* and *mikSi8 [pmai-2:pcmd-1(t3421)::gfp:mai-2]*, were cloned and integrated into the genome as described above. The resulting strains were crossed to the *pcmd-1(t3421)* mutant. The strains, homozygous for the *pcmd-1(t3421)* mutation and homozygous for *mikSi6 [pmai-2:gfp::pcmd-1:mai-2]*, *mikSi7 [pmai-2:gfp::pcmd-1(t3421):mai-2]*, *mikSi9 [pmai-2:pcmd-1::gfp:mai-2]* or *mikSi8 [pmai-2:pcmd-1(t3421)::gfp:mai-2]* allele, were tested for embryonic lethality at restrictive temperature (25 °C, parental animals shifted at L4 stage).

2.3.3. PCMD-1 homology analysis across species

To determine homologous proteins in other species, a sequence similarity search was performed using the NCBI BLAST alignment tool (Table 9). The default parameters were applied. The protein sequences for the homologous proteins found in *C. japonica* (CJA08956), *C. brenneri* (CBN02262), *C. briggsae* (CBG15805) and *C. remanei* (CRE04201) were downloaded from *WormBase* (WS268) and aligned against the *C. elegans* (PCMD-1/C17D12.7) protein sequence using the multiple sequence alignment tool MUSCLE (Table 9). The default parameters were applied.

2.4. RNA mediated interference (RNAi)

2.4.1. RNAi protocol by feeding

For RNAi against *spd-5* or *spd-2*, parental worms were fed with bacteria containing the respective RNAi clones at the L4 stage (Table 4, Table 5). Worms were allowed to feed for 16 to 20 hours at 25 °C. Progeny was scored when the desired age was reached.

For mild RNAi against *plk-1*, parental worms were fed with bacteria containing the respective RNAi clone at the L4 stage (Table 4, Table 5). Worms were allowed to feed for 24 hours at 20 °C.

Table 4: **RNAi experimental protocols**

Gene	Age	Temperature	Duration	Comments
spd-5	L4	25 °C	16-20 h	
spd-2	L4	25 °C	16-20 h	
plk-1	L4	20 °C	24 h	mild *plk-1*(RNAi) phenotype

Table 5: **RNAi clones** used in this study are listed.

Gene	RNAi clone	Reference
mock	L4440	(Kamath and Ahringer, 2003)
spd-5	I-4O08	(Kamath and Ahringer, 2003)
spd-2	I-2G08	(Kamath and Ahringer, 2003)
plk-1	III-4E08	(Kamath and Ahringer, 2003)

2.5. Worm dissection, preparation for immunostainings and life-cell imaging

L4 larvae were grown at 25 °C overnight to adulthood. The next day, worms were dissected to collect embryos shortly after fertilization in H_2O on a coverslip (Carl Roth GmbH; 18 x 18 mm, #1 thickness; Cat. no. 0657.2). Embryos were reversely mounted on a 4 % agarose pad on a microscope slide. If embryos were imaged live at later developmental stages, one-cell embryos were mouth pipetted onto 4 % agar pads and covered with coverslips. The slides were then kept in a petri-dish in a 20 °C incubator until the developmental stage was reached. The duration of this incubation was previously determined by lineaging (see below).

2.6. Fluorescence immunostainings, microscopy and biochemical analysis

2.6.1. Fluorescence immunostainings

Microscope slides were coated with poly-D-lysine (1 mg/ml) and allowed to polymerize on a hot heating plate. 10 - 20 worms were dissected as previously described and the cooled poly-D-lysine coated slide was placed upside-down onto the glass coverslip, thereby enclosing the embryos. The slide was immediately put onto a metal block, pre-cooled on dry ice, for at least 2 min. By using a sharp razor blade, the coverslips were flicked off the microscopy slide to crack open the eggshells. Slides were then immediately fixed in -20°C methanol (100%) for 2-20 min. Slides were then washed two times in PBS for 5 min. Slides were blocked in 2% BSA for 15 - 20 min followed by a 5 min wash in PBT and 5 min in PBS. Slides were removed one after the other to remove access PBS using tissue. A ~18 mm^2 square of PBS was left where embryos were located. 50 µl of the primary antibody solution was pipetted onto the embryos. The slides were placed into a humid chamber and incubated at 4 °C overnight.

The next day slides were washed again for 5 min in PBT and 5 min in PBS. Access PBS was removed as previously described. 50 µl of the secondary antibody dilution, also containing Hoechst (1 mg/ml, Hoechst 33258, Sigma) to visualize DNA, were pipetted onto the embryos. The slides were incubated for 90 min at room temperature. Subsequently, the slides were washed in PBT for 5 min and PBS for at least 5 min. Slides were then removed separately from PBS to remove access PBS as previously described. 6 µl of mounting medium was placed on an 18 mm^2 coverslip, and the microscope slide was placed upside-down onto the glass coverslip enclosing the embryos. After 10-20 min of drying, transparent nail polish was used for sealing the gap between microscope slide and coverslip. Microscopy slides were kept in a microscope slide box at 4 °C until imaging. The dilutions used for primary and secondary antibodies and further information can be found in Table 6 and Table 7.

2.6.2. Microscopy

2.6.2.1. 4D microscopy

Embryos were dissected as previously described. For the images in Figure 9A and B, Figure 11A-E, Figure 12C, Figure 18A and B, and Figure 19A and B embryos were imaged shortly after fertilization until completion of the first or second cell cycle. For the images in Figure 11B, C, E and H, and Figure 22A and B, adult worms were picked and imaged. To determine the temporal development of the IL1 neuron lineage, embryos were imaged from shortly after fertilization or the first cell division on and allowed to develop overnight until hatching. For the images in Figure 26B and C, embryos were allowed to grow until reaching the stage of interest. In the meanwhile, DIC images were taken. Fluorescent images were only taken after photo-conversion using UV light. Images were taken using a Zeiss Axio Imager.M2 equipped with epifluorescence and the Time to Live software from Caenotec. DIC Z-stacks were taken every 35 sec at 20 °C or 25 °C unless indicated otherwise. Fluorescent scans were taken as required. The Simi BioCell software was used for the lineage analysis (Simi Reality Motion Systems GmbH; http://www.simi.com).

2.6.2.2. Confocal microscopy

For the images in Figure 27A, C, D and E embryos were dissected as previously described, and embryos in the stage of interest were imaged subsequently. For the images in Figure 14A-D, Figure 25 and Figure 27F embryos were immunostained as described previously and embryos in the stage of interest were imaged subsequently. Embryos were imaged using a laser scanning confocal TCS SP5 microscope (Leica) with a 63× 1.4-NA Plan-Apochromat oil immersion objective and 405, 488 and 594 nm lasers. The microscope was controlled by the Leica Application Suite Software 2.7.2.

2.6.2.3. Spinning disc confocal microscopy

For the images in Figure 11G, Figure 12A, Figure 13A and B, Figure 15A-D, Figure 16A, Figure 17A-D and Figure 20A-F embryos were imaged shortly after fertilization until

completion of the first or second cell cycle using an eclipse Ti spinning disk confocal (Nikon), controlled by the NIS Elements 4.51 program and equipped with a 100x 1.45-NA Plan-Apochromat oil immersion objective and an Andor DU-888 X-11056 camera (1024 x 1024 pixels). Z-stack were taken every 30 sec at 25 °C. For the images in Figure 24B and D, and Figure 27B, the embryos were allowed to develop at 20 °C for a lineage-specific time frame (previously determined by lineaging) until shortly before the cells of interest were born. The embryos were imaged subsequently at an UltraVIEW VoX spinning disk confocal microscope (Perki- nElmer), which is controlled by Volocity 6.1.1. software (PerkinElmer) and attached to an Axio Observer D1 stand (Zeiss) that was equipped with a 63× 1.4-NA Plan-Apochromat oil immersion objective (Zeiss), EMC CD C9100-50 camera (Hamamatsu), and 488- and 561-nm lasers.

2.6.3. Fluorescence intensity measurements

The Fiji-implemented tool TrackMate was used to measure centrosome and centriole fluorescence intensity in Figure 12B, Figure 15B and C, and Figure 21B (Tinevez *et al.*, 2017). 3D volumes of centrioles and centrosomes were measured in acquired Z-stacks using a 1.001 (PCMD-1), 1.021 (PLK-1) or 2.491 (SPD-5) µm radius. Two background measurements were taken for each, the embryo (embryo background, EB) and the surrounding embryo area (background, B). When low fluorescence intensity prevented automatic recognition of the structures, and for background measurements, manual tracking was applied. The mean background (B) total intensity values were subtracted from the mean embryo background (EB) total values, as well as the individual (anterior (C_a) and posterior (C_p)) total intensity values of the centrioles/centrosomes (C). The resulting mean embryo background (EB-B) was then subtracted from the resulting centriole/centrosome values (C - B). The measurements were summed up to total measurement for each embryo per time point and plotted using Prism. Formula: $((C_a - B) - (EB - B)) + ((C_p - B) - (EB - B))$. Also see Figure 16B.

2.6.4. Western blot analysis

For western blots, a 0.75 mm or 1 mm thick resolving gel containing 7.5 % to 15 % acrylamide was poured. After polymerization, the stacking gel was added. Gels were kept at 4 °C overnight to polymerize fully. The next day the western blot system was mounted, and a PVDF membrane was activated in Ethanol (100 %). Worm lysate samples were allowed to migrate for ~1 hour in running buffer containing 0.1 % SDS. After migration, the membranes were washed in TBST (TBS+0.1 % tween 20) two times for 10 min. Membranes were blocked with TBST containing 5 % milk for 1 hour at 4 °C. After that, the primary antibody, appropriately diluted in TBST containing 5 % milk, was added and incubated overnight at 4 °C (Table 8). The day after the membrane was washed with TBST three times for 10 min at room temperature. The secondary antibody, appropriately diluted in TBST containing 5 % milk, was applied and incubated for 45 min at room temperature (Table 8). The membranes were then washed in TBST three times for 10 min and once in TBS for 10 min at room temperature. For developing the western blot, the Amersham ECL Prime Western Blotting Detection Reagent (GE Healthcare) kit was used. A ChemiDoc XRS+ imaging system from Bio-Rad was used for detection.

2.6.5. Antibodies

Table 6: **Primary antibodies**; Antigen, source, catalogue numbers, manufacturers, and working dilutions are listed.

Antigen	Cat#	Obtained from/provided by	Derived from	Dilution
SAS-4	sc-98949	Santa Cruz Biotechnology	rabbit	1:500
SPD-5	--	gift from B. Bowerman (Hamill *et al.*, 2002)	rabbit	1:5000
GFP	ab290	Abcam	rabbit	1:500
PCMD-1	--	this study	rabbit	1:50
GFP	11814460001	Roche	mouse	1:500
α-tub	T6199 (DM1a) Sigma		mouse	1:500
IFA	--	gift from P. Gönczy (Leung, Hermann and Priess, 1999)	mouse	1:50

PAR-3	P4A1	DSHB	mouse	1:500
		(Nance *et al.*, 2003)		

Table 7: **Secondary antibodies**; Antigen, source, catalogue numbers, manufacturers, and working dilutions are listed.

Antigen/derived from	cat#	obtained from	dilution
goat anti-mouse Alexa 488	A110011	Invitrogen	1:500
goat anti- rabbit Alexa 568	A11011	Invitrogen	1:500

Table 8: **Western blot antibodies**; Antigen, catalogue numbers, manufacturers, source, and working dilutions are listed. Antibodies are divided in (a) primary and (b) secondary antibodies

Antigen	Cat#	Obtained from/provided by	Derived from	Dilution
(a)				
α-Tub	T6199	Sigma-Aldrich	mouse	1:7500
GFP	11814460001	Sigma-Aldrich	mouse	1:500
(b)				
anti-mouse HRP-conj.	1706516	Bio-Rad Laboratories	goat	1:7500

2.6.5.1. PCMD-1 antibody generation

The PCMD-1 antibody was generated by the injection of the peptides DEGFDSSSLKNNPASLQRD and EKSEIRSEKHKNKCKSADLDA into a rabbit by standard protocols of Davids Biotechnologie GmbH (Germany).

2.7. Statistics

Details about the statistical analyses can be found in the text of the results part and the figure legends. Briefly, n represents the number of embryos imaged to determine phenotypes of wild-type and mutant embryos in the first and second cell cycle (Figures 9C-E), the total number of embryos counted for survival assays (Figures 8A and B, Figure 10D, Table 10, Table 11 and Table 13), the number of centrioles used to determine GFP::PCMD-1 and GFP::SAS-4 intensity at centrosomes (Figures 12B), the number of embryos used to determine TPXL-1::mNG at centrosomes (Figure 13B), the number of embryos imaged to determine centriole number per embryo using SAS-4 as a readout (Figure 14E), the number of SAS-4 foci used to determine microtubule nucleation capacity (Figure 14F), the number of microtubule asters associated with SAS-4 foci (Figure 14G), the number of embryos measured to determine GFP::SPD-5 intensities at centrosomes (Figures 15E and F), the number of embryos used to categorize variability of SPD-5 recruitment to centrosomes in *pcmd-1(t3421)* mutants (Figure 16C), the number of embryos used to determine the presence of SPD-5 at centrosomes (Figures 17E, Figure 18C), the number of embryos used to determine the presence of PLK-1::sGFP at centrosomes (Figure 21A), the number of embryos used to determine PLK-1::sGFP intensities at centrosomes (Figure 21B). In quantifications the mean values ± the standard deviations (SD) (Figures 8B, 15E, and Table 11) or mean values ± standard error (SEM) (Figures 8A, 10D, 12B, 15F, 21B, Table 10 and Table 13) are stated. An unpaired t-test with Welch's correction was performed to determine significant differences in centrosomal GFP::SPD-5 intensities at metaphase between control and *pcmd-1(t3421)* mutant embryos (Figure 12B, 15F). To test whether the data met the assumptions of our statistical approach an F-test was performed to compare variances. A one-way ANOVA and Sidak's multiple comparisons test were performed to determine significant differences in centrosomal PLK-1::sGFP intensity levels (Figure 21B). To test whether the data met the assumptions of our statistical approach a Shapiro-Wilk test of normality and BrownForsythe test for homogeneity of variances were performed. Differences are reported as significant when the p-value is < 0.05. Significance levels: ≥ 0.05 = not significant (ns); 0.01 to 0.05 = significant (*); 0.001 to 0.01 = very significant (***); < 0.0001 = very significant (****).

2.8. Software

Table 9: **Software** used in this study

Software	Website	Reference
Fiji	https://fiji.sc/	Schindelin *et al.* 2012
TrackMate	https://imagej.net/TrackMate	Tinevez *et al.*, 2017
Prism 7.04	https://www.graphpad.com/scientific-software/prism/	
MUSCLE	https://www.ebi.ac.uk/Tools/msa/muscle/	Chojnacki *et al.*, 2017
NCBI BLAST	https://www.ebi.ac.uk/Tools/sss/ncbiblast/	Johnson *et al.*, 2008
SMART	http://smart.embl-heidelberg.de/	Schultz *et al.*, 2000

RESULTS

RESULTS

3.1. The previously uncharacterized protein PCMD-1 is required for PCM matrix formation in *C. elegans*

C. elegans is a powerful model system for genetic screenings and the characterization of protein function. The present study describes the molecular function of a previously uncharacterized protein, PCMD-1 (C17D12.7), which is required for bipolar spindle formation. The protein was discovered through the isolation of the *t3421* allele in an EMS mutagenesis screen for temperature-sensitive embryonic lethal mutations (Memar, N. and Schnabel, R., *unpublished data*). The *t3421* allele was chosen for characterization due to its interesting phenotype, forming a monopolar and tripolar spindle in the first and second cell cycle, respectively. The aberrations in spindle formation suggested potential deregulation of centrosome assembly, or function, or both.

3.1.1. PCMD-1 is required for bipolar spindle formation in *C. elegans*

Worms homozygous for the *t3421* mutant allele can survive and reproduce at a permissive temperature of 15 °C (38 % survival, Figure 8A, Table 10; experiment by M. Osepashvili, Erpf *et al*., 2019). However, mutants develop into sterile adults when shifted to a restrictive temperature of 25 °C at early developmental stages (L1-L2 stage, personal communication with T. Mikeladze-Dvali). Similarly, in RNAi experiments against *pcmd-1,* ~50 % of the worms are sterile if exposed to RNAi by feeding for two generations (data not shown). RNAi by injection reduced embryonic viability to 17 % after 39 h at 25 °C (experiment by Lisa Stenzel, Erpf *et al.*, 2019). When *t3421* mutant worms are shifted to restrictive temperature in a later developmental stage (L4 stage) they can produce eggs. However, 100 % of the offspring is embryonic lethal (0 % survival, Figure 8A, Table 10; experiment by M. Osepashvili, Erpf *et al.*, 2019). The F1 generation, derived from parental worms heterozygous for the *t3421* allele, displays ~25 % embryonic lethality at 25 °C, suggesting that *t3421* is a recessive allele (data not shown).

To determine whether the *t3421* mutant effect is maternally or paternally contributed, mating experiments were performed, and embryonic survival of the F1 generation was monitored. Parental worms were maintained at restrictive temperature before mating. *Plg-1(e2001)* males leave a gelatinous blob over the vulva after copulation, which allows the identification of mated hermaphrodites (Hodgkin and Doniach, 1997). The *plg-1(e2001)* males were used in crosses testing the maternal contribution of the *t3421* allele. *Fog-2(q71)* hermaphrodites display feminization of the germline and cannot self-reproduce (Batista *et al.*, 2008). The *fog-2(e2001)* allele was used in crosses testing the paternal contribution of the *t3421* allele. Control matings produced viable offspring with a regular survival rate of 96 % for wild-type hermaphrodites crossed to *plg-1(e2001)* males (n=240, Figure 8B, Table 11) and 91 % for *fog-2(q71)* females crossed to *fog-2(q71)* males (n=359, Figure 8B, Table 11). To test for maternal contribution, homozygous *t3421* mutant hermaphrodites were mated with *plg-1(e2001)* males. The F1 generation displayed only 2 % embryonic viability (n=777, Figure 8B, Table 11). Matings of *fog-2(e2001)* hermaphrodites to *t3421* mutant males, which were performed to test for paternal contribution, showed a less severe impact on viability with 73 % embryonic survival of the F1 generation (n=627, Figure 8B, Table 11). The results suggest a predominantly maternal contribution to the *t3421* mutant phenotype (Mating experiments were performed together with T. Mikeladze-Dvali, Erpf *et al.*, 2019).
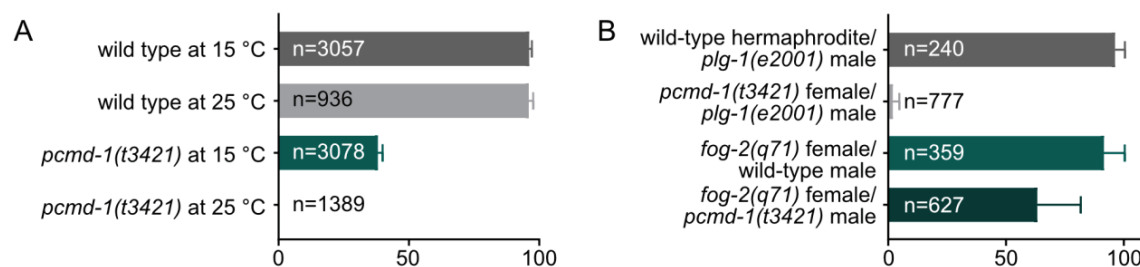
Figure 8: **Temperature sensitivity and parental contribution of the *t3421* mutant allele**. Embryonic viability of wild-type and *t3421* mutant offspring. (A) Embryonic viability of wild-type and *pcmd-1(t3421)* mutant embryos at permissive (15 °C) and restrictive (25 °C) temperature. The graph shows the mean embryonic survival rates ± SEM per worm in percent. The number of n states embryos counted in total. This experiment was performed by M. Osepashvili, Erpf *et al.,* 2019; See also Table 10. (B) Maternal and paternal contribution experiments. Embryonic viability of offspring deriving from control matings, *pcmd-1(t3421)* hermaphrodite and *plg-1(e2001)* male mating and *pcmd-1(t3421)* male and *fog-2(q71)* female

mating at restrictive (25 °C) temperature. The number of n's states embryos counted in total. This experiment was performed together with T. Mikeladze-Dvali; See also Table 11.

Table 10: **Embryonic viability** of wild-type, *pcmd-1(t3421),* and *pcmd-1(syb975)* mutant embryos at permissive (15 °C) and restrictive (25 °C) temperature. The number of n states embryos counted in total. This experiment was performed by M. Osepashvili, Erpf *et al.,* 2019.

Genotype	Temperature	Embryonic viability (in % ± SEM)	
wild type	15°C	96.1 ± 1.1	(n=3057)
pcmd-1(t3421)	15°C	38.0 ± 1.9	(n=3078)
pcmd-1(syb975)	15°C	23.9 ± 1.7	(n=3150)
wild type	25°C	95.9 ± 1.8	(n= 936)
pcmd-1(t3421)	25°C	0.0 ± 0.2	(n=1389)
pcmd-1(syb975)	25°C	0.0 ± 0.0	(n=5560)

Table 11: **Maternal and paternal contribution** to the compromised viability in *t3421* mutants determined by control, *pcmd-1(t3421)* hermaphrodite/*plg-1(e2001)* male and *pcmd-1(t3421)* male/*fog-2(q71)* female matings at restrictive (25 °C) temperature. The number of n states embryos counted in total. This experiment was performed together with T. Mikeladze-Dvali.

Genotype	Temperature	Embryonic viability (in % ± SD)	
wild-type hermaphrodite/*plg-1(e2001)* males	25°C	96.2 ± 4.3	(n= 240)
pcmd-1(t3421) female/*plg-1(e2001)* males	25°C	1.9 ± 2.9	(n= 777)
fog-2(q71)/wild-type male	25°C	91.5 ± 8.9	(n= 359)
fog-2(q71)/*pcmd-1(t3421)* male	25°C	73.2 ± 18.5	(n= 627)

In wild-type embryos, the centrioles are associated with the male pronucleus after fertilization. After their separation, they nucleate microtubules that capture the female pronucleus, and the parental pronuclei start migrating towards each other (Gönczy *et al.*, 1999). In wild-type embryos, the pronuclei meet shortly before the pronuclear envelope

breaks down (PNEB) (n=10, Figure 9A, PNEB, Figure 9C). However, in 50 % of the *t3421* mutant embryos the pronuclei do not meet before PNEB (n=12, Figure 9B, PNEB, Figure 9C).

After PNEB, a bipolar spindle is formed in the wild type (n=10, Figure 9A, metaphase I, Figure 9D). Invariantly between embryos, the following asymmetric cell division then gives rise to a larger anterior and a smaller posterior cell. At restrictive temperature, *t3421* mutants frequently develop a monopolar spindle during metaphase of the first cell division (Figure 9B, metaphase I). The failure of bipolar spindle formation was monitored in 58 % of the embryos (n=12, Figure 9D). The remaining 42 % of the embryos do form bipolar spindles to some degree (Figure 9D). However, in these embryos, the asymmetry of the first cell division, which is typically seen in *C. elegans* wild-type embryos, was lost.

During the second cell division of wild-type embryos the spindles of the anterior and posterior cells are bipolar and oriented perpendicular to one another in metaphase (n=10, Figure 9A, metaphase II; note here that the posterior cell of wild-type *C. elegans* embryos reaches metaphase later than the anterior cell). In *t3421* mutant embryos, 16.7 % of embryos formed a bipolar spindle, 16.7 % a tripolar spindle, and 16.7 % a quadripolar polar spindle (n=12, Figure 9B, metaphase II - tripolar spindle formation, Figure 9E). Each of these embryos underwent monopolar spindle formation in the first cell cycle. Embryos that underwent bipolar cell division in the first cell cycle formed various other phenotypes in the second cell cycle that are not explained here in detail (Figure 9E).
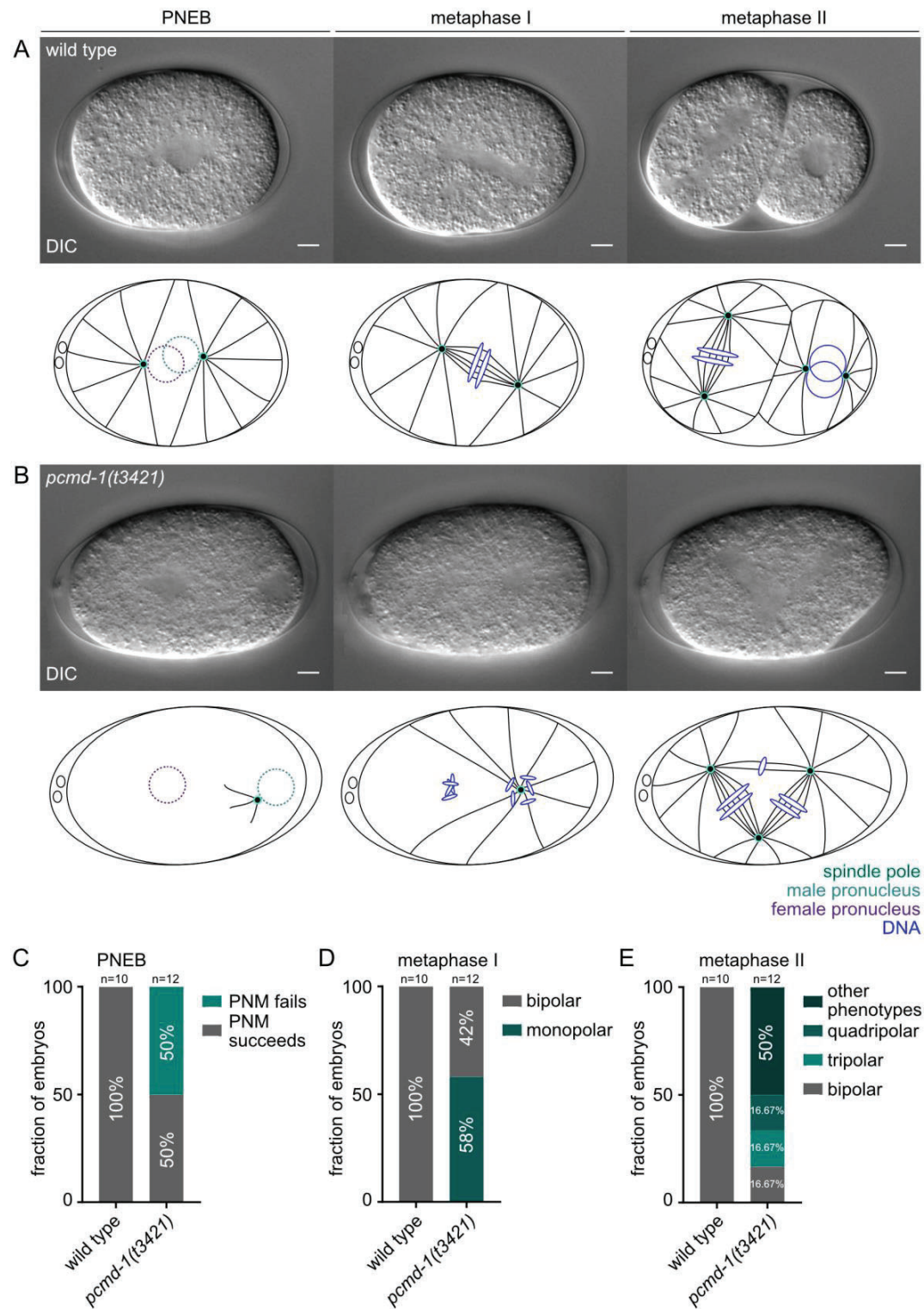
Figure 9: **Abnormal spindle formation in *t3421* mutant embryos**. (A-B) DIC recordings and the corresponding sketches of wild-type and *pcmd-1(t3421)* mutant one- and two-cell embryos. Images were taken at a 4D microscope. Stages: pronuclear envelope breakdown

(PNEB), metaphase I and metaphase II. The anterior side of the embryo is to the left, and the posterior side is to the right. Scale bar: 5 µm. (A) Wild-type *C. elegans* one-cell embryo. At PNEB maternal and paternal pronuclei have met and a bipolar spindle starts to form. At metaphase I a bipolar spindle is visible. In the second cell cycle the anterior cell (AB) is dividing first, and a bipolar spindle is visible at metaphase II. The posterior cell (P1) is dividing later, and PNEB just took place. (B) *Pcmd-1(t3421)* mutant *C. elegans* one-cell embryo. At PNEB maternal and paternal pronuclei have not met and a small monopolar spindle starts to form. At metaphase I a monopolar spindle is forming (Note: Microtubules might nucleate from DNA). In the second cell cycle, after cell division failed in the first cell cycle, a tripolar spindle forms. (C-E) Analysis of phenotypes seen in wild-type and *pcmd-1(t3421)* mutant one- and two-cell embryos. (C) PNM success in wild-type and *pcmd-1(t3421)* mutant embryos at PNEB. The number of n states embryos counted in total. (D) Spindle formation in wild-type and *pcmd-1(t3421)* mutant one-cell embryos. The number of n states embryos counted in total. (E) Spindle formation in wild-type and *pcmd-1(t3421)* mutant two-cell embryos. The number of n states embryos counted in total.

To identify the affected gene underlying the *t3421* mutant phenotype, whole-genome sequencing was performed in combination with single-nucleotide polymorphism (SNP) mapping (*C. elegans* Knockout Facility, Vancouver, B.C., Canada). The mutation was mapped to the right arm of chromosome I between the visual markers *lin-11(n566)* and *unc-101(m1)* (Figure 10A, Table 1, Table 12; experiments were done by M. Osepashvili and T. Mikeladze-Dvali, Erpf *et al.,* 2019). *C17d12.7* was one of the genes carrying an SNP within its coding region (Figure 10A and B). The gene contains a sequence coding for a coiled-coil domain close to the N-terminus of the translated protein (Figure 10 B). Coiled-coil domains are known to be present in many centrosomal proteins (Salisbury, 2003; Kuhn, Hyman and Beyer, 2014). Thus, *c17d12.7* was considered as the most promising of the candidate genes. To determine whether a functional copy of the *c17d12.7* gene can rescue the *t3421* mutant phenotype, I created the single-copy integration allele *mikSi5*, encoding the *c17d12.7* cDNA fused to the *mkate2* fluorophore sequence (Figure 10C, Table 1). The expression of the construct is driven by the *mex-5* promoter, and the protein is visually detectable only in the germline. The strain was crossed to the *t3421* mutant flanked by the *lin-11(n566)* and *unc-101(m1)* visual markers. The resulting strain was assayed for embryonic viability (Figure 10D, Table 13). Progeny deriving from wild-type hermaphrodites showed viability of 98 % at

25 °C (Figure 10D, Table 13). The *t3421* mutant allele displayed 0 % viability (Figure 10D, Table 13). Control strains, carrying the *lin-11(n556)* or *unc-101(m1)* visual markers, displayed 94 % and 62 % embryonic viability, respectively (Figure 10D, Table 13; note here that the strain carrying the *lin-11(n556)* visual marker also has the *unc-75(e950)* visual marker in the background, which is not present in the *lin-11(n556) pcmd-1(t3421) unc-101(m1); mikSi5[pmex-5:mkate2::pcmd-1(c17d12.7):tbb2]* strain (Figure 10A, Table 13). However, since the viability of the strain was not further compromised as the viability of the *unc-101(m1)* allele alone, outcrossing the *unc-75(m1)* allele was not attempted, and possible synergistic effects were ignored at this point). The *t3421* mutant allele, which also carries the *lin-11(n556)* and *unc-101(m1)* visual markers, shows 0 % viability. The *mikSi5[pmex-5:mkate2::pcmd-1(c17d12.7):tbb2]* allele in control genomic background displayed 90 % viability (Figure 10D, Table 13; note here that animals carrying the *mikSi5* allele are not staying on the bacterial lawn most likely due to a cilia defect. This might increase escape rates from Petri dishes). The *mikSi5[pmex-5:mkate2::pcmd-1(c17d12.7):tbb2]* allele was able to restore embryonic viability to 54 % in *t3421* mutant background, a comparable viability rate to what was seen for the *unc-101(m1)* control strain, suggesting that *unc-101(m1)* is responsible for compromised viability in the rescue strain (Figure 10D, Table 13). To avoid this problem, I constructed a transgenic allele *mikSi6,* a single-copy integration of the *c17d12.7* cDNA fused to GFP and flanked by the *mai-2* regulatory elements (Sherrard *et al.*, 2017, Figure 10C, Table 1). This construct is expressed ubiquitously throughout development and in the adult worm. The allele *mikSi6[pmai-2:gfp::pcmd-1:mai-2]* was crossed to the *t3421* mutant stain and scored for embryonic viability (note here that this strain does <u>not</u> carry the *lin-11* or *unc-101* visual markers as genetic background, and therefore, the presence of the mutation was verified by sequencing, Figure 10D). The *mikSi6[pmai-2:gfp::pcmd-1:mai-2]* allele showed 98 % viability in control genomic background and was able to restore embryonic viability to 98 % in *t3421* mutants at restrictive temperature (n=850 and n=855, respectively, Figure 10D, Table 13).

In the *t3421* mutant, the *c17d12.7* gene carries a single nucleotide mutation at the N-terminus, which is located before the coiled-coil domain. The mutation exchanges a Cytosine (C) to Thymidine (T) at nucleotide position 160 (Table 12). On the protein level, the *t3421* mutation leads to the termination of transcription since an early STOP codon is introduced at amino acid position Glutamine 54 (Q54) (Figure 10B). To further validate *pcmd-1* as the candidate gene, I introduced the very same mutation into the cDNA sequence of the *c17d12.7* gene and constructed an allele *mikSi7*, carrying the *c17d12.7(t3421)* cDNA fused to the *gfp*

coding sequence (Figure 10C, Table 1). The strain carrying the mutant construct shows 98 % viability in otherwise control genomic background. Importantly, the *mikSi7[pmai-2:gfp::pcmd-1(t3421):mai-2]* allele was not able to restore embryonic viability in *t3421* mutant background at restrictive temperature (0 % viability, n=662, Figure 10D, Table 13).

Further, a CRISPR deletion allele *syb975* was generated to verify the *t3421* mutant phenotype by an independent allele (Figure 10B, Table 1). A 1201 base pair deletion was introduced, deleting the start codon, the coiled-coil domain and the unstructured regions of the gene (Figure 10B). The strain shows 24 % embryonic viability at 15 °C and 0 % embryonic viability at 25 °C (Figure 10D, Table 13; embryonic viability test was performed by T. Mikeladze-Dvali, Erpf *et al.,* 2019). Similar to the *t3421* mutant allele, the *syb975* allele shows monopolar spindle formation in metaphase of the first cell cycle, as well as tri- and quadripolar spindle formation in the second metaphase (DIC movies recorded by T. Mikeladze-Dvali, Erpf *et al.,* 2019). An existing deletion allele *tm8972*, which lacks 1135 bp spanning part of exon 9 and the 3'UTR of *c17d12.7*, is homozygous viable (National BioResource Project (NBRP), tested by T. Mikeladze-Dvali, Erpf *et al*., 2019, Figure 10B, Table 1, Table 12). The result indicates that the C-terminal part of the protein, which is lacking in the *tm8972* mutant, does not contain any elements required for protein function.

The experiments verify *c17d12.7* as the candidate gene that causes the *t3421* mutant phenotype when functionally compromised. The *c17d12.7* gene was named *pericentriolar matrix deficient 1* (*pcmd-1*) for reasons specified in the text below.
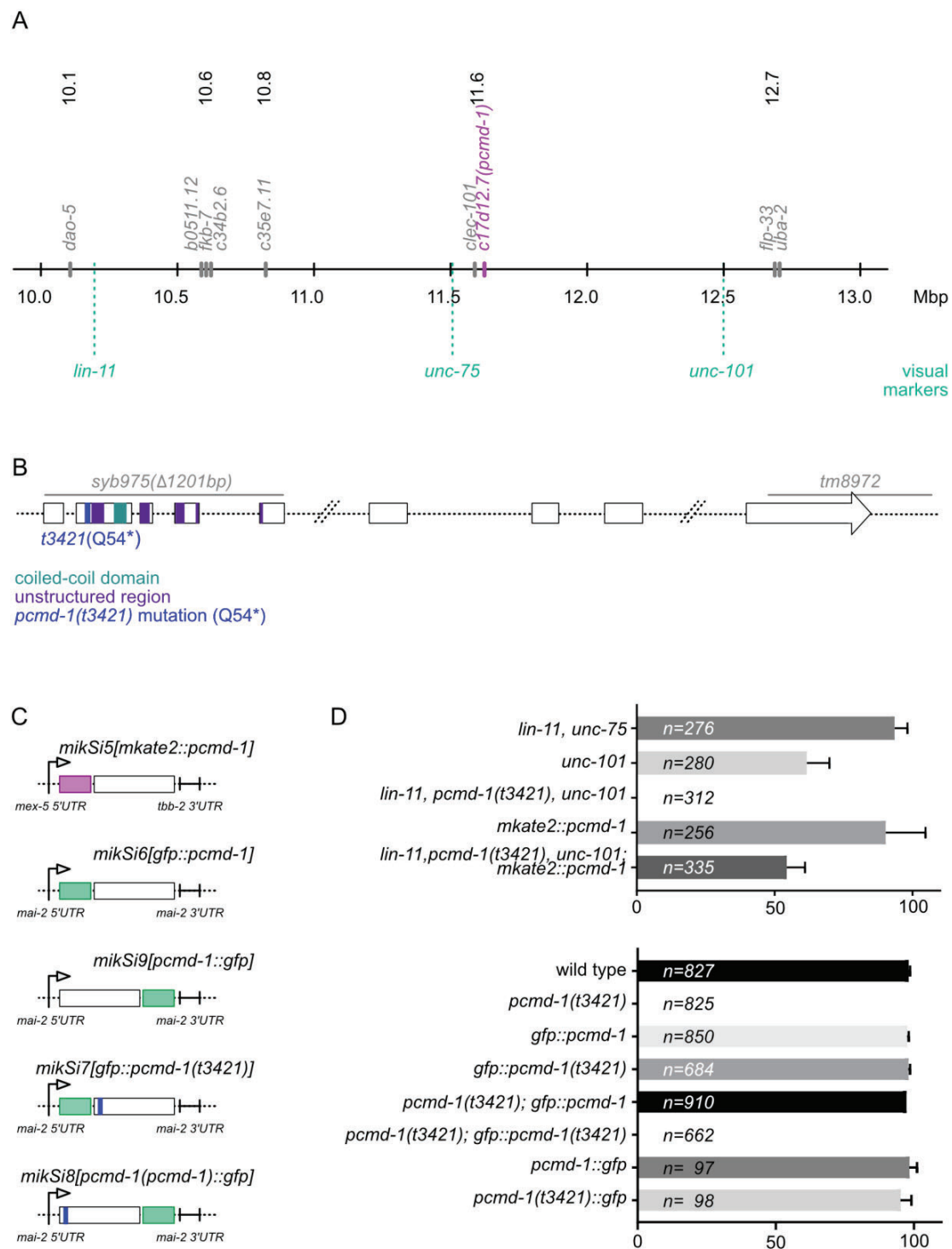
Figure 10: **The *c17d12.7 (pcmd-1)* mutation underlies the *t3421* mutant phenotype**. (A) The illustration shows the genes carrying a mutation in the *t3421* mutant within the mapped region between the visual markers *lin-11(566)* and *unc-101(m1)* (cyan) on chromosome I

(also see Table 10). The mutation in the *c17d12.7* gene (magenta) was identified to underlie the *t3421* mutant phenotype. (B) The *c17d12.7* gene has nine exons and encodes a 630 amino acids (AA) long protein (70.8 kDa), containing a coiled-coil domain (cyan; position (AA): 94-117) and four unstructured regions (purple; positions (AA): 55-75, 132-142, 152-163, 188-199) (predicted by SMART, http://smart.embl-heidelberg.de/). The mutation present in the *t3421* mutant exchanges the Guanine at position 159 to an Adenine. On the protein level, this leads to the introduction of a STOP codon (*) at amino acid position Glutamine 54 (Q54) (blue). The *syb975* allele carries a 1201 bp long N-terminal deletion (grey), including the START codon of the gene. The existing C-terminal deletion allele *tm8972* deletes 1135 bp, spanning the C-terminus and part of the 3'UTR of the gene (grey). Also see Table 12. (C) Illustration of different single-copy insertion *pcmd-1,* and *pcmd-1(t3421)* constructs fused to either *mkate2* or *gfp* fluorophore coding sequences. (D) Rescue experiments. Top: Rescue of *pcmd-1(t3421)* embryonic lethality. The *mikSi5[pmex-5:mkate2::pcmd-1(c17d12.7):tbb2]* allele can partially restore embryonic survival in *pcmd-1(t3421)* mutants. The strain carries different visual markers which likely cause compromised embryonic viability of the rescue strain. Bottom: Rescue of *pcmd-1(t3421)* embryonic lethality. The *mikSi6[pmai-2:gfp::pcmd-1:mai-2]* allele can restore embryonic survival in *pcmd-1(t3421)* mutants to control-like levels (note here that this strain does not carry visual markers). On the contrary, the *mikSi7[pmai-2:gfp::pcmd-1(t3421):mai-2]* allele cannot restore embryonic survival. The number of n states embryos counted in total. Data are represented as mean ± SEM. Also see Table 13.

Table 12: **Gene positions and visual markers**. Displayed are the positions of genes that carry mutations in the *t3421* mutant and the visual markers that were used for narrowing down the mapping region. Positions retrieved from *wormbase* (version WS269).

gene	Genomic position	visual marker
dao-5	I:10187515..10190896	--
lin-11	I:10248256..10255327	*lin-11(566)*
b0511.12	I:10654298..10666933	--
fkb-7	I:10667808..10671301	--
c34b2.6	I:10676922..10682374	--
c35e7.11	I:10844772..10845922	--
unc-75	I:11592302..11602095	*unc-75(e950)*
clec-101	I:11560637..11564387	--

c17d12.7(pcmd-1)	I:11604027..11611314	--
mutation *t3421* in *c17d12.7(pcmd-1)*	I:11611155	--
deletion in *syb975 (pcmd-1)*	I: 11610114..11611314	--
deletion in *tm8972(pcmd-1)*	I:11603963..11605097	--
unc-101	I:12508299..12513419	*unc-101(m1)*
flp-33	I:12624235..12625238	--
uba-2	I:12741588..12749318	--

Table 13: **Rescue of *pcmd-1(t3421)* embryonic lethality**. Different fluorescent fusion constructs of *pcmd-1* cDNA can restore embryonic survival in *pcmd-1(t3421)* mutants. However, a construct carrying the point mutation present in the *pcmd-1(t3421)* mutant cannot restore embryonic survival. The number of n states embryos counted in total. Data are represented as mean ± SEM.

Genotype	Temp.	Embryonic viability (in % ± SEM)	
lin-11(n556), unc-75(e950)	25°C	93.5 ± 4.7	(n= 276)
unc-101(m1)	25°C	61.7 ± 8.2	(n= 280)
lin-11(n556), pcmd-1(t3421), unc-101(m1)	25°C	0.0 ± 0.0	(n= 312)
mkate2::pcmd-1	25°C	90.3 ± 14.4	(n= 256)
lin-11(n556), pcmd-1(t3421), unc-101(m1); mkate2::pcmd-1	25°C	54.4 ± 6.6	(n= 335)
wild type	25°C	98.0 ± 0.6	(n= 827)
pcmd-1(t3421)	25°C	0.0 ± 0.0	(n= 825)
gfp::pcmd-1	25°C	97.5 ± 0.6	(n= 850)
gfp::pcmd-1(t3421)	25°C	97.9 ± 0.7	(n= 684)
pcmd-1(t3421); gfp::pcmd-1	25°C	97.2 ± 0.8	(n= 910)
pcmd-1(t3421); gfp::pcmd-1(t3421)	25°C	0.0 ± 0.0	(n= 662)
pcmd-1::gfp	25°C	98.3 ± 2.8	(n= 97)
pcmd-1(t3421)::gfp	25°C	95.1 ± 4.0	(n= 98)

3.1.2. PCMD-1 is a centrosomal protein

To analyze the subcellular localization of the PCMD-1 protein, I performed fluorescent live-cell imaging. The previously described *mikSi6[pmai-2:gfp::pcmd-1:mai-2]* allele (Figure 10C) is ubiquitously expressed and the GFP signal was detected throughout embryo development, in all larval stages, as well as in the adult animal, where it is detectable in the gonads, at the ciliary base and the sperm (Figure 11A-C, and data not shown).

To analyze the endogenous expression pattern of PCMD-1, the allele *syb370[gfp::pcmd-1]*, carrying a GFP inserted upstream of the *pcmd-1* genomic locus, was generated (Figure 11F, Table 1). GFP::PCMD-1^{syb370} shows the same sub-cellular localization pattern as GFP::PCMD-1^{mikSi6} and is also expressed in all analyzed tissues throughout development up to adulthood (Figure 11D and E). The GFP::PCMD-1^{syb370} signal at the sperm appeared weaker compared to the strain expressing GFP::PCMD-1^{mikSi6} (data not shown). However, this can be an artifact due to the *mai-2* promoter activity in GFP::PCMD-1^{mikSi6} and was therefore not further analyzed or quantified.

The sub-cellular localization of GFP::PCMD-1 resembles that of known centriolar proteins. Thus, a strain, carrying the *mikSi6[pmai-2:gfp::pcmd-1:mai-2]* and the *itIs64[ppie-1:mcherry-TEV-Stag::sas-4]* alleles, was crossed, to verify that PCMD-1 localizes to centrioles (Table 1). GFP::PCMD-1 co-localizes with mCherry::SAS-4 at centrioles (Figure 11G). Similarly, in a strain, carrying the *mikSi5[pmex-5:mkate2::pcmd-1(c17d12.7):tbb2]* and *vieSiIs[psas-4:gfp::sas-4:sas-4]* alleles, mKate2::PCMD-1 localizes at centrioles, as it co-localizes with GFP::SAS-4 in the germline (Figure 11H).

In some images taken at the 4D microscope, GFP::PCMD-1^{mikSi6} appeared as a faint halo around centrioles, which suggests a weak association of the protein with the PCM (Figure 11A). TAC-1 is a centrosomal protein that is only recruited to the mitotic PCM. Thus, a strain, carrying the *mikSi5[pmex-5:mkate2::pcmd-1(c17d12.7):tbb2]* and the *bcSi1[pmex-5:gfp::tac-1]* alleles, was crossed and analyzed for PCM recruitment of mKate2::PCMD-1 at the confocal microscope. In the mitotic part of the germline mKate2::PCMD-1 did not expand but remained localized in the center of the PCM (data not shown). However, since the expression of mKate2::PCMD-1, regulated by *pmex-5*, is not as strong as the expression of GFP::PCMD-1, regulated by *pmai-2*, I generated the *mikSi4[pmex-5:mkate2::tac-1:unc54]* allele (vector cloning performed by E. Abu Khmail), which was crossed to the GFP::PCMD-1 marker (cross by A. Kirgis). Also, with this strain PCM localization could not be verified satisfactorily (data not shown). Hence, super-resolution images of GFP::PCMD-1^{mikSi6}

embryos, stained against GFP and the PCM protein SPD-5, were taken. Indeed, the super-resolution micrographs confirmed the assumption that GFP::PCMD-1 is weakly associated with the PCM (Figure 11I, stainings and imaging by T. Mikeladze Dvali and A. Maiser, Erpf *et al*., 2019).

Together these findings suggest that PCMD-1 localizes to centrosomes, most likely to centrioles or the PCM core and the expandable PCM. However, with the current optical resolution, we cannot discriminate between localization to centrioles or localization to the PCM core. Further, PCMD-1 is present at centrosomes and basal bodies in all life stages of the worm.
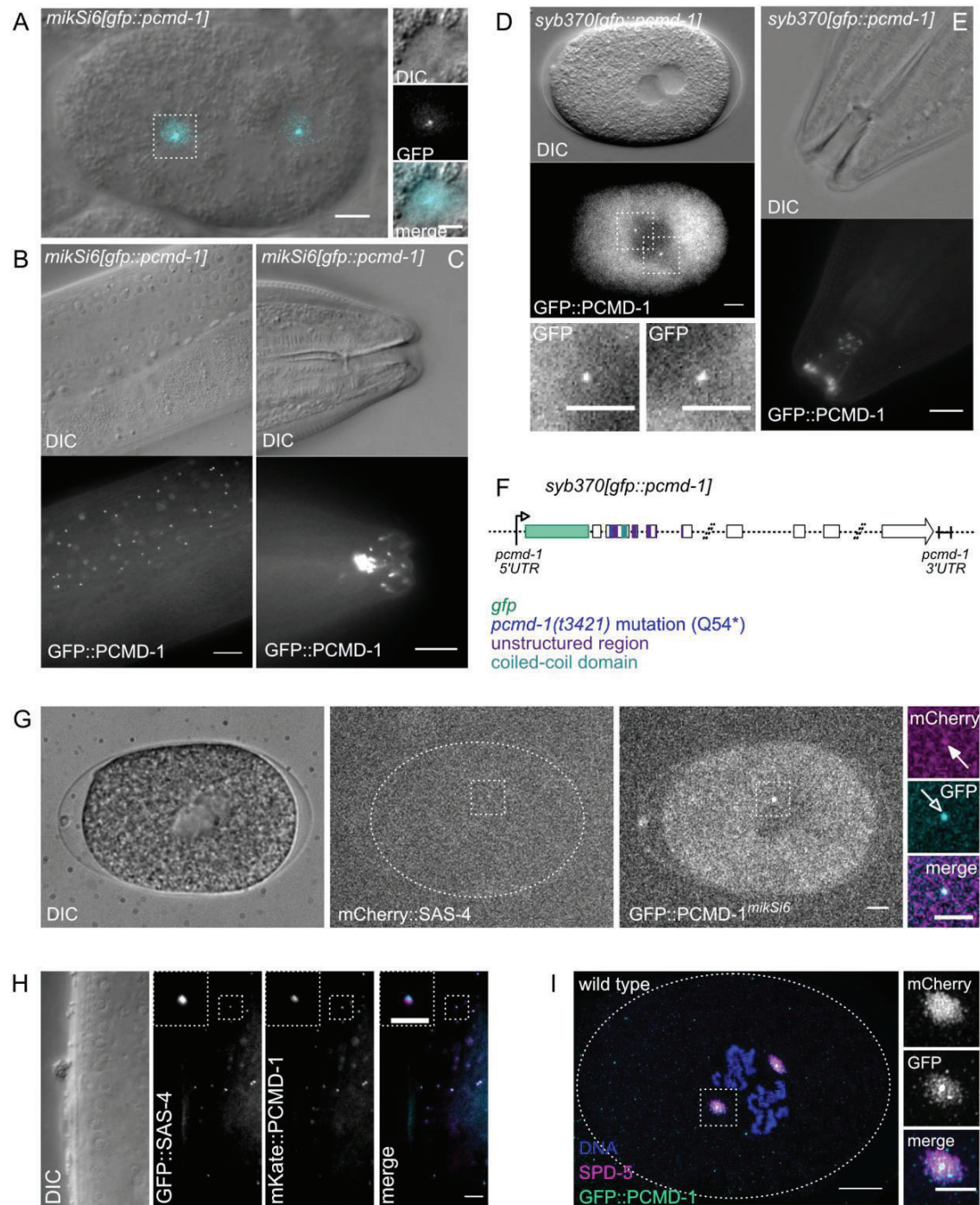
Figure 11: **PCMD-1 localizes to centrosomal structures**. DIC and fluorescence images of (A) a *C. elegans* one-cell embryo, (B) the gonad and (C) the mouth region. GFP::PCMD-1^{mikSi6} localizes to the center of spindle poles, is visible in the gonads and the mouth region. The localization pattern strongly resembles that of known centriolar proteins. Further, in the embryo, the signal seems to be weakly associated with the PCM. Scale bars: 5 µm for

embryo, gonad and mouth region. 2 µm for blow-ups. (D-E) DIC and fluorescence images of (D) a *C. elegans* one-cell embryo and (E) the mouth region. (D) GFP::PCMD-1^{syb370} localizes to a punctate structure in the one-cell embryo, resembling the localization of known centriolar proteins. (E) In the mouth region PCMD-1 is expressed and localizes in a pattern that resembles that of known ciliary proteins (see Figure 10, Table 1). PCM association of the protein is not detectable, presumably due to a lower protein abundance than in the GFP::PCMD-1^{mikSi6} strain. Scale bars: 5 µm for embryo and mouth region. 3 µm for blow-ups. (F) Illustration of the endogenously CRISPR GFP-tagged *pcmd-1* locus, *pcmd-1(syb370)* allele (Table 1). (G) GFP::PCMD-1^{mikSi6} co-localizes with mCherry::SAS-4 in the one-cell embryo, verifying that PCMD-1 localizes to centrioles. Images were taken at a spinning disc microscope. Scale bars: 5 µm for embryo. 2µm for blow-ups. (H) mKate2::PCMD-1 co-localizes with GFP::SAS-4 in the gonad, verifying that PCMD-1 localizes to centrioles. Scale bars: 5 µm for gonad. 3 µm for blow-ups. (I) Super-resolution micrographs of wild-type *C. elegans* one-cell embryo expressing GFP::PCMD-1^{mikSi6} (also see Figure 10, Table 1). Embryos were stained against GFP to visualize PCMD-1 localization and against SPD-5 to visualize pericentriolar material (PCM). Images were taken at a 3D SIM OMX microscope. Stage: Prometaphase II. The anterior side of the embryo is on the left, and the posterior side is on the right. Scale bar: 5 µm for embryo. 2 µm for blow-ups. The GFP::PCMD-1^{mikSi6} protein colocalizes with the PCM protein SPD-5. A bright GFP::PCMD-1^{mikSi6} dot is visible within the broader area of the SPD-5 PCM staining, which represents the centriolar associated fraction of PCMD-1. A faint signal of PCMD-1^{mikSi6} staining is further detectable overlapping with the broader area of the SPD-5 PCM staining, verifying PCM association of PCMD-1.

To analyze dynamic changes of PCMD-1 over the cell cycle, GFP::PCMD-1^{mikSi6} signal intensities were acquired by spinning disc confocal microscopy over time. Interestingly, the GFP::PCMD-1^{mikSi6} signal appears to decrease at centrosomes around metaphase (Figure 12A). The GFP signal intensity was measured at single centrioles over time and compared to GFP::SAS-4 intensity levels at centrioles (Figure 12B). GFP::PCMD-1^{mikSi6} intensity values drop towards metaphase (lowest average intensity at 210 sec after PNEB, Figure 12B). The signal intensity at centrioles undergoes a total recovery thereafter (at 420 sec after PNEB, Figure 12B). On the contrary, such a signal decrease around metaphase was not seen for the intensity measurements of GFP::SAS-4 (at 210 sec after PNEB, Figure 12B). Due to time restrictions, only a few embryos were recorded, and statistical analysis

shows <u>no</u> significant difference between GFP::SAS-4 and GFP::PCMD-1^{mikSi6} measurements. Moreover, the embryos with a drop of the GFP signal intensities at centrioles below the detection limit were not considered for analysis since no suitable centriolar reference marker is available to determine the centriole position in the complete absence of GFP::PCMD-1^{mikSi6}. Thus, the changes in signal intensity of GFP::PCMD-1^{mikSi6} at centrioles are likely underestimated. Further analysis is required to test whether PCMD-1 is down-regulated at centrosomes during metaphase (Figure 12B). Also, the possibility of a bleaching artifact has to be excluded.

A truncated N-terminal part of the protein could still be functional and might be detectable at centrosomes or other cellular structures. To determine whether the PCMD-1(*t3421*) mutant protein has residual activity, the strain carrying the *mikSi7[pmai-2:gfp::pcmd-1(t3421):mai-2]* allele was analyzed over time. No GFP signal was detected at any cellular structure at 15 or 25 °C (data not shown), suggesting that a functional N-terminal part of the protein is not present in detectable amounts in the *pcmd-1(t3421)* mutant. Further, downstream of the *t3421* mutation are several in-frame alternative start codons that might be used and could potentially give rise to a functional truncated C-terminal part of the PCMD-1 protein (Table 14). Thus, also the *mikSi9[pmai-2:pcmd-1::gfp:mai-2]* and *mikSi8[pmai-2:pcmd-1(t3421)::gfp:mai-2]* alleles were analyzed and compared for their protein localization (Figure 10C). Both proteins, PCMD-1::GFP and PCMD-1*(t3421)*::GFP, behave as their N-terminal fusion counterparts at 15 or 25 °C. PCMD-1*(t3421)*::GFP cannot be detected at centrosomes or any other cellular structure (Figure 12C). The result suggests that a truncated C-terminal part of the protein is not present in detectable amounts in the *pcmd-1(t3421)* mutant.

The protein abundance of the N- and C-terminal GFP-PCMD-1 fusion proteins was further checked by western blot analysis. The N- and C- terminal PCMD-1 fusion proteins were visible on the blot at the expected size of 97.95 kDa (Table 15, Figure 12D). The N-terminal strain shows two additional bands at ~28 kDa, which might be cleaved GFP (Figure 12D). On the contrary, no bands were detected for GFP::PCMD-1*(t3421)*, with an expected size of 33,31 kDa, or PCMD-1*(t3421)*::GFP, with an expected size of 85,79 kDa (Table 14 and 15, Figure 12D). In summary, the western blot analysis supports the conjecture that truncated version of PCMD-1 is not present in detectable amounts in *pcmd-1(t3421)* mutants. However, the analysis cannot exclude the possibility that low amounts of truncated PCMD-1, below the detection limit, are generated.
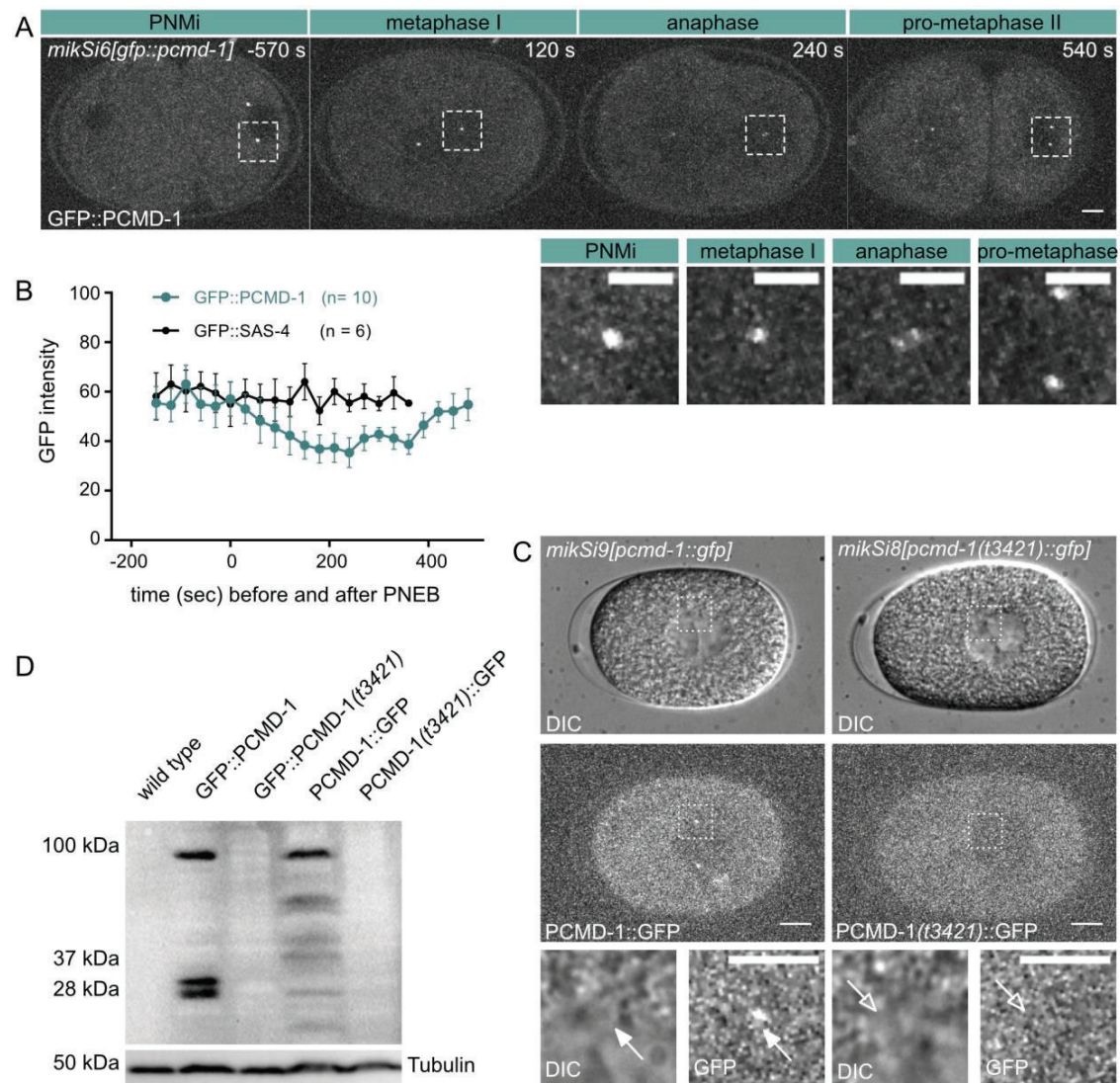
Figure 12: **Analysis of PCMD-1 and PCMD-1(*t3421*) GFP fusion proteins**. (A) GFP::PCMD-1*mikSi6* temporal recordings. An embryo carrying the *mikSi6[pmai-2:gfp::pcmd-1:mai-2]* allele is displayed. Images were taken at a spinning disc microscope. The anterior side of the embryo is on the left and the posterior side is on the right. Timestamps in seconds relative to PNEB. Scale bars: 5 μm for the embryo, 3 μm for the blow-ups. Less GFP::PCMD-1*mikSi6* appears to be localized at centrosomes at meta- and anaphase. (B) GFP intensity measurements of single centrosomes of GFP::PCMD-1*mikSi6* and GFP::SAS-4 in embryos, starting from shortly after fertilization until completion of the first cell division. The images measured correspond to Figure 12A. The radius of measured volume: 1.001 μm. GFP::PCMD-1*mikSi6* intensity drops around meta- and anaphase and recovers after that. Control GFP::SAS-4 measurements do not show this drop of intensity during metaphase.

Note here that only embryos with a residual signal at centrioles in meta- and anaphase were measured to ensure measurements of the right area. Intensities are not significantly different at 180 s after PNEB ($n_{GFP::SAS-4}$ = 6, $n_{GFP::PCMD-1}$ = 10; p = 0,0772; data not shown). The number of n states single centrioles measured. Intensity measurements were performed using TrackMate (Jaqaman *et al.*, 2008) (C) Subcellular localization of C-terminally GFP-tagged PCMD-1 and PCMD-1(*t3421*) fusion proteins at 25 °C (Also see Figure 10C and Table 1). DIC and fluorescent images of one-cell embryos at PNM recorded at a spinning disc confocal microscope. The anterior side of the embryo is on the left and the posterior side is on the right. Scale bars: 5 µm for the embryo, 3 µm for the blow-ups. PCMD-1::GFP localizes to centrioles as previously described for GFP::PCMD-1 constructs (*mikSi6[pmai-2:gfp::pcmd-1:mai-2]* single-copy integration and *syp370[[gfp::pcmd-1]::loxp]* CRISPR alleles). In contrast, PCMD-1(*t3421*)::GFP does neither localize to the centrosome nor any other subcellular structure. (D) Western blot analysis of N- and C-terminally GFP-tagged PCMD-1 and PCMD-1(*t3421*) fusion proteins. An anti-GFP antibody was used for protein detection (Table 6). No bands were detected for control worm lysates. GFP::PCMD-1 shows a band with the expected size of 97.95 kDa (Table 15). Additionally, two bands are detected at around 28 kDa. For GFP::PCMD-1(*t3421*) no band was detected. Expected size for a truncated GFP::PCMD-1(*t3421*) protein would have been 33.31 kDa (Table 15). The C-terminally GFP-tagged PCMD-1 protein shows one band at the expected size of 97.95 kDa. Also the C-terminally tagged PCMD-1(*t3421*) is not detectable (Table 15). In case of the use of the earliest possible alternative START codon after the *t3421* mutation, a protein of 85.78 kDa in size would have been expected (Table 15, also see Table 14).

Table 14: **Alternative in-frame START codons** that occur after the *t3421* mutation in the *pcmd-1* gene. These codons could potentially be used to initiate transcription in the *pcmd-1(t3421)* mutant and lead to the production of a truncated protein at the permissive temperature. The use of an alternative start codon could explain the temperature-sensitive nature of the *pcmd-1(t3421)* and *pcmd-1(syb975)* alleles. * Alternative start codons eliminated in the *pcmd-1(syb975)* deletion allele.

In-frame START codon downstream of *t3421* mutation	Genomic position	bp after original START
Alternative START codon 1	I: 11610944	371*
Alternative START codon 2	I: 11610891	424*
Alternative START codon 3	I: 11610244	1071*

Alternative START codon 4	I: 11610181	1134*
Alternative START codon 5	I: 11610178	1137*
Alternative START codon 6	I: 11610175	1140*
Alternative START codon 7	I: 11607930	3385
Alternative START codon 8	I: 11607690	3625
Alternative START codon 9	I: 11606980	4335
Alternative START codon 10	I: 11606611	4704
Alternative START codon 11	I: 11604938	6377
Alternative START codon 12	I: 11604899	6416

Table 15: **Expected molecular weights of GFP fusion proteins**.

Fusion protein	Expected molecular weight (kDa)
GFP::PCMD-1	97.95
PCMD-1::GFP	97.95
GFP::PCMD-1*(t3421)*	33.31
PCMD-1*(t3421)*::GFP	85.78

3.1.3. A centriole duplication defect cannot account for the *pcmd-1(t3421)* mutant phenotype

To better understand the aberrations present in *pcmd-1(t3421)* mutant embryos, a mutant strain carrying the *estSi121[pmex-5:tpxl-1^{WT}::mNeonGreen:tbb-2]* allele was crossed (Mangal *et al.*, 2018). In the control, TPXL-1::mNG localizes to the centrosome shortly after fertilization. As the PCM expands, TPXL-1 accumulates at the centrosome. It further localizes to microtubules (n = 5; Figure 13A; Özlü *et al.*, 2005; Mangal *et al.*, 2018). Strikingly, in *pcmd-1(t3421)* mutants TPXL-1::mNG is not detectable at centrosomes in 44 % of embryos at PNMi (n = 9, Figure 13B and C). In those forming monopolar spindles in metaphase, TPXL-1::mNG is accumulating in the center of the spindle and localizes to the microtubules emerging from there (Figure 13B). Failed bipolar spindle formation in the first cell cycle can be explained by a centriole duplication or maintenance defect of paternally derived centrioles.

Also a defect in centriole maturation that causes aberrant PCM formation can lead to monopolar spindle formation in early embryos.
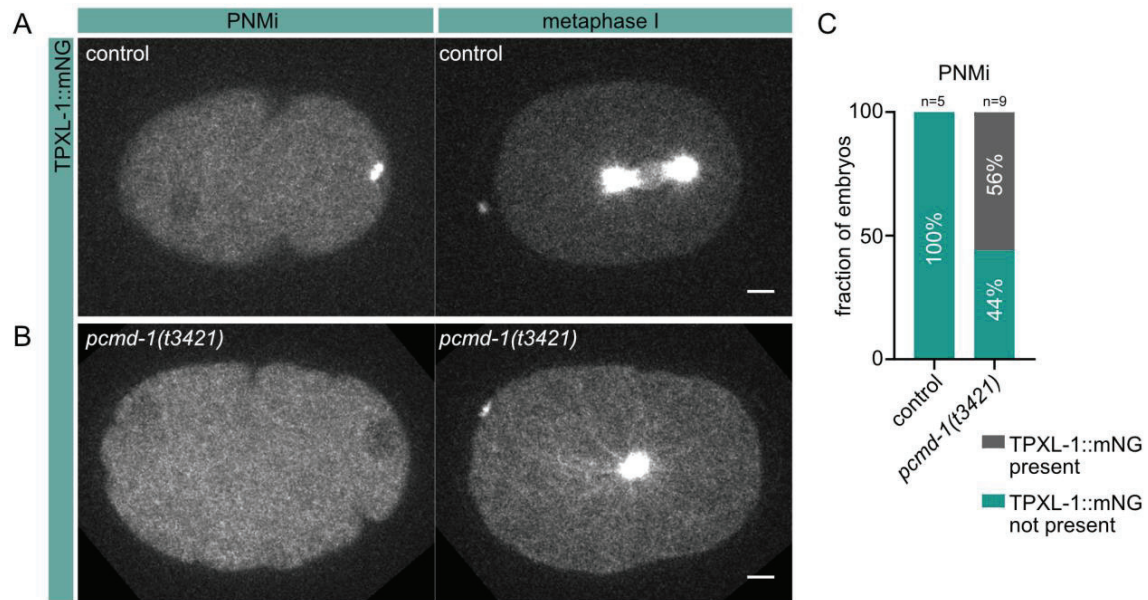
Figure 13: **TPXL-1::mNG in control and *pcmd-1(t3421)* mutant embryos**. (A-B) Images were taken at a spinning disc microscope. The anterior side of the embryo is on the left and the posterior side is on the right. Scale bar: 5 μm. (A) Control embryos show TPXL-1::mNG localization to centrosomes shortly after fertilization. At metaphase TPXL-1::mNG localizes to centrosomes and microtubules. (B) In *pcmd-1(t3421)* mutant embryos GFP does not localize to centrosomes after fertilization. At metaphase the embryo forms a monopolar spindle and TPXL-1::mNG accumulates at the center and localizes to the emanating microtubules. (C) Analysis of TPXL-1::mNG centrosome recruitment in control and *pcmd-1(t3421)* mutant embryos at PNMi. The number of n states embryos counted in total. Embryos were categorized according to their potential to accumulate TPXL-1::mNG during PNMi.

To determine if centriole duplication, maintenance or maturation are impaired in *pcmd-1(t3421)* mutant embryos, immunostainings were performed with antibodies against SAS-4, to analyze centriole number, and α-tubulin, to infer from the microtubule nucleation activity of the centrosomes, whether centrosome function is compromised downstream of centriole formation (Figure 14A-D). Shortly after fertilization centrioles start recruiting PCM

and microtubules start to nucleate. Microtubule mediated pulling forces act on the centrosomes, thereby separating them (Cabral *et al.*, 2013). In wild-type embryos, 50 % of the embryos showed one SAS-4 focus during pronuclear migration (PNMi), whereas the rest of the embryos already carried two separated SAS-4 foci. In contrast, 76 % of the *pcmd-1(t3421)* mutant embryos show a single SAS-4 focus during PNMi. Only 24 % have two SAS-4 foci at that stage (Figure 14E). Interestingly, microtubule nucleation activity was also affected in *pcmd-1(t3421)* mutant embryos during PNMi, with 77 % of the mutant embryos not nucleating microtubules (Figure 14F). In metaphase of the first cell cycle, in 85 % of the wild-type embryos, two SAS-4 foci were detected. Only a small fraction carried three to four SAS-4 foci. These represent embryos, which have started to enter anaphase and centrioles disengaged (n = 20; 2 SAS-4 foci = 5 %, 3 SAS-4 foci = 10%, Figure 14E). 5 % of the *pcmd-1(t3421)* mutants carry only one SAS-4 focus. However, the majority of 69 % of embryos show two SAS-4 foci, while the rest of the embryos have three to four foci (n = 39; 3 SAS-4 foci = 21 %, 4 SAS-4 foci = 5%, Figure 14E). The findings can be explained by either a mild centriole duplication defect or a centriole separation defect, where centrioles in close proximity appear as one SAS-4 focus. Judged from the presence of multiple SAS-4 foci, 95 % of the embryos carry a sufficient number of centrioles to form a bipolar spindle (Figure 14B-D and E). Thus, a centriole duplication or maintenance phenotype cannot explain the formation of monopolar spindles during the first cell cycle (Figure 14B and D). Further supporting this assumption, also in metaphase of the second cell cycle all embryos carry at least 3 SAS-4 foci (29 %) or more (4 SAS-4 foci = 57 % and 5 SAS-4 foci = 14 %, Figure 14E). In mitosis I, 10 % of the centrioles are not associated with microtubules and thus are not contributing to spindle formation (Figure 14F). Strikingly, 27 % of microtubule asters are not emanating from SAS-4 foci (Figure 14G).

Overall, these findings indicate that monopolar spindle formation in one-cell *pcmd-1(t3421)* mutant embryos might be caused by a defect in PCM recruitment to centrioles, rather than a defect in centriole duplication.
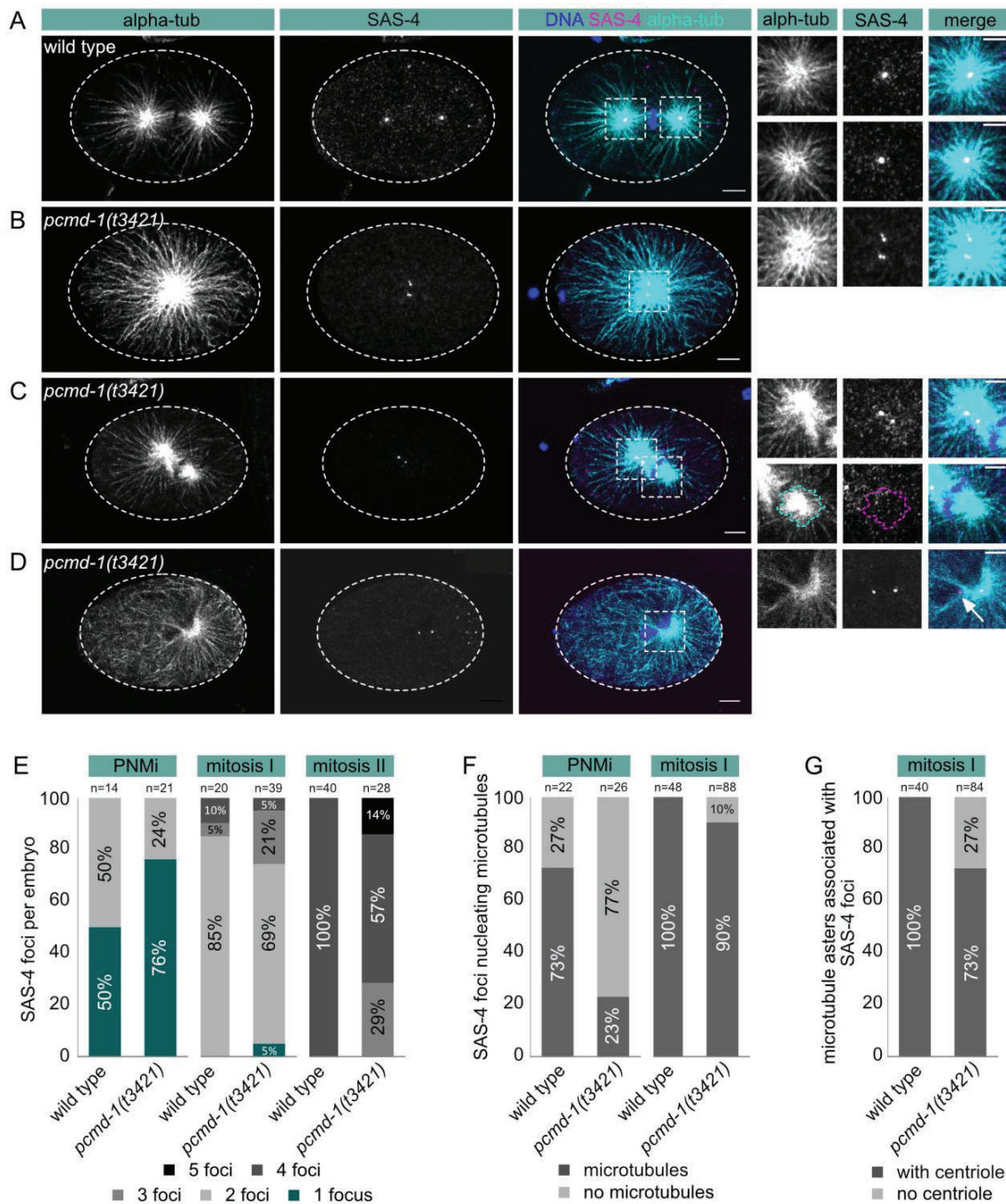
Figure 14: **Centriole duplication in wild-type and _pcmd-1(t3421)_ mutant embryos**. Centriole duplication defects cannot account for the _pcmd-1(t3421)_ mutant phenotype. (A-D) Immunofluorescent images of wild-type and _pcmd-1(t3421) C. elegans_ one-cell embryos and corresponding blow-ups. Embryos were stained against α-Tubulin, to visualize microtubules, and SAS-4, to visualize centrioles. Hoechst staining was used to visualize DNA. Images were taken at a confocal microscope. The anterior side of the embryos is on the left and the posterior side in on the right. Scale bars: 5 μm for the embryos, 3 μ for the blow-ups. (A) In

wild-type embryos, two SAS-4 foci are present at metaphase. At this cell cycle stage, the two SAS-4 foci represent two centriolar pairs, so that in total, four centrioles are present in the embryo. (B) This *pcmd-1(t3421)* mutant embryo forms a monopolar spindle. At the center of the spindle the two centrosomes both harbor two SAS-4 foci. (C) An abnormal bipolar spindle is formed in this *pcmd-1(t3421)* mutant embryo. Two SAS-4 foci are present in the embryo. However, they are both in the center of the anterior spindle pole. The posterior spindle pole does not contain any SAS-4 foci. (D) The embryo forms a monopolar spindle. Two SAS-4 foci are present. They are in close proximity, and only one of the centrosomes shows microtubule nucleation activity. (E) Centriole duplication analysis in wild-type and *pcmd-1(t3421)* mutant embryos at PNMi, in mitosis I and mitosis II. The number of n states the embryos counted in total. SAS-4 foci were counted per embryo. (F) Analysis of the microtubule nucleation capacity of centrosomes in wild-type and *pcmd-1(t3421)* mutant embryos at PNMi and in mitosis I. The number of n states the SAS-4 foci counted in total. (G) Analysis of the microtubule aster formation and their association with SAS-4 foci in wild-type and *pcmd-1(t3421)* mutant embryos in mitosis I. The number of n states the microtubule asters counted in total.

3.1.4. PCMD-1, a long-missing link between centrioles and PCM formation in *C. elegans*

In *C. elegans* it is unknown which component connects the PCM to centrioles. The most upstream known factor that is required for PCM recruitment is the centrosome matrix protein SPD-5. At mitotic entry, SPD-5 gets phosphorylated by PLK-1 and changes its conformation into an assembly competent state (Wueseke *et al.*, 2016). SPD-5 then forms the PCM matrix to recruit downstream factors to the centrosome. Thus, to determine whether PCM recruitment is compromised in *pcmd-1(t3421)* mutants, the *itSi202[pspd-2::gfp::spd-5]* allele was crossed into the mutant to monitor the matrix protein over time (Table 1). In control *C. elegans* embryos, GFP::SPD-5 localizes to centrosomes shortly after fertilization and accumulates until metaphase, reaching peak intensity in early anaphase, ~180s after NEBD (n = 10, Figure 15A and E). *Pcmd-1(t3421)* mutant embryos show a very severe but diverse defect in PCM recruitment. In 42 % of the embryos, no GFP signal is detected after fertilization until PNEB (n = 12, Figure 15D), consistent with what was seen in mutant embryos expressing TPXL-1::mNG. In 25 % of the embryos, GFP::SPD-5 starts

accumulating within the embryo after PNEB and around metaphase only (Figure 15C). The remaining mutant embryos (25 %, n = 12) show early GFP::SPD-5 accumulation after fertilization. However, in all *pcmd-1(t3421)* mutant embryos, overall PCM formation was strongly perturbed, and the PCM appeared unstable and fragmented (Figure 15B). To compare GFP::SPD-5 recruitment efficiencies in control and *pcmd-1(t3421)* mutants, intensity measurements were performed through Z-stacks using TrackMate (Figure 16, Tinevez *et al.*, 2017). The intensity measurements of GFP::SPD-5 in control and mutant embryos show a significant difference of GFP::SPD-5 accumulation at centrosomes over time (control: n = 10, *pcmd-1(t3421)*: n = 4, Figure 15E). Note here that intensity measurements were only performed for mutant embryos, which accumulated PCM shortly after fertilization. Ideally, a counter marker for centrioles should have been used to determine the centrosome position and to measure intensities in all embryos. However, an existing strain *ItIs64[ppie-1:mcherry-TEV-Stage::sas-4]* and a newly generated strain *mikSi10[psas-4:mKate2::sas-4:sas-4]* bleached too fast during recordings, and are therefore not suitable for long term imaging. Thus, the measurements underestimate the GFP::SPD-5 accumulation phenotype. Especially at metaphase, GFP::SPD-5 showed a strongly significant difference between GFP intensity in control and *pcmd-1(t3421)* mutant embryos (control: n = 10, *pcmd-1(t3421)*: n = 7, p < 0.0001; Figure 15C). Embryos were categorized according to their signal intensity (Figure 16A, C). Note here that only GFP levels in mutant embryos of the categories II-IV with a GFP signal at metaphase were measured (16A, C).

The results suggest that PCMD-1 is required for effective SPD-5 localization to non-mitotic centrosomes. Further, in *pcmd-1(t3421)* mutants, mitotic SPD-5 accumulations appear fragmented and unstable. Similar observations were made for other PCM proteins such as SPD-2 and TAC-1 (data not shown), suggesting an additional PCM stabilizing role of PCMD-1. This phenotype has not been described previously in *C. elegans*.
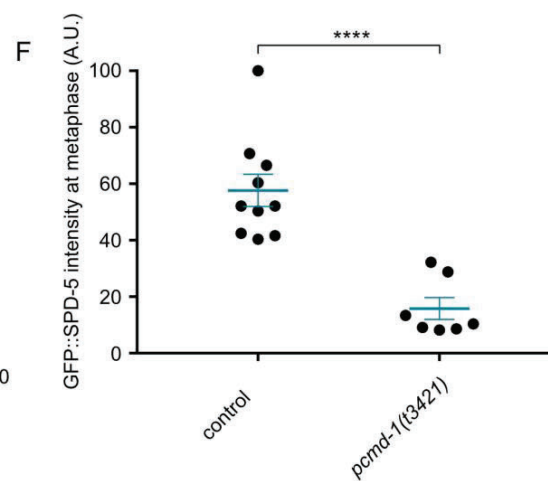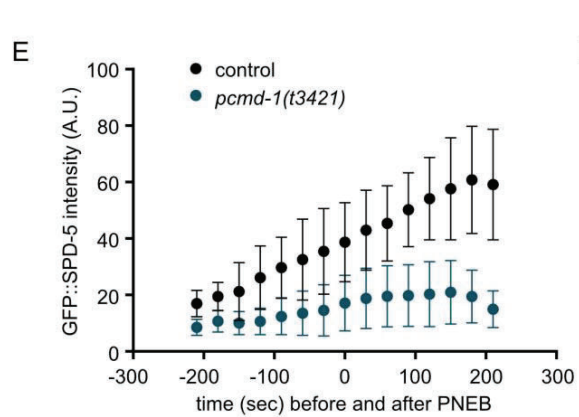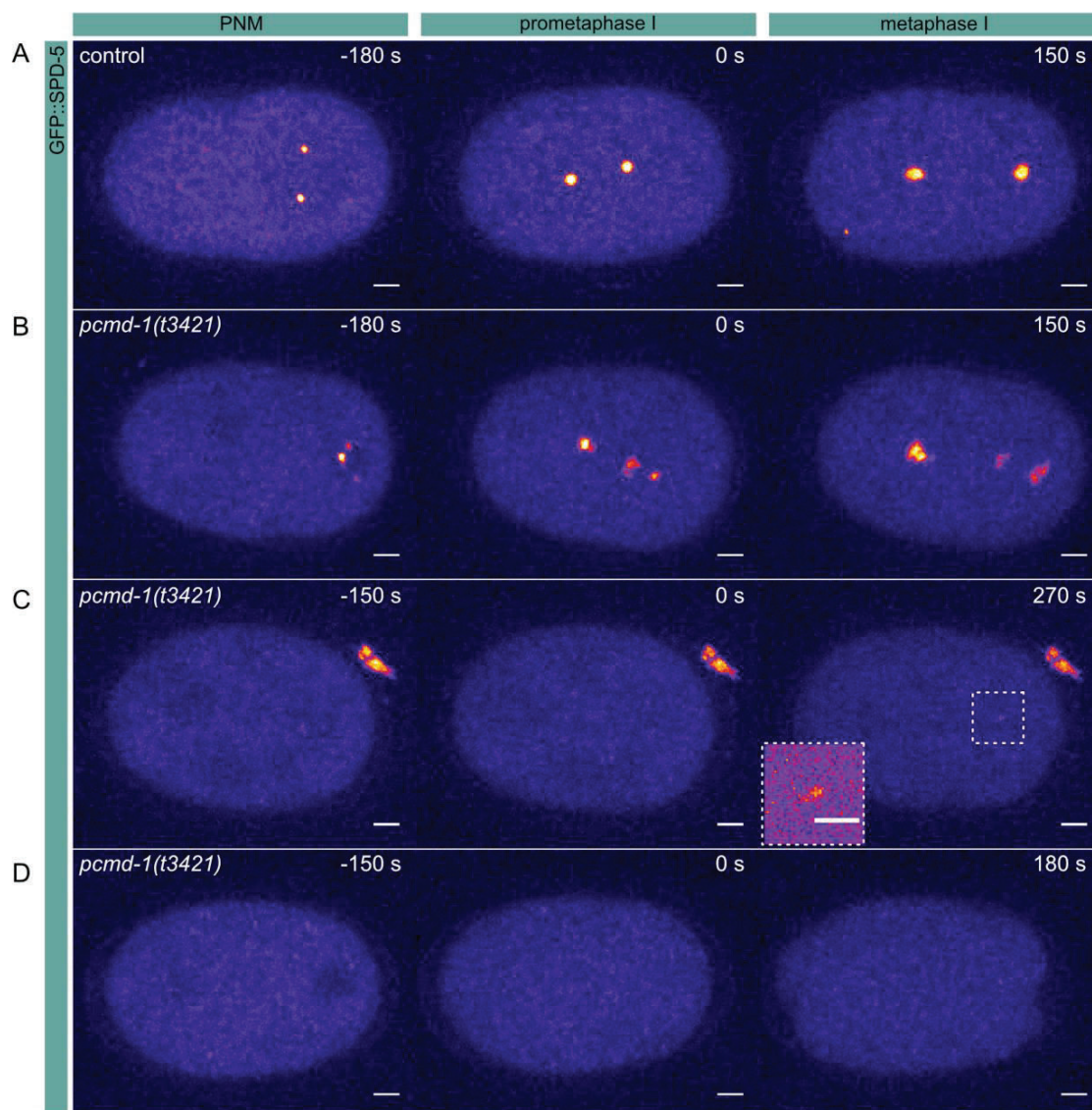
Figure 15: **Aberrant PCM formation in *pcmd-1(t3421)* mutant embryos.** Analysis of the SPD-5 centrosome matrix formation in control and *pcmd-1(t3421)* mutant embryos. SPD-5 accumulates non-spherically in *pcmd-1(t3421)* mutant embryos. (A-D) Fluorescence images of control and *pcmd-1(t3421)* mutant one-cell embryos expressing GFP::SPD-5. Images were taken at a spinning disc confocal microscope. Stages: PNM, prometaphase I and metaphase I. The anterior side of the embryo is on the left and the posterior side is on the right. Maximum projections of z-stacks through the embryo. Scale bars: 5 µm for the embryos, 3 µm for the blow-up in (C). (A) Control one-cell embryo. GFP::SPD-5 accumulates spherically at centrosomes shortly after fertilization. The signal at centrosomes increases at mitotic entry. (B) *Pcmd-1(t3421)* mutant one-cell embryo. Embryo showing high levels of GFP::SPD-5. The centrosome matrix appears highly fragmented. This phenotype was detected in 16.7% of the analyzed embryos. (C) *Pcmd-1(t3421)* mutant one-cell embryo. Embryo showing low levels of GFP::SPD-5. Also here, a fragmentation of the matrix was observed. This phenotype was detected in 41,6% of the analyzed embryos. Magnification of GFP::SPD-5 accumulation: Z-stack of 3 planes. (D) *Pcmd-1(t3421)* mutant one-cell embryo. Embryo showing no GFP::SPD-5 at any cell cycle stage. This phenotype was detected in 41,7% of the analyzed embryos. (E) Intensity quantifications of GFP::SPD-5 accumulations in control and *pcmd-1(t3421)* mutant embryos over time (shortly after fertilization until end of cell cycle I; control: n = 10, *pcmd-1(t3421)*: n = 4). The number of n states the embryos measured in total. The radius of measured volume: 2.491 µm. Intensity measurements were performed using TrackMate (Jaqaman, Loerke and Mettlen, 2008). (F) Intensity quantifications of GFP::SPD-5 accumulation in control and *pcmd-1(t3421)* mutant embryos at metaphase I. The difference in intensity between control and *pcmd-1(t3421)* embryos is significant. (control: n = 10, *pcmd-1(t3421)*: n = 7, p-value: < 0.0001). The number of n states the embryos measured in total. The radius of measured volume: 2.491 µm. Intensity measurements were performed using TrackMate (Jaqaman, Loerke and Mettlen, 2008).

79
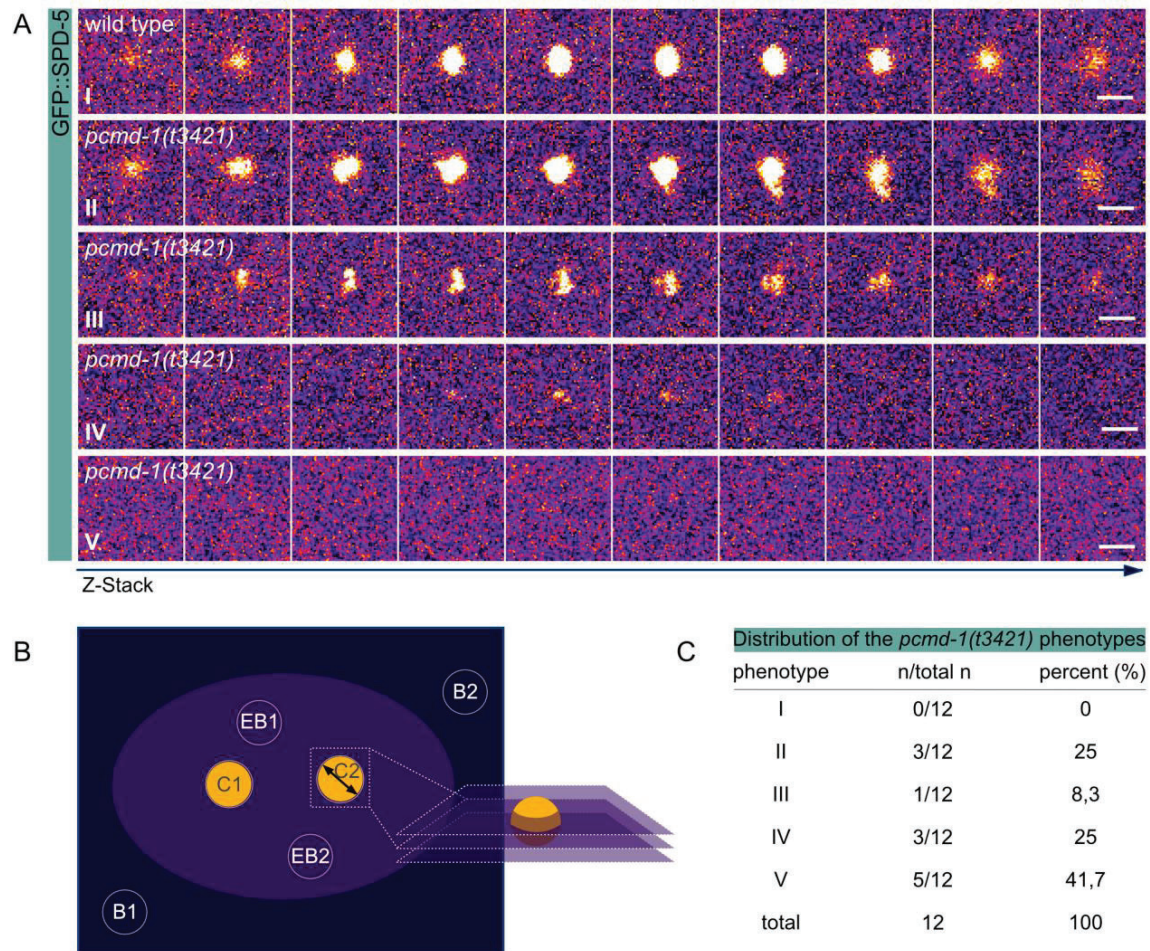
Figure 16: **Aberrant PCM formation in *pcmd-1(t3421)* mutants in mitosis.** GFP::SPD-5 measurements in control and *pcmd-1(t3421)* mutant embryos. The *pcmd-1(t3421)* centrosome matrix fragmentation phenotype is diverse. (A) Fluorescence images of GFP::SPD-5 accumulations in control and *pcmd-1(t3421)* mutant one-cell embryos expressing GFP::SPD-5. Images were taken at a spinning disc confocal microscope. Single z-planes through GFP::SPD-5 accumulations are shown. Stages: Metaphase I. Scale bar: 3 µm. (B) Scheme of GFP::SPD-5 signal quantifications. GFP intensities were measured through z-stacks using track mate. Radius: 2.491 µm. Measurements of the image background (B1 and 2), embryo background (EB1 and 2), and GFP::SPD-5 accumulations (C1 and 2) were taken. (C) Table showing the frequencies of GFP::SPD-5 phenotypes in *pcmd-1(t3421)* mutants (n = 12). The number of n states the embryos counted in total. Frequencies are shown in percentages. Data were taken from fluorescence recordings taken at a spinning disc confocal as shown in Figure 16B. Intensity cut-off values: I: >35%, II: >10%, III: >9.1%, IV: >8% (or still detectable by eye), V: ≤8 (or not detectable by eye).

3.1.5. PCMD-1 cooperates with key centrosomal components and ensures structured centrosome matrix formation in the *C. elegans* one-cell embryo

As known from other organisms, CDK5RAP2^{SPD-5} is part of a conserved module, which ensures efficient PCM formation in mitosis (Conduit *et al.*, 2014). CDK5RAP2^{SPD-5} forms this module together with pericentrin, the kinase PLK1^{PLK-1}, and Cep192^{SPD-2}. It was shown in *C. elegans* that SPD-5 could undergo a conformational change and thereby transition into a self-assembly competent state. The protein can then form micrometer-sized porous networks *in vitro* (Woodruff *et al.*, 2015). Moreover, phosphorylation by PLK-1, beginning with the mitotic entry *in vivo*, strongly accelerates the self-assembly rate of SPD-5 (Woodruff *et al.*, 2015; Wueseke *et al.*, 2016). Further, the centrosomal protein SPD-2 is required for centrosome matrix expansion upon mitotic entry (Kemp *et al.*, 2004; Pelletier *et al.*, 2004; Decker *et al.*, 2011). SPD-2 was shown to also accelerate SPD-5 self-assembly into networks *in vitro* (Woodruff *et al.*, 2015).

As described above, GFP::SPD-5 is absent from non-mitotic centrosomes in *pcmd-1(t3421)* mutant embryos, suggesting that PCMD-1 is required for the PCM core formation. However, in metaphase, more than half of the *pcmd-1(t3421)* mutants accumulate some PCM on at least one of the centrosomes (n = 7 of 12). Since SPD-2 and PLK-1 have been previously shown to be required for efficient SPD-5 self-assembly, I examined their role in establishing the remaining GFP::SPD-5 formations in the *pcmd-1(t3421)* mutant. To test whether SPD-2 and PCMD-1 genetically interact or work in parallel to organize PCM recruitment, GFP::SPD-5 localization to the centrosome was monitored in *pcmd-1(t3421)* mutants exposed to *spd-2* RNAi (RNAi experiments performed by M. Antoniolli, live imaging performed together with M. Antoniolli). In control embryos, treated with control *mock* RNAi, GFP::SPD-5 is recruited to centrosomes after fertilization and PCM expansion takes place normally (n = 10, Figure 17A and E). Further, control *pcmd-1(t3421)* mutant embryos show the anticipated phenotype, with most embryos (83 %) not recruiting GFP::SPD-5 to centrosomes after fertilization, and a severely reduced and fragmented PCM phenotype during mitosis (n = 6, Figure 17B and E). As previously reported, in *spd-2* RNAi treated control embryos, GFP::SPD-5 still localized to centrioles, but mitotic PCM expansion is not taking place (n = 10, Figure 17C and E; Kemp *et al.*, 2004; Pelletier *et al.*, 2004). GFP::SPD-5 is completely absent in *pcmd-1(t3421)* mutant embryos treated with *spd-2* RNAi, indicating an additive role of PCMD-1 and SPD-2 in GFP::SPD-5 recruitment (n = 10, Figure 17D and E). Due to the complete lack of detectable GFP::SPD-5 signal in *spd-2* RNAi treated

pcmd-1(t3421) embryos, intensity measurements were not performed. Overall the results suggest a collaborative role of PCMD-1 and SPD-2 in mitotic PCM expansion.
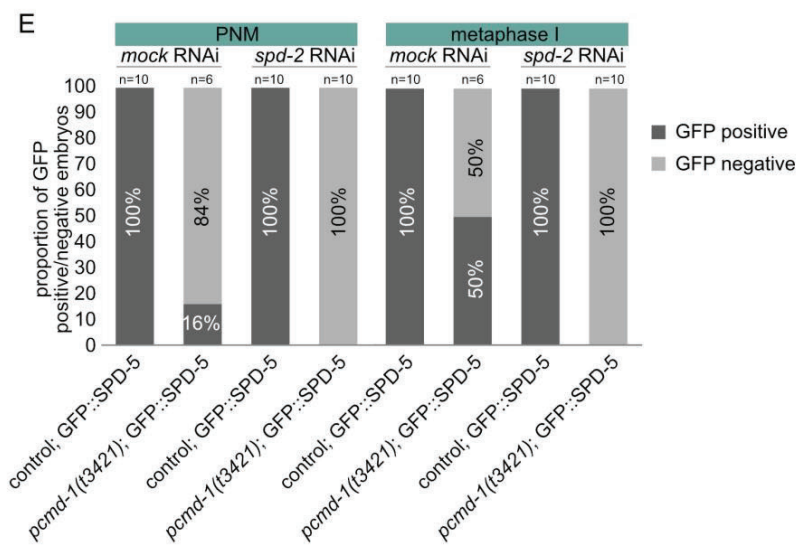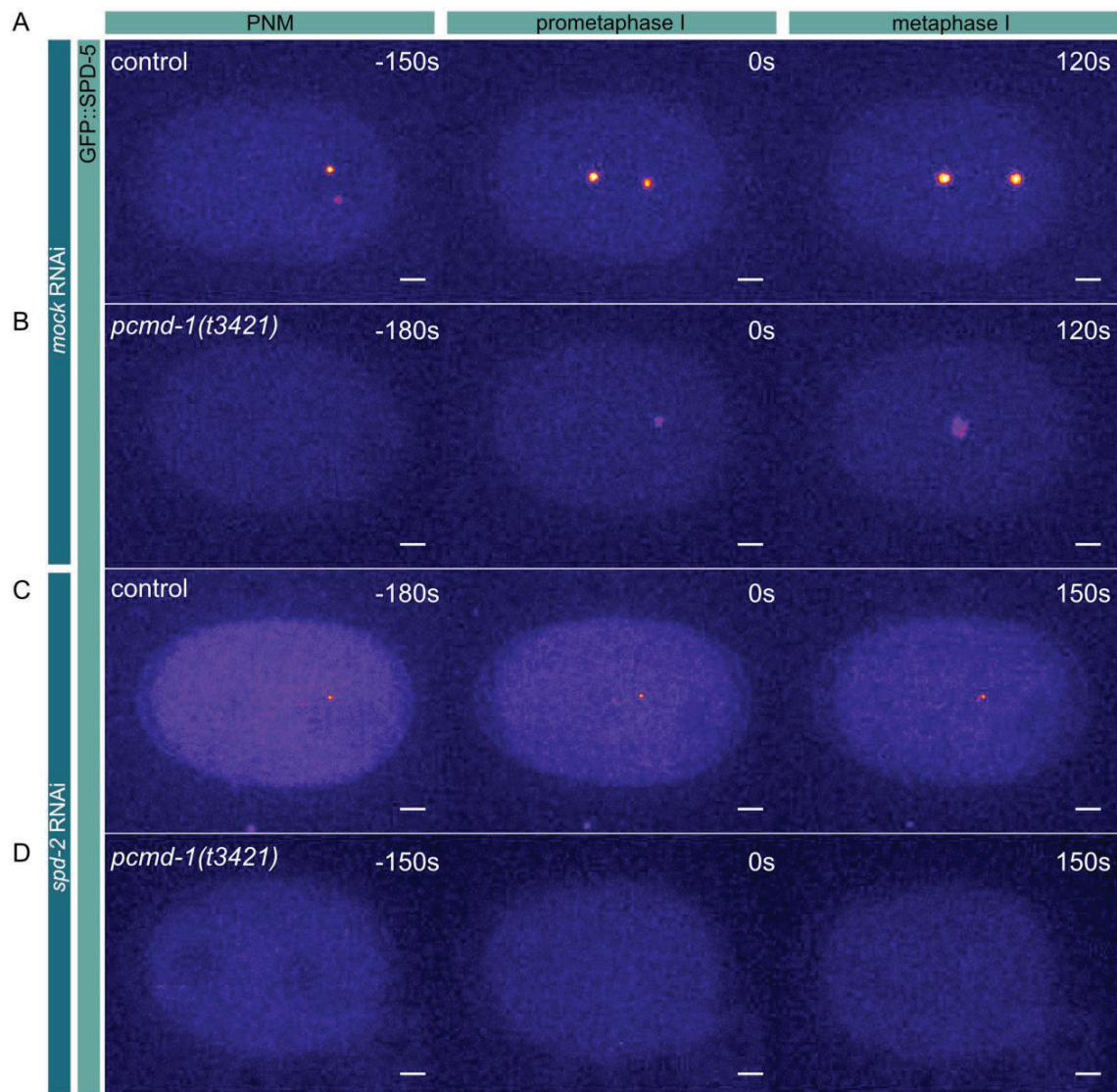
Figure 17: **PCMD-1 and SPD-2 collaborate for mitotic PCM formation.** Analysis of the SPD-5 centrosome matrix formation in control and *pcmd-1(t3421)* mutant embryos treated by *mock* and *spd-2* RNAi. Downregulation of SPD-2 eliminates residual GFP::SPD-5 accumulation in *pcmd-1(t3421)* mutant embryos. (A-D) Fluorescence images of control and *pcmd-1(t3421)* mutant one-cell embryos expressing GFP::SPD-5 treated by RNAi. Images were taken at a spinning disc confocal microscope. Stages: PNM, prometaphase I and metaphase I. The anterior side of the embryo is on the left and the posterior side is on the right. Maximum projections of z-stacks of 29 planes through the embryo. Scale bars: 5 μm for the embryos. (A) Control one-cell embryo treated with *mock* RNAi. GFP::SPD-5 accumulates spherically at centrosomes shortly after fertilization, as previously described for embryos not treated with RNAi. The signal at centrosomes increases at mitotic entry. (B) *Pcmd-1(t3421)* mutant one-cell embryos treated with *mock* RNAi. GFP::SPD-5 accumulates only around metaphase and appears fragmented, as previously described for embryos not treated by RNAi. (C) Control one-cell embryo treated with *spd-2* RNAi. GFP::SPD-5 localizes to centrosomes shortly after fertilization. If SPD-2 is downregulated, the PCM does not expand upon mitotic entry. (D) *Pcmd-1(t3421)* mutant one-cell embryos treated with *spd-2* RNAi. GFP::SPD-5 does not accumulate at any structure at any cell cycle stage. (E) Analysis of GFP::SPD-5 centrosome matrix protein accumulations in control and *pcmd-1(t3421)* mutant embryos treated by *mock* and *spd-2* RNAi. Embryos were categorized according to their potential to accumulate GFP::SPD-5 during PNM and metaphase I. Since no GFP::SPD-5 signal is detectable in *pcmd-1(t3421)* mutant embryos treated by *spd-2* RNAi, no intensity measurement were performed. The number of n states embryos counted in total.

Next, I analyzed the role of PLK-1 in the formation of residual GFP::SPD-5 accumulations in *pcmd-1(t3421)* mutant embryos. As mentioned earlier, PLK-1 phosphorylates SPD-5 to initiate mitotic centrosome expansion. Thus, PLK-1 might facilitate the residual SPD-5 accumulations similar to SPD-2. I used RNAi to downregulate PLK-1. However, since strongly penetrant *plk-1* RNAi conditions (25 °C for 16 h) lead to embryonic arrest as single cells (Chase *et al.*, 2000), I employed a milder RNAi treatment at 20 °C for 24 h. Control embryos exposed to *mock* RNAi did phenotypically not differ from untreated wild-type embryos (Figure 18A and B). The temperature-sensitive *pcmd-1(t3421)* mutants exposed to a semi-permissive temperature of 20 °C, and treated by *mock* RNAi, can recruit GFP::SPD-5 to centrosomes before mitotic entry (Figure 18A and B). In metaphase I, these embryos do

form bipolar spindles. However, under these conditions, the PCM does appear highly fragmented and instable (Figure 18A and B). Control embryos exposed to the mild *plk-1* RNAi do localize GFP::SPD-5 at centrosomes, but mitotic expansion of the PCM is compromised (Figures 17A and B, note here that the PNEB does not take place in *plk-1* RNAi treated embryos (Chase *et al.*, 2000; Rahman *et al.*, 2015). Since, at 20 °C, *mock* RNAi treated *pcmd-1(t3421)* mutant embryos still localize GFP::SPD-5 to the centrosome before mitotic entry (before mitotic onset of SPD-5 phosphorylation by PLK-1), and since the mild *plk-1* RNAi alone is only compromising PCM expansion, I would expect that *pcmd-1(t3421)* mutant embryos, exposed to mild *plk-1* RNAi, are still accumulating reduced levels of GFP::SPD-5 at centrosomes prior to mitotic onset. Further, I would expect that the expansion of the PCM does not take place, as expected for an additive effect of the PCMD-1 and PLK-1 compromised functions. Importantly, not any GFP signal was detectable in 83 % of the embryos (n=24, Figures 18A and B). The embryos appeared extremely sick and arrested in development as single cells (Figures 18A and B). This experiment suggests that the partial downregulation of the two proteins has a synergistic effect, indicating a genetic interaction of PCMD-1 and PLK-1 that remains to be investigated.
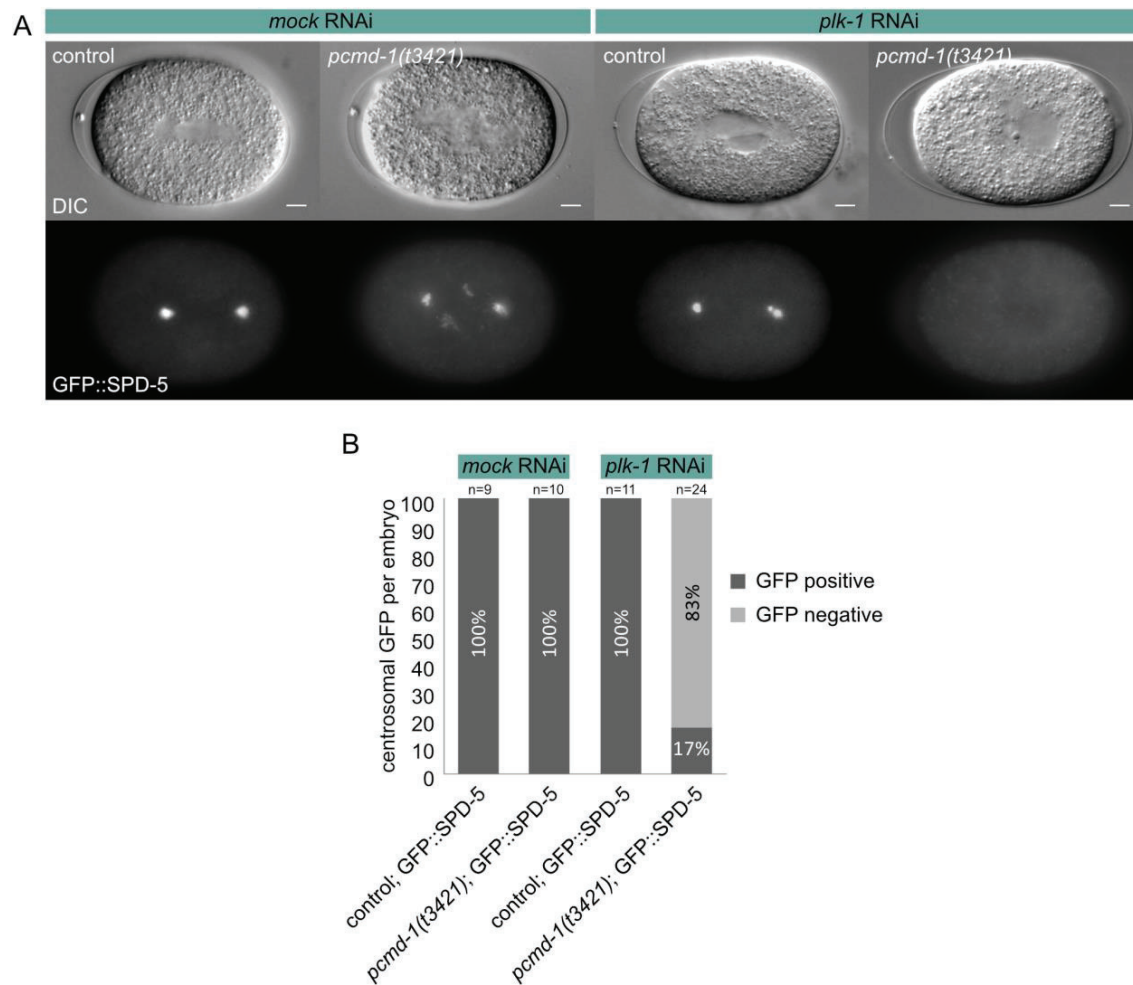
Figure 18: **PCMD-1 and PLK-1 facilitate SPD-5 centrosome matrix formation**. Analysis of the SPD-5 centrosome matrix formation in control and *pcmd-1(t3421)* mutant embryos treated by *mock* and *plk-1* RNAi. Downregulation of PLK-1 eliminates residual GFP::SPD-5 accumulation in *pcmd-1(t3421)* mutant embryos. (A) Fluorescence images of control and *pcmd-1(t3421)* mutant one-cell embryos expressing GFP::SPD-5 treated by RNAi. Images were taken at a 4D microscope. Stages: metaphase I. The anterior side of the embryo is on the left, and the posterior side is on the right. Scale bars: 5 μm. Control embryos treated by *mock* RNAi show normal GFP::SPD-5 accumulation at centrosomes. *Pcmd-1(t3421)* mutant embryos treated with *mock* RNAi show fragmented GFP::SPD-5 accumulations. Control embryos treated with *plk-1* RNAi show reduced GFP::SPD-5 PCM expansion at metaphase. *Pcmd-1(t3421)* mutant embryos treated with control *plk-1* RNAi lack detectable GFP::SPD-5 accumulations. Only 17% of the embryos have residual GFP::SPD-5 signal (n = 24). (B) Analysis of GFP::SPD-5 accumulations in control and *pcmd-1(t3421)* mutant embryos treated by *mock* and *plk-1* RNAi. Embryos were categorized according to their potential to

accumulate GFP::SPD-5 at metaphase I. Since no GFP::SPD-5 signal is detectable in *pcmd-1(t3421)* mutant embryos treated by *plk-1* RNAi, no intensity measurements were performed. The number of n states embryos counted in total.

Subsequently, I investigated how SPD-2 is regulated at the centrosome in *pcmd-1(t3421)* mutant embryos. To analyze SPD-2 recruitment to centrosomes, the *ItIs69[ppie-1:mcherry::spd-2]* allele was crossed into the *pcmd-1(t3421)* mutant. In the control embryo, mCherry::SPD-2 localizes to centrosomes (Figure 19A, n=1). It was previously shown that a centriolar and a PCM pool of SPD-2 exist (Kemp *et al.*, 2004; Pelletier *et al.*, 2004). The PCM levels were diminished in recordings of mCherry::SPD-2 expressing *pcmd-1(t3421)* mutant embryos, similarly to what I previously described for GFP::SPD-5 in *pcmd-1(t3421)* mutants. However, at the center of a spindle, SPD-2 was still present in those embryos (Figure 19B, n=2). In the gonad of mCherry::SPD-2 expressing mutant embryos, the protein still localized to centrioles (n=4, control: n=4; data not shown). The data suggest that only the PCM pool of SPD-2 is recruited to the centrosome downstream of PCMD-1.
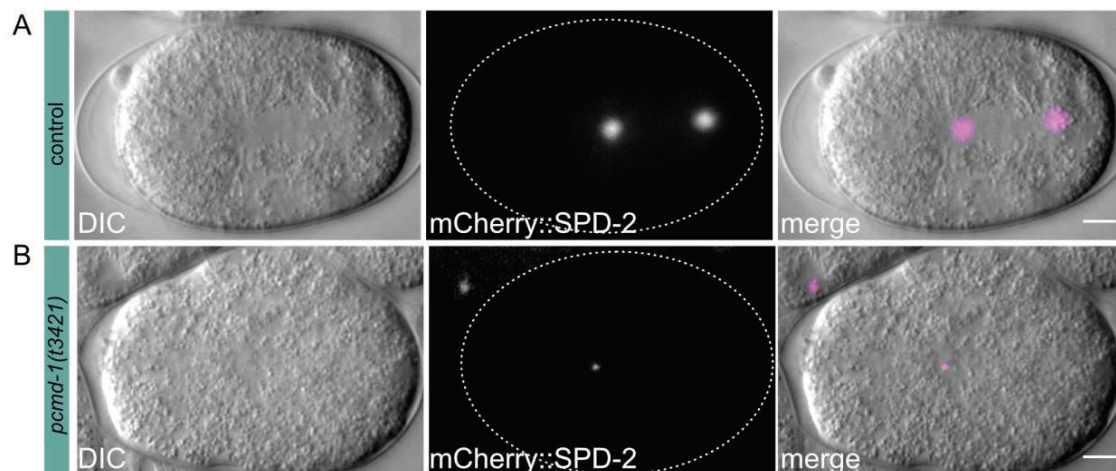
Figure 19: **SPD-2 is present at centrioles in *pcmd-1(t3421)* mutant embryos.** Analysis of the SPD-2 centrosome matrix formation in control and *pcmd-1(t3421)* mutant embryos. Fluorescence images of control and *pcmd-1(t3421)* mutant one-cell embryos expressing mCherry::SPD-2. Images were taken at a 4D microscope. Stages: metaphase I. The anterior side of the embryo is on the left, and the posterior side is on the right. Scale bars: 5 µm. (A) Control embryos show mCherry::SPD-2 localizing to the expanded PCM. (B) In *pcmd-*

1(t3421) mutant embryos mCherry::SPD-2 does not expand. A weak fluorescent signal is still visible at the center of the monopolar spindle.

As mentioned above, PLK-1 is the kinase that phosphorylates the centrosome matrix protein SPD-5 upon mitotic entry for SPD-5 transition into a self-assembly competent state, and thus, triggers PCM expansion (Wueseke *et al.*, 2016). PLK-1 was shown to localize to centrosomes and kinetochores in *C. elegans* (Chase *et al.*, 2000). To test for abnormalities of PLK-1 dynamics in *pcmd-1(t3421)* mutant embryos, a strain, carrying the *it18[[plk-1::sgfp]::loxp]* single-insertion and *pcmd-1(t3421)* mutant alleles, was generated. Control embryos showed robust PLK-1::sGFP accumulation at centrosomes shortly after fertilization, and an increase of intensity at centrosomes until metaphase as the cell cycle progresses (data not shown, Wang *et al.*, 2017). PLK-1::sGFP also localizes to kinetochores upon nuclear envelope breakdown (data not shown, Wang *et al.*, 2017). In contrast, the PLK-1::sGFP signal is barely detectable at centrosomes in *pcmd-1(t3421)* mutant embryos. Moreover, the PLK-1::sGFP signal does not expand in mutants upon mitotic entry (data not shown).

The residual PLK-1::sGFP at centrosomes might be recruited by the other components of the conserved centrosome module, namely SPD-5 or SPD-2. To distinguish the cell cycle stages more easily, the *itIs37[ppie-1:mcherry::h2b:pie-1]* allele was crossed into the strains that carry the *it18[[plk-1::sgfp]::loxp]* allele in either control or *pcmd-1(t3421)* mutant background (Table 1, cross done by M. Museridze). SPD-5 is not or barely detectable at centrosomes in 67% of *pcmd-1(t3421)* mutants (Figure 15 C and D, Figure 16A and C, phenotype IV and V). Thus, SPD-5 is unlikely responsible for residual PLK-1::sGFP recruitment to centrosomes in the mutants. To proof this, *spd-5* RNAi was employed to downregulate the protein in control and *pcmd-1(t3421)* mutant embryos. As expected, in control embryos exposed to *mock* RNAi, PLK-1::sGFP localizes to centrosomes and kinetochores (n = 9; Figure 20A, Figure 21A). In *pcmd-1(t3421)* mutants treated with *mock* RNAi, signal intensity is strongly reduced, but a small fraction of PLK-1::sGFP is still detectable at centrosomes (n = 8; Figure 20B, Figure 21A). When control embryos were exposed to *spd-5* RNAi, PLK-1::sGFP does still localize to centrosomes. However, the signal intensity does not increase towards metaphase (n = 8; Figure 20C, Figure 21A). As expected, in *spd-5* RNAi treated *pcmd-1(t3421)* mutant embryos, PLK-1::sGFP is still present at centrosomes, and only PCM expansion is compromised as seen for control embryos (n = 7; Figure 20D, Figure 21A). To determine PLK-1 recruitment efficiency to centrosomes, PLK-

1::sGFP intensities were measured in control and mutant background. Measurements were taken before PNEB, to ensure that the kinetochore PLK-1::sGFP protein pool accumulating upon mitosis was not mistaken for the centrosomal fraction of the protein (Figure 21B). The overall signal intensity of PLK-1::sGFP at centrosomes is drastically reduced in *pcmd-1(t3421)* mutant embryos exposed to *mock* RNAi, and the residual signal is barely detectable by eye. In control embryos exposed to *spd-5* RNAi, PLK-1::sGFP is reduced at centrosomes. However, the signal is not significantly different from *pcmd-1(t3421)* mutant embryos treated with control RNAi. Further, in *pcmd-1(t3421)* embryos treated with *spd-5* RNAi, PLK-1::sGFP levels are reduced. The signal intensity is not significantly different from *pcmd-1(t3421)* mutant embryos treated with control RNAi, and PLK-1::sGFP is still detectable at centrosomes. Taken together, the results show that PCMD-1 is critical for efficient PLK-1 recruitment to centrosomes and that SPD-5 does not recruit residual PLK-1::sGFP to centrosomes in *pcmd-1(t3421)* mutant embryos. On the other hand, SPD-2 is still present at centrioles in *pcmd-1(t3421)* mutant embryos (Figure 19). Further, SPD-2 was shown to be required for PLK-1 recruitment to the PCM (Decker *et al.*, 2011), and thus might recruit the residual PLK-1::sGFP to centrosomes in *pcmd-1(t3421)* mutant embryos. To test this possibility, *spd-2* RNAi was used to downregulate the protein in control and mutant embryos. Importantly, PLK-1::sGFP was not detectable at centrosomes in *spd-2* RNAi treated control embryos (n = 9; Figure 20E, Figure 21A). As expected, none of the *spd-2* RNAi treated *pcmd-1(t3421)* mutant embryos recruit PLK-1::sGFP to centrosomes (n = 10; Figure 20F, Figure 21A). Since PLK-1::sGFP is not detectable in *spd-2* RNAi treated embryos, no GFP intensity measurements were performed. Taken together the results suggest that the centriolar PLK-1 pool is recruited to centrosomes by SPD-2 in *C. elegans*.
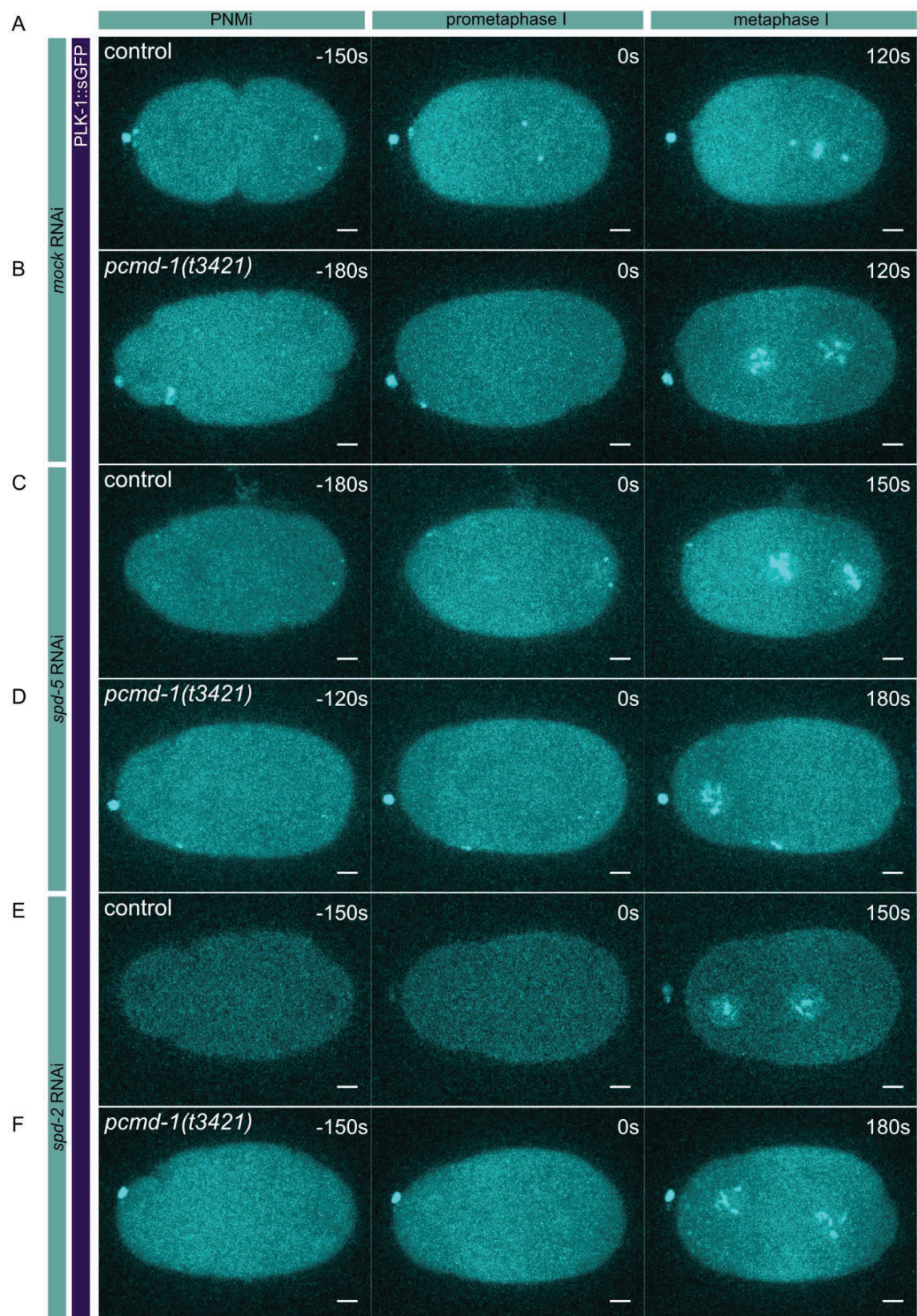
Figure 20: **PLK-1 localization to centrosomes depends on SPD-2**. Analysis of the PLK-1 recruitment to the PCM in control and *pcmd-1(t3421)* mutant embryos treated by *mock*, *spd-5,* and *spd-2* RNAi. Fluorescence images of control and *pcmd-1(t3421)* mutant one-cell embryos expressing PLK-1::sGFP treated by RNAi. Images were taken at a spinning disc confocal microscope. Stages: PNMi, prometaphase I, and metaphase I. The anterior side of the embryo is on the left, and the posterior side is on the right. Maximum projections of z-stacks through the embryo. Scale bars: 5 µm for the embryos. (A) Control one-cell embryo treated with *mock* RNAi. PLK-1::sGFP normally accumulates at centrosomes shortly after fertilization. The signal at centrosomes normally increases at mitotic entry, and upon nuclear envelope breakdown, PLK-1::sGFP localizes to the DNA. (B) *Pcmd-1(t3421)* mutant embryos treated with *mock* RNAi. PLK-1::sGFP is strongly reduced but still detectable in these embryos. (C-D) Control and *pcmd-1(t3421)* mutant embryos treated with *spd-5* RNAi. PLK-1::sGFP is strongly reduced but still detectable in these embryos. (E-F) In *spd-2* RNAi treated control and *pcmd-1(t3421)* mutant embryos, PLK-1::sGFP is not detectable.
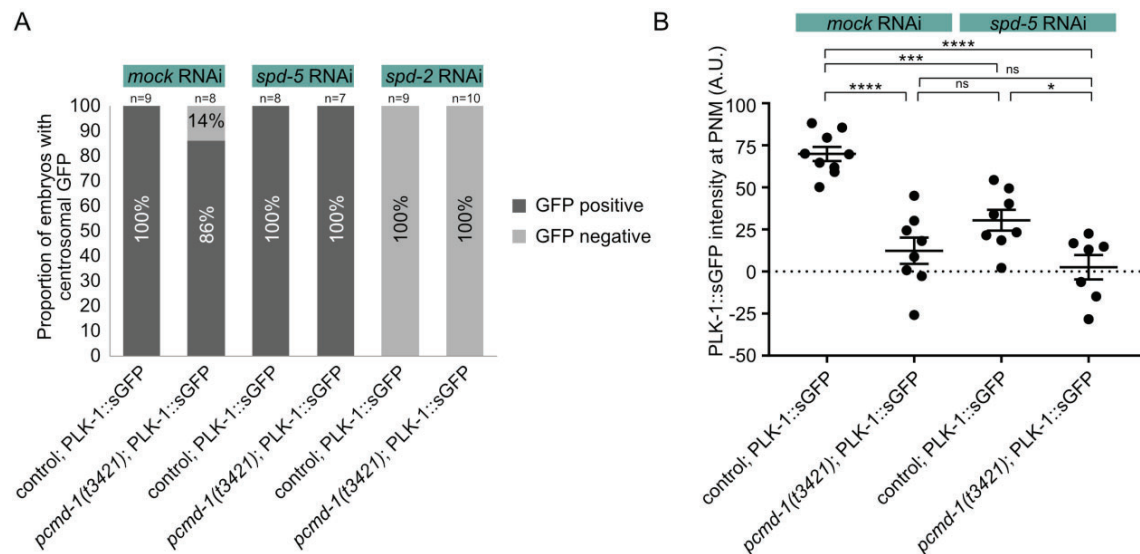
Figure 21: **Analysis of PLK-1::sGFP centrosome recruitment** in control and *pcmd-1(t3421)* mutant embryos treated by *mock*, *spd-5,* and *spd-2* RNAi (Figure 20). (A) Embryos were categorized according to their potential to accumulate PLK-1::sGFP before PNEB. The number of n states embryos counted in total. (B) Intensity measurements of PLK-1::sGFP at centrosomes in control and *pcmd-1(t3421)* mutant embryos treated with *mock* and *spd-5* RNAi. The radius of measured volume: 1.021 µm. Note here that negative intensity values

can occur if the measured background levels are higher than measured values in an area that contains very low residual PLK-1::sGFP signal. Since no PLK-1::sGFP signal is detectable in *pcmd-1(t3421)* mutant embryos treated by *spd-2* RNAi, no intensity measurement was performed for these embryos. Intensity measurements were performed using TrackMate (Jaqaman, Loerke and Mettlen, 2008). The number of n states embryos measured in total.

PCMD-1 appears to be part of the conserved centrosome module. Thus, the centrosomal localization of PCMD-1 itself might be regulated by the components of the centrosome module, namely SPD-5, SPD-2 or PLK-1. Therefore, the *spd-2(or298)* and *spd-5(or213)* mutants were each crossed to the *mikSi5[pmex-5:mkate2::pcmd-1(c17d12.7):tbb2]* allele to monitor PCMD-1 recruitment in the *spd-2* and *spd-5* mutant backgrounds (Table 1). In *spd-2(or298)* and *spd-5(or213)* mutants, mKate2::PCMD-1 is still present at centrioles in the gonad at restrictive temperature of 25 ºC (data not shown, and Figure 22A and B, respectively). The result was further validated in embryos by monitoring GFP::PCMD-1[syb486] in *spd-5(or213)* and *spd-2(or293)* embryos (experiment done by T. Mikeladze-Dvali, Erpf *et al.,* 2019). Thus, PCMD-1 localization to centrosomes is independent of SPD-2 and SPD-5. These conclusions can only be made for a fraction of PCMD-1 localizing to the centriole since the PCM fraction of PCMD-1 is not detectable with conventional confocal microscopy. Similarly, in embryos depleted of PLK-1 by *plk-1* RNAi, GFP::PCMD-1 is still present at centrioles (experiment by Tamara Mikeladze-Dvali, Erpf *et al.,* 2019). Again, this can only be inferred for the centriolar fraction of PCMD-1.
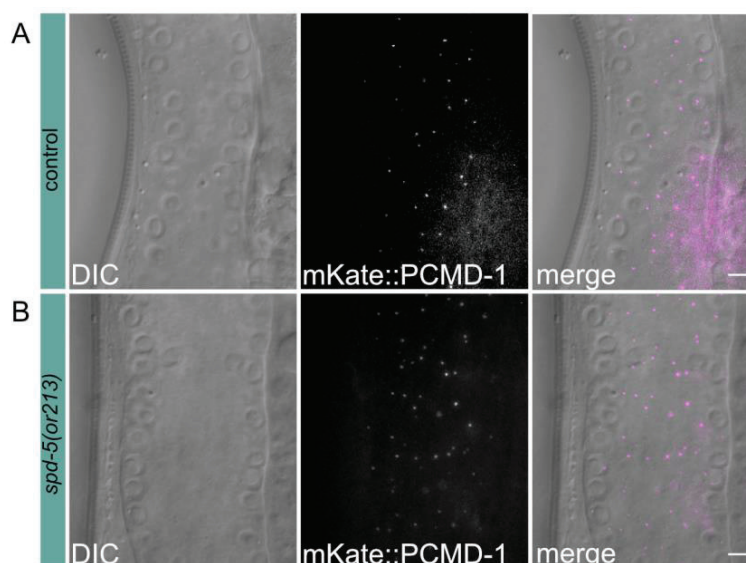
Figure 22: **PCMD-1 localization to centrosomes does not depend on SPD-5**. MKate2::PCMD-1 still localizes to centrosomes in *spd-5(or213)* mutant embryos at the restrictive temperature. DIC (single planes) and fluorescence images (maximum intensity projections of 6 planes through part of gonad) of control and *pcmd-1(t3421)* mutant gonads expressing mKate2::PCMD-1. Images were taken at a 4D microscope. Stages: adult. Scale bars: 5 µm. (A) Control embryos show mKate2::PCMD-1 localizing to centrioles. (B) In *spd-5(or213)* mutant embryos mKate2::PCMD-1 does still localize to centrioles.

Taken together, PCMD-1 interacts with the conserved SPD-5/SPD-2/PLK-1 centrosome module in *C. elegans*. The interaction suggests that it might be the homologue of pericentrin. However, a BLAST search (NCBI BLAST) for homologues only shows conservation of the protein among nematodes (Figure 23, Table 9). Thus, similar to other centrosomal proteins such as SPD-5 or ZYG-1, PCMD-1 could represent a functional homologue of human pericentrin (Tsou *et al.*, 2009; Kim, Lee and Rhee, 2015).
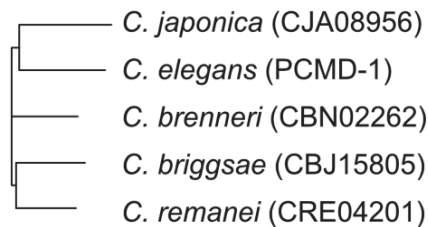
Figure 23: **Homology analysis for the PCMD-1 protein across nematode species**. Homology tree generated from protein sequence comparisons between PCMD-1 and homologues found in other nematode species by BLAST search (https://www.ebi.ac.uk/Tools/sss/ncbiblast/).

3.2. Establishing the IL1 neuron lineage to study asymmetric centrosome inheritance in *C. elegans*

Based on the invariant cell lineage of *C. elegans* and the transparency of the worm, the fate of individual cell lineages can be followed by conventional DIC microscopy throughout embryo development. In the IL1 neuron lineage, the IL1 neuroblast divides asymmetrically and generates two daughters adopting different fates, the ciliated IL1 sensory neuron and its sister cell, which undergoes apoptosis. Thus, this cell lineage gives rise to one daughter that requires centrioles/basal bodies post-mitotically for cilia formation. I established the IL1 lineage as a model system to study asymmetric centrosome inheritance in *C. elegans*.

3.2.1. IL1 neurons elongate their dendrites via retrograde extension during *C. elegans* development

To monitor the IL1nb division, different promoters were considered. Based on their expression pattern, transgenic animals carrying the *kdIs66[agr-1:gfp]* were analyzed. Under the *agrin-1* promoter, GFP is strongly expressed in the dorsal and ventral IL1 neurons (IL1DL, IL1DR, IL1VL, IL1VR) throughout all larval stages and in the adult. Further, GFP is weakly expressed in the lateral IL1 neurons (IL1L and IL1R) until the L1 larval stage. Also, the buccal epithelial cells are labeled (Hrus *et al.*, 2007). To define when the *agrin-1* promoter starts to be expressed in the IL neuron lineage, I characterized the expression in the lineage at a 4D microscope and by confocal microscopy in the *C. elegans* embryo. The *agrin-1* promoter drives the expression of GFP in the IL neuron lineage from 320 min after the first embryonic cell division (Figure 24A). Thus GFP expression starts before the IL1nb division takes place, allowing me to monitor early events in this lineage (Figure 24A; Sulston and Schierenberg, 1983; *WormAtlas 1.0*). During my analysis, I noticed that the IL1 neurons form a dendrite by retrograde extension. While the dendritic tip stays anchored in place, the cell body of these neurons migrates backward, and the dendrite is formed (Figure 24B and C). Heiman *et al.* (2009) were the first to describe the mechanism of retrograde dendrite extension for the amphid neurons (Heiman and Shaham, 2009). It was later shown that the ciliary transition zone is required for dendrite anchoring of these neurons (Schouteden *et al.*, 2015). However, what seems somewhat surprising is that the IL1nb appears to be highly polarized, with a dendrite anchored and forming, before the division into the IL1 neuron and its dying sister cell takes place: In the bean stage embryo, the dendrite tip is already anchored, and a

projection is forming (Figure 24B and C). The IL1nb division occurs in the comma stage embryo around 400 min after the first embryonic cell division, and approximately 80 min after retrograde extension initiated (Figure 24A and D). The IL1 neuron and its sister cell are clearly distinguishable when the IL1sc starts rounding up towards undergoing cell death in the late embryonic 1.5-fold stage (Figure 24D). This result was completely unexpected and requires further investigation. A strain, carrying the *itIs37[ppie-1:mcherry::h2b:pie-1]* and the *kdIs66[agr-1:gfp]* alleles, was constructed, to examine the IL1nb division in more detail, and to determine the exact time point of the division (Table 1). Detailed recordings remain to be taken, and further analysis should be performed.
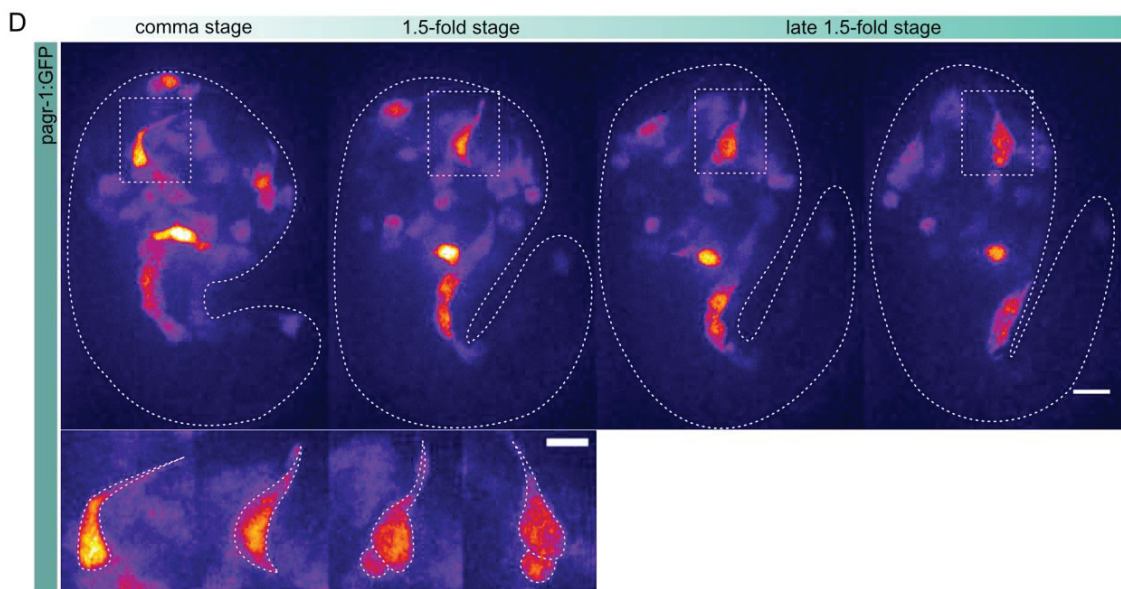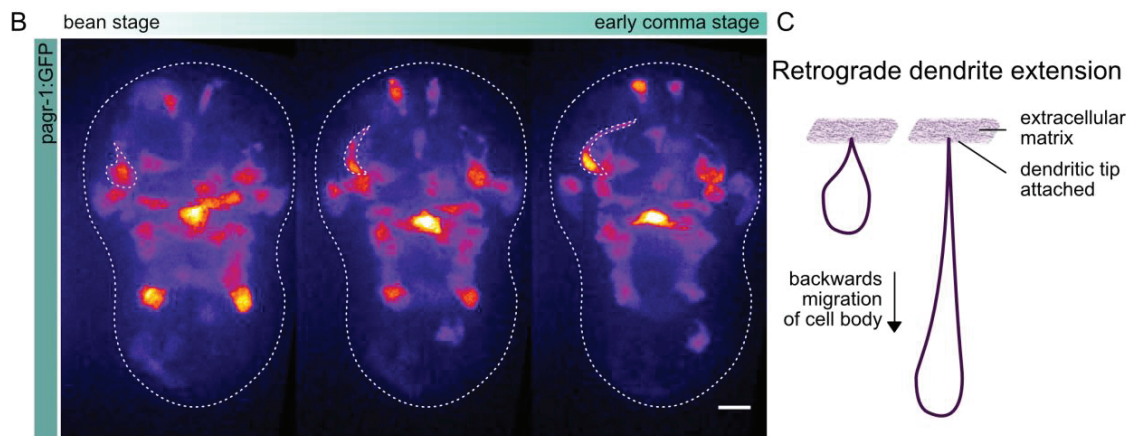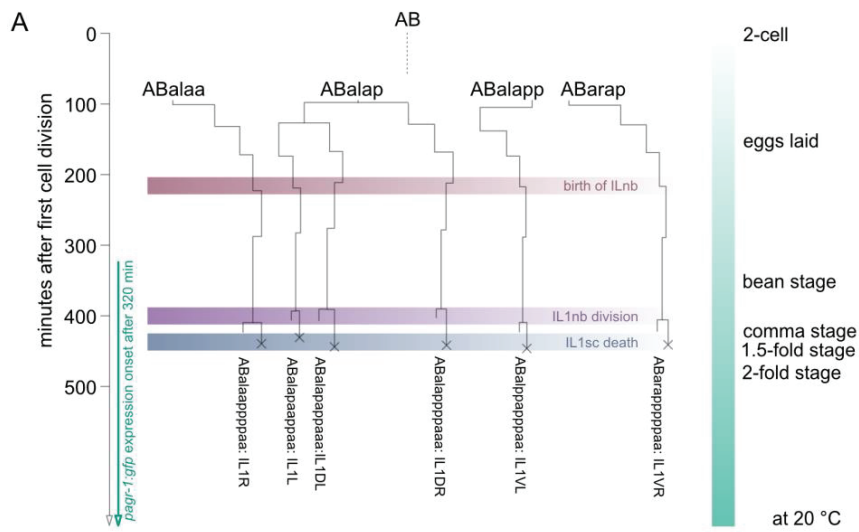
A

B bean stage — early comma stage

pagr-1:GFP

C

Retrograde dendrite extension

extracellular matrix

dendritic tip attached

backwards migration of cell body

D comma stage — 1.5-fold stage — late 1.5-fold stage

pagr-1:GFP

Figure 24: **IL1 neuron development**. (A) Cell lineages of the IL1 neurons. Lineages are displayed after the 5th cell division after fertilization. Vertical lines correspond to the time that passed after the last division. Horizontal lines indicate a cell division, which goes to the left if the anterior cell continues in the lineage, or to the right if it is the posterior cell. Timeline of the *pagrin-1* driven GFP expression in the IL neuron lineage is indicated on the left. At 20 °C, the ILnb is born about 210 min after the first cell division takes place (red bar). The IL1nb divides into the IL1 neuron, and its dying sister cell about 400 min after the first cell division takes place (purple bar). The cell death of the IL1sc takes place about 430 min after the first embryonic cell division (blue bar). Illustration partially adapted from Sulston and Schierenberg (1983), and *WormAtlas* 0.1. (B) IL1 neuron anchorage and retrograde dendrite extension. Fluorescence images of embryos with *pagrin-1* driven GFP expression between embryonic bean and comma stages. Images were taken at a spinning disc confocal microscope. The anterior side of the embryo is on the top and the posterior side is on the bottom. Maximum projections of z-stacks through the embryo. Scale bars: 5 µm. (C) Illustration of the retrograde dendrite extension in *C. elegans*. The dendritic tip attaches to an extracellular matrix, and the cell body migrates backward (adapted from Hrus *et al.*, 2007). (D) IL1nb division and IL1sc death. Fluorescence images of embryos with *pagrin-1* driven GFP expression in the embryonic comma and 1.5-fold stage. Images were taken at a spinning disc confocal microscope. The anterior side of the embryo is on the top and the posterior side is on the bottom. Maximum projections of z-stacks through the embryo. Scale bars: 5 µm for the embryo and 3 µm for the blow-ups. The IL1 neuron divides in embryonic comma stage, while the neuron is already highly polarised. The IL1sc undergoes cell death in embryonic 1.5-fold stage.

3.2.2. Centrioles/basal bodies are localizing at dendritic tips in prospective mouth region in *C. elegans*

Heiman *et al.* (2009) illustrate that dendrite anchorage, and subsequent elongation of the dendrite requires an extracellular matrix for successful attachment, namely the secreted abnormal dye filling 7 (DYF-7), and dendrite extension defective 1 (DEX-1) proteins (Heiman and Shaham, 2009). A more recent publication of Schouteden *et al.* (2015) reports a function of the ciliary transition zone in mediating dendrite attachment through interactions with this extracellular matrix (Schouteden *et al.*, 2015). The role of the ciliary transition zone in mediating adhesion of dendritic tips requires the anchorage of the basal body to the cell

membrane to serve as a template for cilium formation. In consistence with these findings, I found that in live recordings of 1.5-fold *C. elegans* embryos, carrying the *vieSiIs18[psas-4:gfp::sas-4:sas-4],* and *itIs44[ppie-1:mcherry::ph]* alleles, GFP::SAS-4 foci are detectable in a ring like structure at the prospective mouth region, where dendrites are anchoring (Figure 25). However, despite visualization of cell boundaries by mCherry::PH, it is difficult to determine whether those centrioles are localizing at dendritic tips of neurons, specifically of the IL1 neurons. To further investigate this question, an allele *mikSi10[psas-4:mkate2::sas-4:sas-4]* was made, to mark centrioles in red. The allele can be used in combination with the *kdIs66[agr-1:gfp]* allele, labeling the IL1 neurons, to determine centriole localization at the dendritic tips of IL1 neurons at different stages of dendrite formation in the embryo. Further, for a similar readout, an allele *mikSi3[pagr-1:mkate2:unc-54]*, driving the red mKate2 fluorophore expression cytoplasmically in IL1 neurons, was generated, and can be used in combination with the *vieSiIs18[psas-4:gfp::sas-4:sas-4]* allele, to mark centrioles (Table 1). However, both, the *mikSi10[psas-4:mkate2::sas-4:sas-4]* and *mikSi3[pagr-1:mkate2:unc-54]* alleles, are photo-bleaching fast and are therefore not well suitable for long term recordings. In summary, the results show that SAS-4 localizes in the region where dendrites anchor at the time of dendrite elongation. However, for the subsequent analysis, it is important to establish an imaging setup that allows to distinguish between dendrites and the correct assignment of the SAS-4 foci.
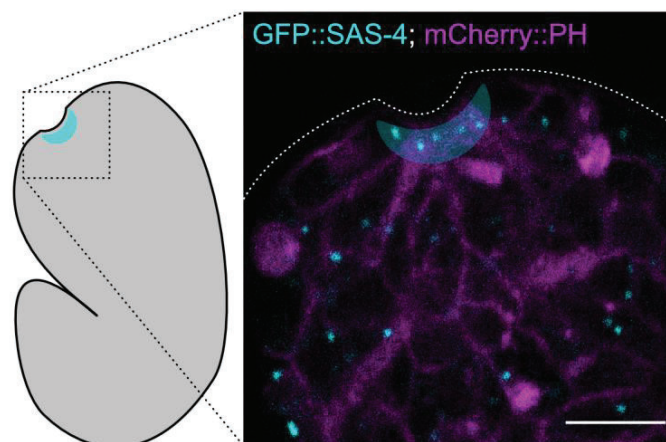

Figure 25: **Centriole localization at presumptive dendrite anchorage sites**. Centrioles localize in a ring-like structure at the mouth region of *C. elegans* 1.5-fold stage embryos.

Fluorescence image of the mouth region of a 1.5-fold stage embryo expressing GFP::SAS-4 to label centrioles and mCherry::PH to mark cell boundaries. Images were taken at a confocal. The anterior side of the embryo is on the top and the posterior side is on the bottom. Displayed is a single z-plane through the mouth region on the anterior of the embryo. Scale bars: 5 µm.

3.2.3. Analyzing the inherent age difference of mother-centrosomes and their biological function in *C. elegans*

In mammalian cell culture, it has been shown that the inherent age difference of mother-centrosomes inherited by two daughter cells entails a functional difference. The cell receiving the older mother-centrosome usually forms a primary cilium first (Anderson and Stearns, 2009). For *C. elegans* ciliated sensory neurons that form their dendrites via retrograde extension, it might be of biological relevance, which daughter cell inherits the centrosome with the older mother-centrosome. Which daughter inherits the older centrosome might be relevant since Heiman *et al*. (2009) report a critical initiation phase for the anchoring process of the dendritic tip (Heiman and Shaham, 2009). The authors report that if the dendrite is not anchored within the specific time window, dendrites do not elongate, and cilia are detected at the cell body (Heiman and Shaham, 2009). In the IL1 neuron lineage, the cell receiving the older centrosome might be competent to grow a projection soon enough to anchor within this critical initiation phase. Therefore, the older centrosome might be inherited by the IL1 neuron during the asymmetric cell division of the IL1nb. In *C. elegans*, to date, no protein was identified that associates specifically with mother- or daughter-centrioles. Hence, it is not possible to discriminate their inheritance by selectively labeling one or the other centriole specifically. To overcome this limitation, I generated the *mikSi1[psas-4:dendra2::sas-4:sas-4]* allele (Table 1; Kirkham *et al.*, 2003). Photo-conversion of the photo-switchable Dendra2 fluorophore coupled to the centriole protein SAS-4 allows to distinguish centrosome age two cell divisions after photo-conversion (Figure 26A). As a proof of principle, I tested the system in other, easier accessible embryonic lineages than the IL1 neuron lineage. The divisions of the ABprpppaa and the ABprpppap cells occur ~150 min post the four-cell stage at 25 °C. At this developmental stage, cell divisions can be monitored more easily than in a later division, such as the division of the IL1 neuroblast. Dendra2::SAS-4 was photo-converted in the grandmother cell (ABprppp) shortly after the cell was born. In the division of the ABprpppaa cell, the anterior daughter inherited the red Dendra2::SAS-4

focus in 57 % of the cases (n=7). For the division of the ABprpppap cell, the red Dendra2::SAS-4 focus partitioned into the anterior cell in 80 % of the divisions (n=5). The experiment shows, that photo-conversion of the Dendra2::SAS-4 construct works efficiently and enables to monitor mother-centrosome inheritance in *C. elegans* (Figure 26B and C). In the analyzed lineages, centrosomes are inherited randomly. However, whether centrosomes are inherited age dependently may differ between lineages and may be crucial in sensory neuron lineages that require centrosomes postmitotically.

To simplify the photo-conversion protocol in late divisions, and to circumvent possible errors during lineaging, lineage-specific promoters that are specifically expressed in the target cell are beneficial. Unfortunately, no promoter is available that drives expression specifically in the ILnb, the grandmother cell of the IL1 neuron. Thus, it is not possible to use an IL neuron lineage-specific marker to determine the time point for the Dendra2::SAS-4 photo-conversion in this lineage. However, since the *C. elegans* cell lineage is highly invariant, and because cell divisions occur at specific time points if embryos are raised at the same constant temperature, photo-conversion of centrioles ~210 min after the first cell division and subsequent imaging at the time the IL1 neurons are born, would allow to monitor the inheritance of centrosomes in the IL1 neuron lineage (Figure 24A, Figure 26A). Alternatively, if promoters in other lineages turn on at the time of the IL neuroblast division, they could be used as an indirect measure to determine the timing for the photo-conversion. A strain, carrying the *mikSi1[psas-4:dendra2::sas-4:sas-4]* and the *kdIs66[pagr-1:gfp]* alleles, was constructed and can be used to determine whether older mother centrosomes are inherited by the IL1 neuron as presumed. Moreover, centrosome size can differ between mother and daughter centrosomes in *C. elegans* (Chakraborty *et al.*, 2015). The Dendra2::SAS-4 construct could be used to analyze whether the inherent age difference between centrosomes in metaphase correlates with differences in centrosome size, determined for example by using GFP::TAC-1 (*bcSi1[pmex-5:gfp::tac-1]*) as a readout. If centrosome age correlates with centrosome size, the latter can be used as a readout for age-dependent centrosome inheritance. For a size-dependent readout, a strain was constructed, which carries the *mikSi4[pmex-5:mkate2::tac-1:unc54]* allele, to determine the centrosome size, and the *kdIs66[agr-1:gfp]* allele, to monitor the IL1nb division. If TAC-1 levels at centrosomes depend on centrosome age in *C. elegans*, mKate2::TAC-1 levels can be used as an indirect readout for mother-centrosome inheritance in the IL1 neuron lineage. In summary, the Dendra2::SAS-4 construct works efficiently and allows tracking the mother-centrosome inheritance in *C. elegans*.

Further, several tools are available that can help to overcome the difficulties specific to tracking mother-centriole inheritance in the late divisions of the IL neuron lineages.
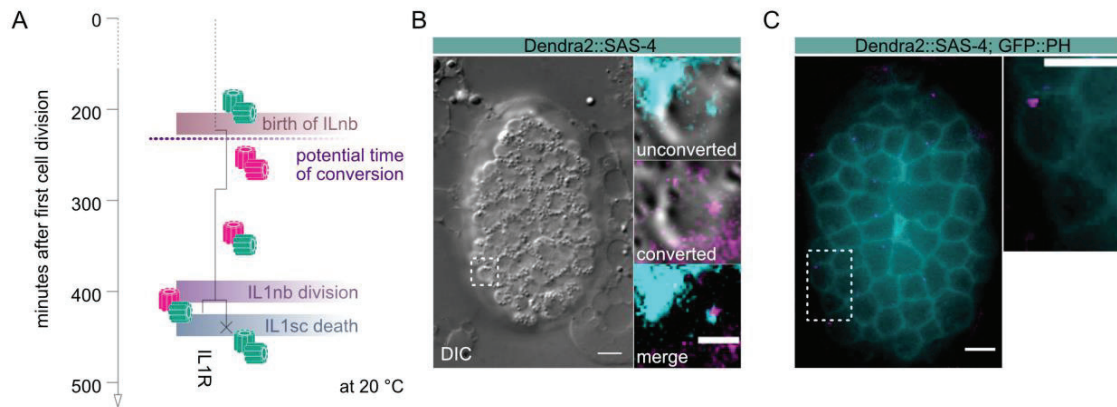
Figure 26: **Determining centrosome age** by coupling a photo-convertible fluorophore to the stably incorporated centriolar protein SAS-4. (A) Illustration of Dendra2::SAS-4 inheritance in the IL1R neuron lineage. Photo-conversion has to take place before the centrosome duplicates in the ILnb (the grandmother cell of the IL1 neuron), for the newly forming daughter centrioles to incorporate unconverted Dendra2::SAS-4 (green). The ILnb will inherit a centrosome with one converted centriole (magenta) and one unconverted centriole (green) to each daughter cell. Thus, centrosome age is not distinguishable between the IL1nb and its sister cell. However, when the IL1nb divides into the IL1 neuron and the dying IL1sc, only the oldest centrosome will hold one converted centriole (magenta). Thus, only one of the sister cells will inherit a centrosome with one converted centriole (magenta), and centrosome age will be distinguishable between the two sister cells. (B) DIC and fluorescence images of a *C. elegans* embryo expressing Dendra2::SAS-4 to distinguish centriole age. The anterior side of the embryo is on the top and the posterior side is on the bottom. The blow-ups show a single cell that holds a centrosome with one unconverted daughter (cyan) and one converted mother (magenta) centriole. Images were taken at a 4D microscope. Stages: ~110 min after the first cell division. Scale bars: 5 μm for the embryo and 2 μm for the blow-ups. (C) In the second generation after photo-conversion, centrosome age is distinguishable in sister cells. Fluorescence images of a *C. elegans* embryo expressing Dendra2::SAS-4, to follow centrosome inheritance, and GFP::PH, to mark cell boundaries. The anterior side of the embryo is on the top and the posterior side is on the bottom. The blow-up shows two sister cells. Photo-conversion took place in their grandmother cell. Only the anterior sister cell holds

a converted centriole (magenta) and thus inherited the older mother centrosome. Images were taken at a 4D microscope. Stages: ~110 min after the first cell division. Scale bars: 5 μm for the embryo and blow-up.

3.2.4. Polarity factors PAR-3 and PAR-6 are enriched at dendrite anchorage sites

E-cadherin is required for centrosome anchoring in *D. melanogaster* male germline stem cells (GSCs) (Inaba, Venkei and Yamashita, 2015). HMR-1, the sole homologue of E-cadherin in *C. elegans* (Costa *et al.*, 1998), might play a similar role in basal body positioning in *C. elegans* sensory neurons. A strain, carrying the *xnIs96[phmr-1:hmr-1::gfp:unc-54]* allele, was monitored (Table 1; Achilleos *et al.*, 2010). As determined by confocal imaging of 1.5-fold stage embryos, HMR-1::GFP is detected at distinct regions at the prospective mouth region, where dendrites are anchoring, at adherens junctions within the pharynx and the intestine, as well as the tip of the tail (Figure 27A). Further, the polarity protein Bazooka[PAR-3] was shown to be required for the docking of the centrosome in the *D. melanogaster* GSCs. As known from studies in mammalian cell culture, *D. melanogaster*, and *C. elegans*, the polarity proteins ASIP/Bazooka/PAR-3 and hsPAR6α/β/γ/Par-6/PAR-6 are found in a complex along with the atypical protein kinase C, aPKCλ/ζ/aPKC/PKC-3, which is referred to as the anterior PAR complex (Tabuse *et al.*, 1998; Hung and Kemphues, 1999). The *xnIs312[ppar-6::par-6::mcherry]* and *zuIs20[pjn271:par-3::par-3::zf1::gfp+unc-119(+)]* alleles were examined for PAR-6 and PAR-3 protein localization (Table 1; Nance, Munro and Priess, 2003; Armenti, Chan and Nance, 2014). Both, PAR-6 and PAR-3, show a similar localization pattern to HMR-1 in *C. elegans* 1.5-fold embryos (Figure 27B and not shown, respectively). Of particular interest for this study is the localization at the prospective mouth region of the worm, where dendrites are attaching. Time-lapse spinning disk confocal recordings of PAR-6::mCherry show that the protein is distributed in small punctate accumulations in bean stage embryos (Figure 27B). Over time these punctate spots move towards the prospective mouth where they accumulate in 1.5-fold stage (Figure 27B). The lateral sides of the embryo each show one very prominent PAR-6 spot, which supposedly corresponds to the anchorage site of the amphid neurons (Figure 27B). This finding was confirmed recently by Fan *et al*. (Fan *et al.*, 2019). The authors show that the amphid neurons form rosettes together with their sheath and socket glial cells. The rosettes are easily detectable in images of bean stage embryos that express PAR-6::mCherry and a cell boundary marker GFP::PH (Figure 27C, Fan *et al.*, 2019). As previously described, the dendritic tips of the amphid neurons are attached to an

extracellular matrix and the anteriorly migrating epidermis, while the cell body migrates backward, and retrograde dendrite elongation takes place (Heiman and Shaham, 2009; Fan *et al.*, 2019). The adhesion molecules DYF-7, sensory axon guidance 7 (SAX-7), hammerhead embryonic lethal 1 (HMR-1), and drosophila disc large homolog 1 (DLG-1) are required for dendritic tip attachment to the migrating epidermis (Fan *et al.*, 2019). As presumed from my PAR-6::mCherry time-lapse recordings, the authors show, that PAR-6 is located at the site of amphid dendrite tip anchorage and is required for DYF-7 localization, dendrite tip attachment, and dendrite extension (Fan *et al.*, 2019). Other, smaller PAR-6::mCherry punctate accumulations, which migrate towards the prospective mouth region of the worm, might represent the anchorage sites of other neurons, including the IL1 neurons (Figure 27B). A strain, carrying the *xnIs312[ppar-6:par-6::mcherry]* and the *kdIs66[pagr-1:gfp]* alleles, was crossed, to monitor PAR-6 accumulation at the dendritic tips of the IL1 neurons (Table 1). It remains to be determined whether PAR proteins play a role in localizing centrosomes in *C. elegans* sensory neuron lineages, mechanistically similar to what was previously described in the *D. melanogaster* male germline (Inaba *et al.*, 2015). Live recordings of 1.5-fold stage embryos, carrying the *xnIs312[ppar-6:par-6::mcherry]* and *vieSiIs18[psas-4:gfp::sas-4:sas-4]* alleles, show that centrioles nicely arrange at PAR-6::mCherry accumulation sites in the mouth region of the worm (Figure 27D, Table 1). Within migrating amphid neuron associated PAR-6::mCherry accumulations in the comma stage embryo, multiple centrioles are detectable (Figure 27E). SAS-4 foci accumulate at the dendrite anchorage site of the amphid neurons together with PAR-6 (Figure 27E). At least 10 SAS-4 foci can be distinguished by eye in the lateral PAR-6 spots. Further, 1.5-fold stage embryo stainings against PAR-3 and SAS-4 show that SAS-4 foci localize to PAR-3 in the prospective mouth region, similar to what was observed for PAR-6 (Figure 27F). Taken together, the results suggest that the anterior PAR complex might be involved in centrosome positioning in sensory neurons. However, a molecular mechanism remains to be determined.
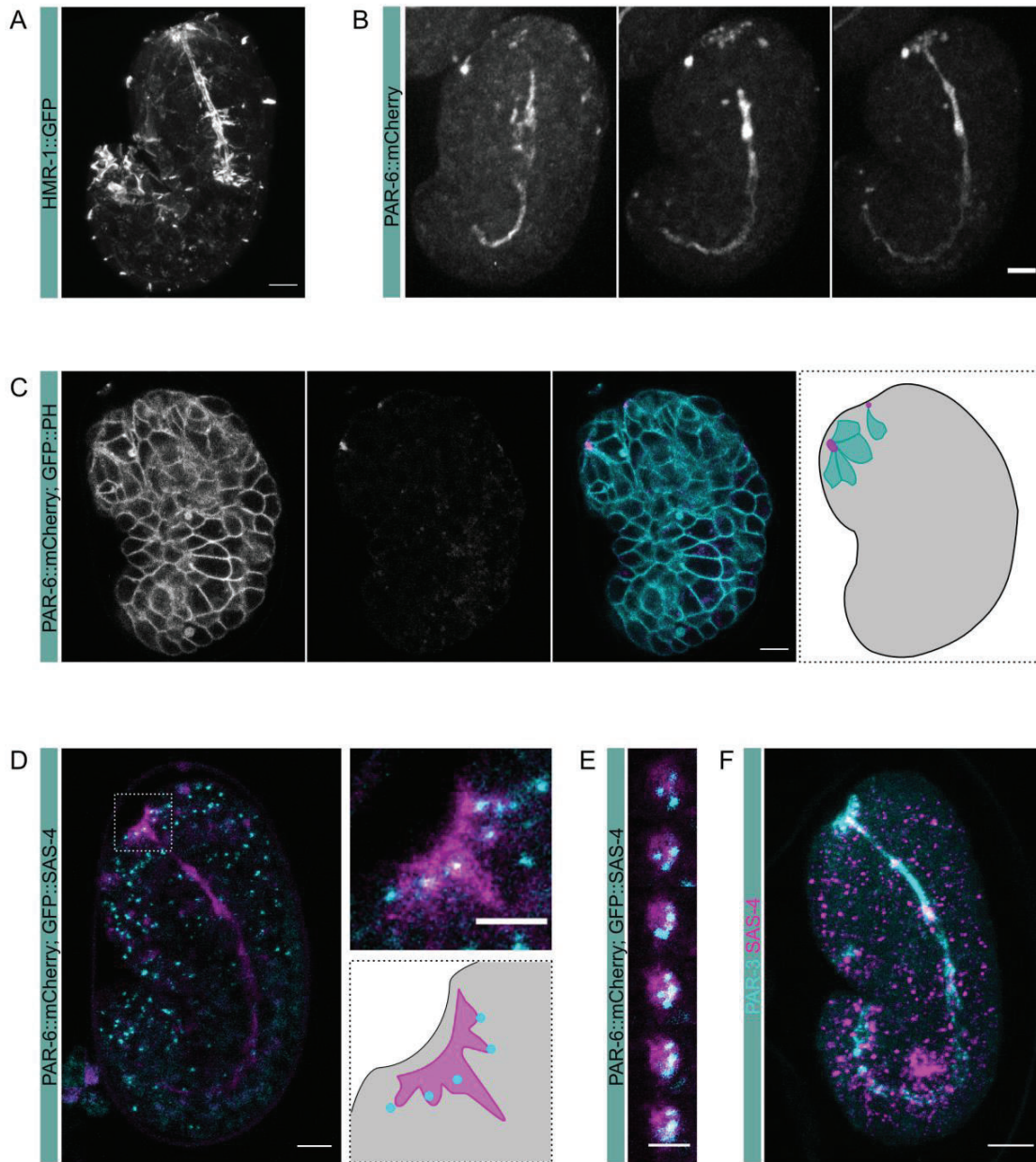
Figure 27: **Polarity markers and centriole positioning**. (A) Fluorescence image of a 1.5-fold stage embryo expressing HMR-1::GFP. The image was taken at a confocal microscope. In *C. elegans* 1.5-fold embryos, HMR-1::GFP is enriched at the prospective mouth region, the intestine, and the tail tip. (B) Fluorescence images of a PAR-6::mCherry expression embryo from bean to 1.5-fold stage. The image was taken at a spinning disc confocal microscope. The PAR-6::mCherry punctate accumulations at the prospective mouth region migrate towards the forming nose tip where dendrites are attached. (C) Fluorescent image of a PAR-6::mCherry and GFP::PH expressing bean stage embryo. The image was taken at a confocal microscope.

The amphid neuron rosette formation is visible. The corresponding cartoon illustrates rosette formation. (D-F) Centrioles localize to PAR punctate accumulations. (D) In PAR-6::mCherry and GFP::SAS-4 expressing embryos, SAS-4 foci are organized around the prospective mouth region where PAR-6 is localizing. The image was taken at a confocal microscope. The corresponding cartoon illustrates how the SAS-4 foci arrange at PAR-6 accumulations. (E) Fluorescent image of a PAR-6::mCherry accumulation corresponding to the amphid neuron anchorage site in a PAR-6::mCherry and GFP::SAS-4 expressing bean stage embryo. The image was taken at a confocal microscope. Blow-ups of single planes of a z-stack through the tip anchorage site of an amphid neuron is shown. Scale bar: 3 µm. Multiple SAS-4 foci are visible within the PAR-6 punctate accumulation. (F) Fluorescent image of a 1.5-fold stage embryo stained against PAR-3 and SAS-4 is shown. The image was taken at a confocal microscope. PAR-3 shows the same localization pattern as PAR-6. (A-D, F) The anterior side of the embryo is on the top, and the posterior side is on the bottom. Maximum projection of z-stack through part of the embryo. Scale bar: 5 µm.

DISCUSSION

DISCUSSION

4.1. PCMD-1 is a coiled-coil protein required for the formation of the centrosome matrix in *C. elegans* one-cell embryos

In this study, I demonstrate that the coiled-coil protein PCMD-1 plays an essential role in centrosome formation in the early *C. elegans* embryo. PCMD-1 is recruiting the centrosome matrix protein SPD-5[CDK5RAP2, Cnn] to the centrosome for PCM core formation. Further, the protein ensures stable PCM expansion upon mitosis. To date, in *C. elegans,* no protein with a similar function has been described. PCMD-1 is most likely a functional homologue of pericentrin[Plp], a protein required for anchoring other centrosomal proteins in humans and has been associated with human diseases, such as primordial dwarfism, ciliopathies, and cancer (Nigg and Raff, 2009; Waters and Beales, 2011).

4.1.1. PCMD-1 localization to centrosomes

By analyzing the localization pattern of PCMD-1, I found that the protein is present at centrioles throughout development and in the adult worm (Figure 11). However, it is not yet clear whether PCMD-1 is part of the centriole or the PCM core. Conventional confocal microscopy cannot resolve the exact positioning of the protein at centrosomes. Also, the 3D SIM super-resolution micrographs taken of one-cell *C. elegans* embryos do not have sufficient resolution to determine whether PCMD-1 is part of the centriolar structure or the surrounding PCM core. If PCMD-1 is a centriolar protein and can be preserved at centrosomes in electron microscopy experiments, correlative fluorescence electron microscopy can be applied to determine PCMD-1 localization (Watanabe *et al.*, 2011). Moreover, super-resolution techniques optimized for thick samples can be used to clarify where the protein is localized at the centrosome. A small amount of PCMD-1 was found to localize to the expandable PCM (Figure 11A). A similar localization pattern was reported for the proteins SPD-2[Cep192, Spd-2] and SAS-4[CPAP, Sas-4] in *C. elegans* (Kirkham *et al.*, 2003; Leidel and Gönczy, 2003; Dammermann *et al.*, 2004; Kemp *et al.*, 2004; Pelletier *et al.*, 2004). Nevertheless, PCMD-1 displays functional differences to SPD-2[Cep192, Spd-2], and SAS-4[CPAP, Sas-4], as it does not seem to be required for centriole duplication.

4.1.2. The regulation of the PCMD-1 protein at centrosomes

In recordings of GFP::PCMD-1^{mikSi6} over time, the protein appears to be downregulated at centrosomes upon mitotic exit (Figure 12A and B). A similar phenotype has been reported for pericentrin^{Plp}, the presumable human orthologue of PCMD-1 (see discussion below: PCMD-1 homologues). Pericentrin^{Plp} is cleaved by separase$^{SSE, SEP-1}$ at mitotic exit for effective PCM disassembly (Kim, Lee and Rhee, 2015). The cleavage requires phosphorylation of pericentrin^{Plp} by PLK1$^{Polo, PLK-1}$ (Kim, Lee and Rhee, 2015). In the analysis of the GFP::PCMD-1^{mikSi6} recordings, only a small subset of the recorded embryos was quantifiable, and signal intensities were not significantly different to control embryos (Figure 12B). Thus, it remains to be validated whether PCMD-1 is indeed downregulated at centrosomes. For further analysis, the endogenously tagged PCMD-1 should preferably be used. If the protein is downregulated at centrosomes, a similar mechanism as reported for pericentrin^{Plp} regulation by PLK1$^{Polo, PLK-1}$ might apply and can be tested. Upon identification of PLK-1$^{PLK1, Polo}$ phosphorylation sites, phosphodeficient, and phosphomimetic mutant alleles can be generated. With a phosphodeficient variant of the protein, fused to GFP, one could test whether the protein remains present at centrosomes throughout mitosis. Intensity measurements of the phosphodeficient and the wild-type PCMD-1 variants could be analysed and compared. Moreover, if PLK-1$^{PLK1, Polo}$ is required for PCMD-1 cleavage and downregulation at the centrosome, an allele carrying the phosphomimetic mutations would presumably give rise to a PCMD-1 protein that is repeatedly removed from centrosomes throughout the cell cycle, or is not loaded onto the centrosome in the first place. Thus, a strain carrying the phosphomimetic allele of *pcmd-1* as a GFP fusion might not be detectable at centrosomes throughout the cell cycle. Moreover, the mutant allele might have a similar phenotype to the *pcmd-1(t3421)* mutant. A strain carrying the phosphomimetic allele, might not be able to rescue the *pcmd-1(t3421)* or *pcmd-1(syb975)* mutant phenotypes. The experiment would prove that the site is required for the removal of PCMD-1 from centrosomes if phosphorylated.

PCMD-1 has further been shown to interact with the F-box domain containing protein FBXA-171 in a yeast two-hybrid screen (Simonis *et al.*, 2009). Thus, PCMD-1 might be subject to ubiquitinylation by the Skp, Cullin, F-box containing (SCF) complex, and subsequent degradation (Kipreos and Pagano, 2000). Interestingly, the Cep68 protein in humans was shown to be targeted for degradation by the Skp1-Cul1-F-box protein (SCFβTrCP) ubiquitin ligase complex upon PLK-1 phosphorylation on Ser332. The

degradation of the protein is, together with the separase[SSE, SEP-1] mediated cleavage of pericentrin[Plp], required for effective CDK5RAP2[Cnn, SPD-5] removal from centrosomes (Pagan *et al.*, 2015). A similar regulatory mechanism might apply for PCMD-1.

4.1.3. A centriole duplication defect cannot account for the *pcmd-1(t3421)* mutant phenotype

As mentioned above, PCMD-1 does not seem to be implicated in centriole duplication. By immunofluorescence stainings against the most downstream centriolar protein SAS-4[CPAP, Sas-4], I was able to show that enough centrioles are present during the first cell cycle in *pcmd-1(t3421)* mutants to form a bipolar spindle (Figure 14). Further, centrioles are duplicating in the second cell cycle, even if cell division failed in cell cycle one (Figure 14E). However, not all centrioles in *pcmd-1(t3421)* mutants seem to have microtubule nucleation activity or are capable of recruiting the PCM (Figure 14C, D and F, Figure 15C and D), which explains the frequently monitored formation of monopolar spindles during the first cell cycle (Figure 9). Nevertheless, to validate that centriole formation or duplication is not affected in the absence of PCMD-1, mutant embryos could be analyzed by electron microscopy.

4.1.4. PCMD-1, a long-missing link

The most conspicuous phenotype apparent in *pcmd-1(t3421)* mutant embryos is that SPD-5[CDK5RAP2, Cnn] is not detectable at non-mitotic centrosomes. SPD-5 is a critical centrosomal protein that, together with SPD-2[Cep192, Spd-2], forms a scaffold to recruit other PCM components. For a long time, the PCM was thought to be an amorphous accumulation of proteins around centrioles. In recent years, by availing super-resolution microscopy in *D. melanogaster* and human cells, primarily the interphase PCM was found to be highly organized instead (Fu and Glover, 2012; Lawo *et al.*, 2012; Mennella *et al.*, 2012; Sonnen *et al.*, 2012). This inner PCM core was shown to underlie mitotic PCM expansion (Mennella *et al.*, 2012). As observed in *pcmd-1(t3421)* mutant embryos, impaired PCM core formation also leads to severe problems with mitotic PCM assembly in *C. elegans,* entailing aberrations in embryo development (Figure 9, 15). However, PCM formation defects in *pcmd-1(t3421)* mutants are phenotypically diverse. In 42 % of GFP::SPD-5 expressing embryos, PCM is

absent from centrosomes, or only minimal amounts of PCM are visible during mitosis (33 %). Relatively robust accumulations can be observed in 25 % of the embryos (Figure 15, Figure 16). The SPD-5$^{\text{CDK5RAP2, Cnn}}$ centrosome matrix accumulations in mutant embryos are unusual insofar, as they appear fragmented and less dense in comparison to the wild-type. Importantly, no such phenotype has been previously reported. The rather flared nature of GFP::SPD-5 assemblies in mutants somewhat resembles SPD-5$^{\text{CDK5RAP2, Cnn}}$ networks forming under certain conditions in *in vitro* experiments conducted by Woodruff *et al.* (Woodruff *et al.*, 2015). These *in vitro* assays revealed that SPD-5$^{\text{CDK5RAP2, Cnn}}$ can polymerize into networks in a density and time-dependent manner (Woodruff *et al.*, 2015). In this context, network assembly was accelerated in the presence of PLK-1$^{\text{PLK1, Polo}}$, and SPD-2$^{\text{Cep192, Spd-2}}$. However, only SPD-5$^{\text{CDK5RAP2, Cnn}}$ assembled into networks that were able to recruit downstream PCM factors (Woodruff *et al.*, 2015). Moreover, Woodruff *et al.* (2017) observed that SPD-5$^{\text{CDK5RAP2, Cnn}}$ assembles into more dense structures in a crowded environment *in vitro*, resembling the spherical structure of centrosomes *in vivo* (Woodruff et al., 2017). Since SPD-5$^{\text{CDK5RAP2, Cnn}}$ accumulations in *pcmd-1(t3421)* mutant embryos resemble the SPD-5$^{\text{CDK5RAP2, Cnn}}$ assemblies observed in low-density environments *in vitro*, PCMD-1 might act to favor a specific conformational change of the SPD-5$^{\text{CDK5RAP2, Cnn}}$ protein. PCMD-1 could contribute to SPD-5$^{\text{CDK5RAP2, Cnn}}$ assembly *in vivo* by decreasing the threshold for SPD-5$^{\text{CDK5RAP2, Cnn}}$ density-dependent accumulation, thereby providing a dose-dependent regulatory mechanism to centrosome matrix formation at non-mitotic and mitotic centrosomes.

Importantly, it was previously not possible in *C. elegans* to strip centrosomes from their innermost PCM core. Thus, *pcmd-1* mutants offer a unique opportunity to study the implications of PCM core formation in the worm.

4.1.5. PCMD-1 homologues

The sequence homology analysis across species was not conclusive. Apart from identifying homologues in closely related species of the genus *Caenorhabditis*, no sequence homology to proteins of other species was found (Figure 23). However, functionally PCMD-1 resembles the role of Asl/Cep152 or D-Plp/pericentrin in centrosome assembly. In *D. melanogaster*, loss of Asl$^{\text{Cep152}}$ strongly impacts the stabilization of PCM around centrioles (Varmark *et al.*, 2007). Conduit *et al.* (2014) report that in *D. melanogaster* syncytial embryos Cnn$^{\text{CDK5RAP2, SPD-5}}$, and Spd-2$^{\text{Cep192, SPD-2}}$ are incorporated into the PCM in close proximity to

the mother-centriole and spread outwards to form the scaffold structure. Asl initiates this process by recruiting Spd-2$^{\text{Cep192, SPD-2}}$, which in turn helps to recruit Cnn$^{\text{CDK5RAP2, SPD-5}}$ for scaffold formation (Conduit *et al.*, 2014). In *C. elegans* SPD-5$^{\text{CDK5RAP2, Cnn}}$ recruitment to centrosomes occurs throughout the PCM and not at specific nucleation sites at centrioles as reported for its fly homolog Cnn$^{\text{CDK5RAP2, SPD-5}}$ (Conduit *et al.*, 2014; Laos, Cabral and Dammermann, 2015). However, PCMD-1 function is comparable to that of Asl$^{\text{Cep152}}$, as it is required for the initiation of efficient PCM assembly in embryos. On the other hand, Asl is implicated in the process of centriole duplication, similar to its human homologue Cep152 (Blachon *et al.*, 2008; Dzhindzhev *et al.*, 2010). In contrast, no significant implication for centriole duplication was observed in *pcmd-1* mutants (Figure 14A-D and E). Moreover, other than PCMD-1, Asl$^{\text{Cep152}}$ is only found at centrioles but not the PCM (Varmark *et al.*, 2007). Thus, despite their functional overlap in PCM recruitment, the differences in localization and their role in centriole duplication argue against Asl and Cep152 being the PCMD-1 *D. melanogaster* and human homologues, respectively.

The *Drosophila* Plp$^{\text{pericentrin}}$ protein was shown to be implicated in interphase PCM core organization in cultured *D. melanogaster* cells by forming fibrils stretching away from the centriole wall to the outer PCM matrix (Lawo *et al.*, 2012; Mennella *et al.*, 2012). Plp$^{\text{pericentrin}}$ fibrils are further required for proper assembly of the mitotic PCM (Mennella *et al.*, 2012), similar to what is seen in *pcmd-1(t3421)* mutants. Rough *et al.* 2018 report that mitosis is not severely compromised in *D. melanogaster* Plp$^{\text{pericentrin}}$ mutants. However, centrioles separate prematurely in this mutant background (Roque *et al.*, 2018). Likewise, centrioles were observed to disengage shortly after fertilization in *pcmd-1(t3421)* mutant embryos (observation by A. Kirgis and M. Antoniolli). In mice, PCM integrity has been shown to contribute to centriole engagement (Barrera *et al.*, 2010). PCM levels are low in early *C. elegans* embryos but might be strong enough to hold together the centriolar pair. Thus, in the absence of the PCMD-1 dependent PCM core, centrioles might fall apart. Another possibility is that PCMD-1 plays a direct role in centriole engagement, independent of its role in PCM core assembly. SEP-1$^{\text{Separase, SSE}}$ is required for centriole disengagement specifically at the meiosis-mitosis transition in the one-cell embryo (Cabral *et al.*, 2013). PCMD-1 might be a substrate of SEP-1$^{\text{separase, SSE}}$, and removed from the centrosome by cleavage. It was mentioned earlier, that the human protein pericentrin$^{\text{Plp}}$ is downregulated at centrosomes upon mitotic exit in a separase$^{\text{SSE, SEP-1}}$ dependant manner in humans (Kim, Lee and Rhee, 2015). Further, the pericentrin$^{\text{Plp}}$ protein controls the localization of CDK5RAP2$^{\text{Cnn, SPD-5}}$ to centrosomes in interphase and mitosis (Haren, Stearns and Lüders,

2009; Lee and Rhee, 2011; Lawo *et al.*, 2012; Mennella *et al.*, 2012; Sonnen *et al.*, 2012; Conduit *et al.*, 2014; Kim and Rhee, 2014). Similar to PCMD-1, pericentrin[Plp] is found at centrioles and in the PCM (Flory *et al.*, 2002; Lawo *et al.*, 2012). In human cells, depletion of pericentrin[Plp] causes the reduction of PCM recruitment to centrosomes and monopolar spindle formation (Zimmerman *et al.*, 2004). In summary, the reports of pericentrin/Plp function and regulation are in stark resemblance to the observations made for PCMD-1. Therefore, PCMD-1 is most likely the functional homologue of the human pericentrin and the *D. melanogaster* Plp proteins in *C. elegans*.

4.1.6. PCMD-1 cooperates with key centrosomal components and ensures structured centrosome matrix formation in the *C. elegans* one-cell embryo

As previously mentioned, the PCM core organization depends on Plp in *D. melanogaster* (Mennella *et al.*, 2012). The same holds true for the human and mouse homologues pericentrin and Pcnt (Lawo *et al.*, 2012; Chen *et al.*, 2014). As discussed above, PCMD-1 is most likely the functional homologue of pericentrin and Plp in *C. elegans*. Pericentrin/Plp are present in an evolutionary conserved module, comprising Cep215/Cnn[SPD-5], Cep192/Spd-2[SPD-2] and PLK1/Polo[PLK-1], to regulate mitotic PCM expansion in human and *D. melanogaster* (Haren, Stearns and Lüders, 2009; Lee and Rhee, 2011; Lawo *et al.*, 2012; Mennella *et al.*, 2012; Sonnen *et al.*, 2012; Conduit *et al.*, 2014; Kim and Rhee, 2014). In *C. elegans* SPD-2[Cep192, Spd-2] and SPD-5[CDK5RAP2, Cnn] have been reported to be interdependent for their localization to the mitotic PCM (Kemp *et al.*, 2004; Pelletier *et al.*, 2004). Thus, the inefficient recruitment of SPD-5[CDK5RAP2, Cnn] to centrosomes in *pcmd-1(t3421)* mutants can explain why also SPD-2[Cep192, Spd-2] is not efficiently recruited to the PCM in mutants (Figure 19B). It was recently shown in *C. elegans* that a centriolar fraction of SPD-2[Cep192, Spd-2] is recruited to the centrosome by SAS-7[Cep295, Ana1] (Sugioka *et al.*, 2017). Thus, it is most likely the SAS-7[Cep295, Ana1] dependent centriolar fraction of SPD-2[Cep192, Spd-2] that remains at centrosomes in *pcmd-1(t3421)* mutants. SPD-2[Cep192, Spd-2] was shown to physically interact with PLK-1 (Boxem *et al.*, 2008) and to be required for mitotic recruitment of the kinase in worms (Decker *et al.*, 2011). In *pcmd-1(t3421)* mutants, the small fraction of PLK-1[PLK1, Polo] that remains around centrioles, was shown to depend on the residual centriolar fraction of SPD-2[Cep192, Spd-2] (Figure 20E and F, Figure 21A). This observation was previously made in mammalian tissue culture, where PLK-1 is absent from the centrosome in CEP192[Spd-2, SPD-2]

siRNA treated HeLa cells (Joukov, Walter and De Nicolo, 2014). Moreover, *pcmd-1(t3421)* mutants treated by *spd-2* RNAi show that GFP::SPD-5 accumulation is completely abolished (Figure 17D and E). If SPD-2$^{Cep192, Spd-2}$ is downregulated at the centrosome, PLK-1$^{PLK1, Polo}$ recruitment to centrosomes is further diminished, and consequently also the phosphorylation of SPD-5$^{CDK5RAP2, Cnn}$ by PLK-1$^{PLK1, Polo}$. Thus, the shift towards a self-assembly state of SPD-5$^{CDK5RAP2, Cnn}$ is lessened. Taken together these results suggest that PCMD-1 is part of the evolutionarily conserved centrosome module in *C. elegans* and functions to bring SPD-5$^{CDK5RAP2, Cnn}$ into close proximity of SPD-2$^{Cep192, Spd-2}$ recruited PLK-1$^{PLK1, Polo}$ before mitotic centrosome activation (Figure 29).

The seeding function of PCMD-1 seems to be required for efficient PCM expansion. However, it is also needed to link the PCM to centrioles reliably. Thereby, the determination of the centrosome as the dominant nucleator of microtubules in the cell is secured, since in *pcmd-1(t3421)* mutants, PCM detaches from centrioles and microtubules can nucleate in ectopic places, potentially the chromatin (Figure 14C, 15B, 18A and 28).

Strikingly, in *plk-1* RNAi (mild) treated *pcmd-1(t3421)* mutants, GFP::SPD-5 is not only absent from centrosomes, but there seems to be a strong genetic interaction between the factors (Figure 18A and B). These embryos do not progress beyond the first cell cycle in their development. Since PLK-1$^{PLK1, Polo}$ is only partially downregulated and *pcmd-1(t3421)* mutants treated by control RNAi form bipolar spindles and also progress through the first cell cycle under the given conditions, it was completely unexpected to observe such a severe phenotype when the factors are downregulated simultaneously. The phenotype resembles a strong PLK-1$^{PLK1, Polo}$ loss of function phenotype (Chase *et al.*, 2000). The outcome cannot solely be explained by the absence of PLK-1$^{PLK1, Polo}$ from centrosomes, as this is also the case for *spd-2* RNAi treated embryos (Figure 20E). Thus, the interaction of PLK-1$^{PLK1, Polo}$ and PCMD-1 is of particular interest and requires further analysis.

4.1.7. Temperature dependence and high variability of the *pcmd-1* mutant phenotype

The PCMD-1 mutants, *pcmd-1(t3421)* and *pcmd-1(syb975)*, are temperature-sensitive mutants. Both alleles can be maintained at low temperature (15 °C) and exhibit embryonic lethality when exposed to high temperature (25 °C). Since gene function is disrupted in *pcmd-1(t3421)* mutants by a single nucleotide exchange, which introduces a premature STOP codon

early in the coding sequence, it is unlikely that functional protein is made by transcription from the original START site. However, several alternative in-frame start codons exist downstream of the point mutation in *pcmd-1(t3421)* mutants, which could explain the residual activity of the *pcmd-1* gene (Table 13). In case the first available alternative START codon is used in *pcmd-1(t3421)* mutants, a truncated protein would still carry three of the four *in silico* predicted unstructured domains. The *in silico* predicted coiled-coil domain would be deleted. Further, also downstream of the 1201 bp deletion in *pcmd-1(syb975)* mutants, in-frame start codons exist (Table 13). In *pcmd-1(syb975)* mutants, the predicted coiled-coil and the four unstructured domains are deleted. The increased lethality of *pcmd-1(syb975)* compared to the *pcmd-1(t3421)* mutant might arise from differences between the residual proteins made in the mutants. Moreover, the temperature sensitivity of the mutants could be explained by differences in residual protein stability or efficacy of transcription initiation at alternative START sites. In the case that alternative START codons are used in *pcmd-1(t3421)* and *pcmd-1(syb975)* mutants, the alleles would be hypomorphic. In western blot analysis against the C-terminally GFP tagged PCMD-1 protein, and immunofluorescence stainings, no residual protein was detected (Figure 12). However, if protein is made by the use of an alternative start codon, the amount of protein might be below the detection limits of western blot analyses and fluorescence imaging. Only small quantities of the PCMD-1 protein might be required in the embryo. If an alternative start codon is used, enough truncated protein might be generated in a subset of the embryos, which can make it through development. Ideally, a full deletion allele of the *pcmd-1* gene should be generated.

The variability of the *pcmd-1* mutant phenotype can alternatively be explained by differences in SPD-5$^{CDK5RAP2, Cnn}$ protein folding kinetics at different temperatures. SPD-5$^{CDK5RAP2, Cnn}$ can transition into a self-assembly competent state *in vitro* (Woodruff *et al.*, 2015). The SPD-5$^{CDK5RAP2, Cnn}$ self-assembly rate could be determined in an *in vitro* assay as performed by Woodruff *et al*. (2015) and analyzed for variability at different temperatures, and whether the addition of PCMD-1 changes the rate of SPD-5$^{CDK5RAP2, Cnn}$ self-assembly. Also, at lower temperatures embryonic development is slower in *C. elegans* embryos, and cell cycles are prolonged (Begasse *et al.*, 2015). SPD-5$^{CDK5RAP2, Cnn}$ might have more time to self-assemble under these conditions.

4.1.8. A model of PCMD-1 function

Only a limited number of proteins required for PCM formation were discovered in *C. elegans* through large-scale RNAi screens and genetic analyses, namely SPD-5[CDK5RAP2, Cnn] (Hamill *et al.*, 2002), SPD-2[Cep192, Spd-2] (Kemp *et al.*, 2004; Pelletier *et al.*, 2004) and PLK-1[PLK1, Polo] (Decker *et al.*, 2011), which together form an evolutionary conserved PCM module. In other organisms, this conserved module comprises another factor, Plp in *D. melanogaster* or pericentrin in humans. For a long time, the *C. elegans* PCM matrix protein SPD-5[CDK5RAP2, Cnn] was thought to comprise pericentrin and CDK5RAP2 function (Hamill *et al.*, 2002; Zimmerman *et al.*, 2004; Conduit *et al.*, 2010). In this study, I identified PCMD-1 as the *C. elegans* functional homologue of pericentrin. PCMD-1 is necessary for PCM recruitment to non-mitotic centrosomes in worms. The protein is further needed for the efficient and orderly expansion of PCM upon mitotic entry. PCMD-1 recruits the centrosome matrix protein SPD-5[CDK5RAP2, Cnn] to centrosomes to establish an inner PCM core. Moreover, SPD-2[Cep192, Spd-2] was found to recruit PLK-1[PLK1, Polo] to centrioles. Together, PCMD-1 and SPD-2[Cep192, Spd-2] form a platform for initial seeding of the core PCM factors before mitosis. Thus, upon mitotic entry SPD-5[CDK5RAP2, Cnn] can effectively be phosphorylated by PLK-1[PLK1, Polo] for centrosome matrix expansion. *In vitro*, SPD-5[CDK5RAP2, Cnn] can assemble into micrometer-sized porous networks, and the polymerization of the network accelerates in the presence of PLK-1[PLK1, Polo] and SPD-2[Cep192, Spd-2] (Woodruff *et al.*, 2015). *In vivo*, most likely SPD-2[Cep192, Spd-2], which is recruited to the mitotic PCM by SPD-5[CDK5RAP2, Cnn], recruits PLK-1[PLK1, Polo] to secure subsequent mitotic phosphorylation of SPD-5[CDK5RAP2, Cnn]. It is generally assumed that SPD-2[Cep192, Spd-2] and SPD-5[CDK5RAP2, Cnn] are interdependent for their localization to the centrosome (Kemp *et al.*, 2004; Pelletier *et al.*, 2004). However, the proteins might, together with PLK-1[PLK1, Polo], instead act in a feed-back loop for PCM assembly (Figure 29). This hypothesis is reconcilable with the previous findings that only SPD-5[CDK5RAP2, Cnn] can self-assemble into network-like structures *in vitro*, and that SPD-2[Cep192, Spd-2] is regulating centrosome size *in vivo* (Decker *et al.*, 2011; Woodruff *et al.*, 2015).
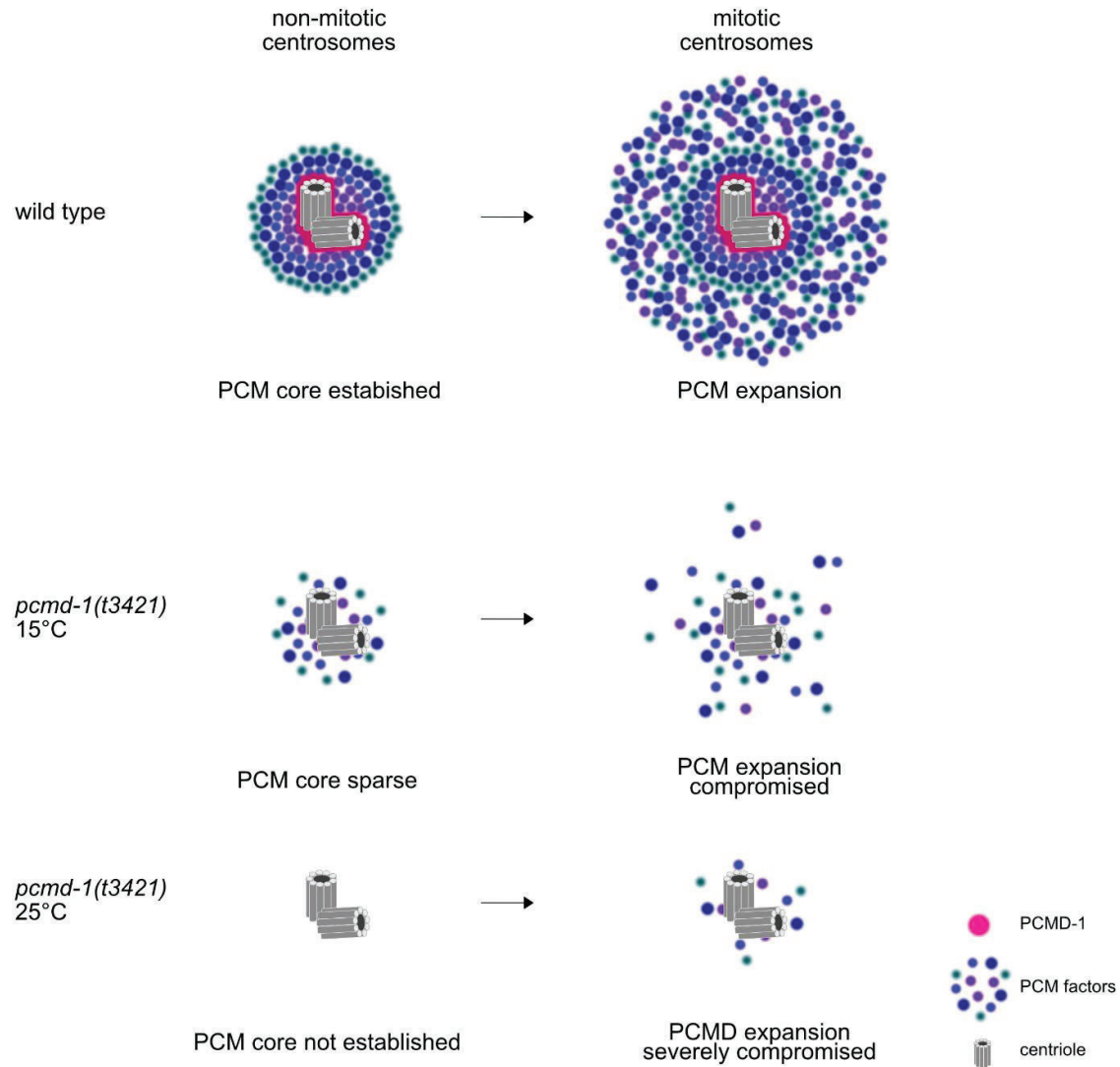
Figure 28: **Aberrations of PCM formation in *pcmd-1(t3421)* one-cell mutant embryos**. PCMD-1 is required for PCM core formation in the wild type. Thereafter, PCM can stably expand during mitosis. In *pcmd-1(t3421)* mutant embryos, PCM core formation, and mitotic PCM expansion are compromised at 15 °C. However, 38 % of the mutant embryos grow into adults. Whereas, at 25 °C, PCM core formation and mitotic PCM expansion are severely compromised, leading to 100 % embryonic lethality.
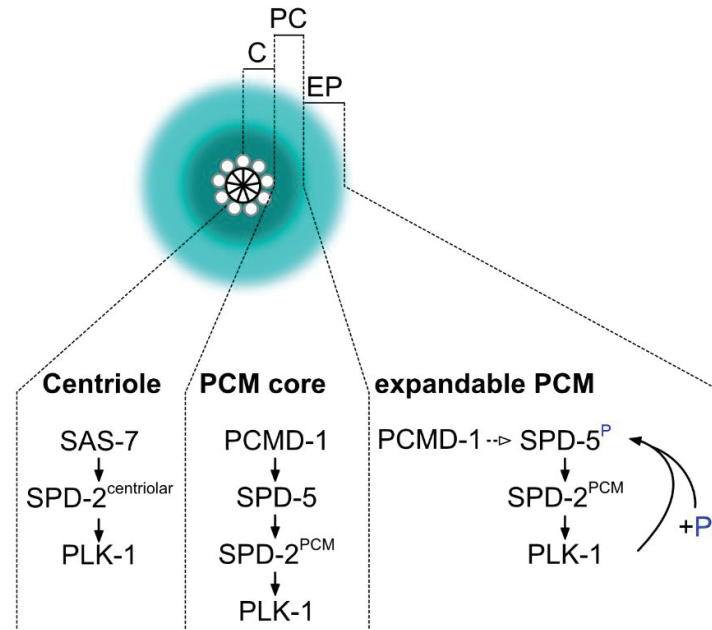
Figure 29: **Model of PCM recruitment in *C. elegans***. Shown is the schematic of a mitotic centrosome (Note that the recruitment of centriole and PCM core factors takes place before the centrosome enters mitosis). (C) A SAS-7$^{\text{Cep195, Ana1}}$ dependent centriolar pool of SPD-2$^{\text{Cep192, Spd-2}}$ recruits PLK-1$^{\text{PLK1, Polo}}$ to centrioles. (PC) Further, PCMD-1 recruits SPD-5$^{\text{CDK5RAP2, Cnn}}$ to centrosomes to form the PCM core. Through SPD-5$^{\text{CDK5RAP2, Cnn}}$ also more SPD-2$^{\text{Cep192, Spd-2}}$ is recruited to the PCM core, which in turn increases the amount of PLK-1$^{\text{PLK1, Polo}}$ at the PCM core. Note that it is unclear whether PCMD-1 is part of the centriole or the PCM core. (EP) Upon mitosis, PLK-1$^{\text{PLK1, Polo}}$ phosphorylates SPD-5$^{\text{CDK5RAP2, Cnn}}$ for PCM matrix expansion. In a feedback loop, SPD-5$^{\text{CDK5RAP2, Cnn}}$ recruits SPD-2$^{\text{Cep192, Spd-2}}$, which accumulates more PLK-1$^{\text{PLK1, Polo}}$ at centrosomes for further SPD-5$^{\text{CDK5RAP2, Cnn}}$ phosphorylation. At mitotic centrosomes, PCMD-1 might lead to increased stabilization of the SPD-5$^{\text{CDK5RAP2, Cnn}}$ self-assembly state.

4.2. Centrosome inheritance and development of the IL1 neuron lineage

4.2.1. IL1 neuron dendrite growth by retrograde extension and centrosome inheritance

In *C. elegans*, sensory neurons are the only cell type that forms cilia and thus require centrioles as basal bodies post mitotically. I established a system to analyze centrosome inheritance in the IL1 neuron lineage. The IL1nb gives rise to the IL1 ciliated sensory neuron and the IL1 dying sister cell, of which the latter does not require centrioles post-mitotically. In cell culture it was shown that cells with older mother centrosomes grow cilia earlier than the ones that received younger mother centrosomes after cell division (Anderson and Stearns, 2009). The potential of a cell to grow out a cilium earlier than its sister cell might be biologically relevant in some systems. As previously described for amphid and phasmid neurons (Heiman and Shaham, 2009; Schouteden *et al.*, 2015), I found that also IL1 neurons grow their dendrites via retrograde extension (Figure 24B and C). Interestingly, amphid neurons are known to require their ciliary transition zone to anchor their dendrites for successful dendrite elongation (Schouteden *et al.*, 2015). Further, amphid dendrite anchorage has to take place in a confined time window during development (Heiman and Shaham, 2009). Thus, the timely outgrowth of a cilium might be essential for successful dendrite anchorage. During the IL1nb division, it might be necessary that the future IL1 neuron inherits the older mother centrosome to be competent to grow a cilium early enough. Centrioles localize in the prospective mouth region where dendrites anchor (Figure 25). By using the photo-convertible centriole protein I generated, which comprises the green-to-red switchable fluorescent protein Dandra2 fused to SAS-4$^{CPAP, Sas-4}$ (Figure 26), it will now be possible to determine whether the older or the younger centrosome is inherited by the dendrite forming neuron. The photo-conversion of the Dendra2 fluorophore at centrioles has to take place in the grandmother cell, which is the ILnb in the case of the IL1 neuron and its dying sister cell (Figure 26A). Unfortunately, to my knowledge, no promoter is described that marks explicitly the ILnb and the ILnb descendants. However, there are several possibilities to overcome this limitation: 1. To lineage each embryo live until the ILnb is born and subsequently photo-convert. 2. To photo-convert blindly around the time the ILnb is born. 3. Applying an indirect approach by using centrosome size as a readout for centrosome age. The first approach is the most precise. However, the ILnb division takes place very late in development, at about 210 min after fertilization at a maintenance temperature of 20 °C.

Thus, the lineaging approach is labor-intensive and challenging. By contrast, blind photo-conversion might be easy to establish, since *C. elegans* development is highly invariant. A strain carrying the *mikSi1[psas-4:dendra2::sas-4:sas-4]* and *kdIs66[pagr-1:gfp]* allele was generated and can be used to establish the assay for centrosome inheritance in IL1 neurons (Table 1). Since the *agrin-1* promoter is expressed in more cells than the IL1 neurons, an additional verification step is required. The *aakg-1(y111b2a.8)* promoter drives expression specifically in IL1 neurons in larvae (WormAtlas, Altun *et al.*, 2002-2019). An allele *paakg-1:gfp* or *paakg-1:mKate2* would drive expression late enough in development to not interfere with the readout of centrosome inheritance in IL1 neurons after Dendra2::SAS-4 photo-conversion. The allele could be used to prove IL1 neuron identity in retrospect. Alternatively, it can be tested whether older mother centrosomes accumulate more PCM at the centrosome in *C. elegans*. It was previously shown that TAC-1$^{TACC1/2/3, D-TACC}$ levels differ at centrosomes in metaphase in some cell divisions (Chakraborty *et al.*, 2015). Using the Dendra2::SAS-4 tool it can now be determined whether these differences are dependent on centrosome age. TAC-1$^{TACC1/2/3, D-TACC}$ levels could then be used as a readout for centrosome age in the IL1nb division.

4.2.2. The IL1nb is already highly polarized

Unexpectedly, the IL1nb appears to be already highly polarized, with its dendrite already anchored and forming, before the division into the IL1 neuron and its dying sister cell takes place (Figure 24D, Figure 30). In the monitored comma stage embryos, a projection formed and anchored already before the IL1nb division. In the 1.5-fold embryo, the division occurred, and the IL1 neuron and its sister cell are distinguishable, as the IL1sc starts rounding up to prepare for its cell death in the 2-fold stage. This result was completely unexpected and raised new questions concerning the behavior of the centrosome and basal body in this division. It has to be clarified how centrosome and basal body function can be carried out simultaneously in this system since centrosome function is required for cell division, but also basal body function to template the cilium. Both functions are mediated by centrioles. A strain carrying the *kdIs66[pagr-1:gfp]* allele, to determine IL1 neuron identity, and the *itIs37[ppie-1:mcherry::h2b:pie-1 + unc119(+)]* allele, to visualize DNA, was generated and can be analyzed to determine the exact time point of IL1nb division (Table 1).

4.2.3. PAR protein requirement for cilium formation and dendrite attachment in *C. elegans*

As previously described, IL1 neurons elongate their dendrites by retrograde extension. The dendritic tip stays anchored in place, while the cell body of these neurons migrates backward, and the dendrite is formed (Figure 24B). Heiman *et al*. (2009) were the first to describe this mechanism and identified the tectorin-related proteins DEX-1[SNED1, Ndg], and DYF-7 to be involved in this process. These proteins are thought to be secreted and form an extracellular matrix necessary for anchoring the amphid neurons (Heiman and Shaham, 2009). Most interestingly, Schouteden *et al*. (2015) have found that the anchoring process is mediated by the transition zone of the cilium, which required basal body anchorage to the cell membrane (Schouteden *et al.*, 2015). In a recent publication, Fan *et al*. (2019) show that PAR-6 proteins localize in the region where dendritic tips of amphid neurons are anchoring, which I can confirm by my experiments (Figure 27; Fan *et al.* 2019). Further, PAR-6 is required for DYF-7 localization and dendrite tip attachment (Fan *et al.*, 2019). Thus, in dendrites elongating by retrograde extension, basal body attachment might be compromised. As previously mentioned, PAR-3[ASIP, Bazooka], and PAR-6[hsPAR6α/β/γ, Par-6] form a complex together with PKC-3[aPKCλ/ζ, aPKC] (Tabuse *et al.*, 1998; Hung and Kemphues, 1999). Analysis of the role of this complex in dendrite attachment and basal body positioning in retrograde extending neurons might give valuable insights about PAR function apart of their role in cell polarity. Fan *et al.* (2004) and Sfakianos *et al.* (2007) found that PAR3 localizes to the primary cilium in mammalian cell culture and is required for cilium elongation (Fan *et al.*, 2004; Sfakianos *et al.*, 2007). PAR-3[ASIP, Bazooka] might play a similar role in cilium formation in *C. elegans*. Sfakianos *et al.* (2007) report that the C-terminus of PAR3 is required for cilium formation in Madin-Darby canine kidney (MDCK) cells, and more specifically, the kinesin family member 3A (KIF3A) binding domain (Sfakianos *et al.*, 2007). KIF3A[klp64D, KLP-11] is a subunit of Kinesin II and is required in primary cilium formation, centriole cohesion and subdistal appendage organization (Kodani *et al.*, 2013). It would be interesting to test whether one of the PAR-3[ASIP, Bazooka] splice variants, or a specific binding domain of the protein is required for cilium formation in worms. Different GFP fusion constructs, mimicking the PAR-3[ASIP, Bazooka] splice variants, or consisting of individual binding domains, could be tested for their localization to cilia to determine which part of *C. elegans* PAR-3[ASIP, Bazooka] is responsible for targeting the protein to the cilium. More importantly, in combination with *par-3* RNAi, the PAR-3[ASIP, Bazooka] splice variants could be tested for their embryonic rescue potential and analyzed for aberrations specifically in cilium formation (Li *et al.*, 2010).

Similarly, embryos expressing GFP::PAR-3 constructs, which carry deletions of individual domains, could be used to determine which domains might be necessary for ciliogenesis. Embryos, surviving RNAi mediated silencing of the endogenous PAR-3[ASIP, Bazooka] protein, could be analyzed for aberrations in ciliogenesis. Alternatively, a degradation system to conditionally perturb protein function exists in *C. elegans*, and strains for PAR-3[ASIP, Bazooka]/-6[hsPAR6α/β/γ, Par-6] degradation in late embryonic development are available (Armenti *et al.*, 2014). IL1, amphid, and phasmid neurons could be analyzed in those mutants to determine the role of the PAR-3[ASIP, Bazooka]/-6[hsPAR6α/β/γ, Par-6] proteins in centrosome positioning.

4.2.4. Observations are conflicting with the current model for retrograde dendrite extension

Since centrioles are required for cell division but also cilia formation, the observation that IL1nbs divide, when the cell is already highly polarized with a dendrite attached and elongating, is challenging the current view that the ciliary transition zone is required for dendrite tip attachment to an extracellular matrix. Further, in amphid neurons, transition zone formation is reported to take place in the 2-fold stage (Serwas *et al.*, 2017). Thus, transition zone formation occurs much later than dendrite attachment and rosette formation, which take place in bean to comma stage embryos (Fan *et al.*, 2019). However, I find centrioles to be present within PAR-6[hsPAR6α/β/γ, Par-6] accumulations at dendritic tips of sensory neurons, which corroborates the theory that cilia are forming. Nevertheless, cilia should be retracted before cell division. Hence, how IL1 neurons divide, with their dendrites anchored at the same time, is obscure. Further analysis of centrioles/basal bodies in dendrite attachment during retrograde extension and the IL1nb division is required.
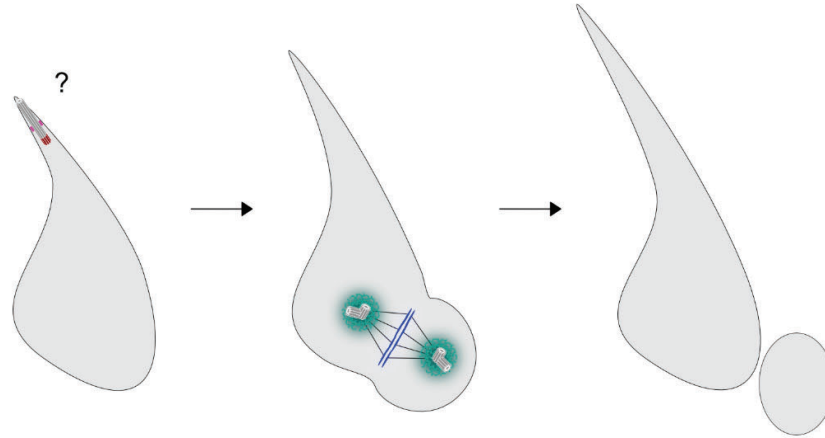
Figure 30: **Contradicting observations during the IL1nb division**. The IL1nb divides after dendrites attached, and retrograde extension is ongoing. Dendrite attachment during retrograde extension was reported to be mediated by the ciliary transition zone (Schouteden *et al.*, 2015). In amphids neurons, dendrite attachment takes place already in bean stage embryos (Heiman and Shaham, 2009; Fan *et al.*, 2019). Whereas, the transition zone is only formed in the 2-fold embryonic stage in these neurons (Serwas *et al.*, 2017). Centrioles were observed at presumptive dendritic tips in bean stage embryos (Figure 27). However, the IL1nb divides later in development, ~400 min after the first embryonic division, which corresponds to the embryonic comma stage. How dendrites of IL1 neurons attach and how they divide remains to be determined.

REFERENCES

REFERENCES

Achilleos *et al.* (2010) 'PAR-3 mediates the initial clustering and apical localization of junction and polarity proteins during C. elegans intestinal epithelial cell polarization', *Development*, 137(11), pp. 1833–1842. doi: 10.1242/dev.047647.

Albertson, D. G. and Thomson, J. N. (1993) 'Segregation of holocentric chromosomes at meiosis in the nematode, Caenorhabditis elegans', *Chromosome Research*, 1(1), pp. 15-26. doi:10.1007/BF00710603

WormAtlas, Altun, Z.F., Herndon, L.A., Wolkow, C.A., Crocker, C., Lints, R. and Hall, D.H. (ed.s) 2002-2019. Available at: http://www.wormatlas.org.

Andersen, J. S., Wilkinson, C. J. and Mayor, T. (2003) 'Proteomic characterization of the human centrosome by protein correlation profiling', *Nature*, 426(6966), pp. 570-574. doi: 10.1038/nature02166.

Anderson, C. T. and Stearns, T. (2009) 'Centriole age Underlies Asynchronous Primary Cilium Growth in Mammalian Cells', *Current Biology*, 19(17), pp. 1498–1502. doi: 10.1016/j.cub.2009.07.034.

Archambault, V. and Glover, D. M. (2009) 'Polo-like kinases: Conservation and divergence in their functions and regulation', *Nature Reviews Molecular Cell Biology*, 10(4), pp. 265–275. doi: 10.1038/nrm2653.

Armenti, S. T. *et al.* (2014) 'Repurposing an endogenous degradation system for rapid and targeted depletion of C. elegans proteins', *Development*, 141(23), pp. 4640–4647. doi: 10.1242/dev.115048.

Armenti, S. T., Chan, E. and Nance, J. (2014) 'Polarized exocyst-mediated vesicle fusion directs intracellular lumenogenesis within the C. elegans excretory cell', *Developmental Biology*, 394(1), pp. 110–121. doi: 10.1016/j.ydbio.2014.07.019.

Arquint, C. *et al.* (2015) 'STIL binding to Polo-box 3 of PLK4 regulates centriole duplication', *eLife*, 4, e07888. doi: 10.7554/eLife.07888.

Arquint, C., Gabryjonczyk, A. and Nigg, E. A. (2014) 'Centrosomes as signalling centres', *Phil. Trans. R. Soc. B.,* 369(1650), 20130464. doi: 10.1098/rstb.2013.0464

Arquint, C. and Nigg, E. A. (2016) 'The PLK4–STIL–SAS-6 module at the core of centriole duplication', *Biochemical Society Transactions*, 44(5), pp. 1253–1263. doi: 10.1042/BST20160116.

Azimzadeh, J. (2014) 'Exploring the evolutionary history of centrosomes', *Phil. Trans. R. Soc. B.*, 369(1650), 20130453. doi: 10.1098/rstb.2013.0453.

Bae, Y. K. and Barr, M. M. (2008) 'Sensory roles of neuronal cilia: Cilia development, morphogenesis, and function in C. elegans', *Frontiers in Bioscience*, 13, pp. 5959–5974. doi:10.2741/3129.

Barbelanne, M. and Tsang, W. (2014) 'Molecular and cellular basis of autosomal recessive primary microcephaly', *Biomed Res Int. 2014, 547986.* doi: 10.1155/2014/547986.

Barrera, J. A. *et al.* (2010) 'CDK5RAP2 regulates centriole engagement and cohesion in mice', *Developmental Cell*, 18(6), pp. 913–926. doi: 10.1016/j.devcel.2010.05.017.

Basto, R. *et al.* (2008) 'Centrosome Amplification Can Initiate Tumorigenesis in Flies', *Cell*, 133(6), pp. 1032–1042. doi: 10.1016/j.cell.2008.05.039.

Batista, P. J. *et al.* (2008) 'PRG-1 and 21U-RNAs Interact to Form the piRNA Complex Required for Fertility in C. elegans', *Molecular Cell*, 31(1), pp. 67–78. doi: 10.1016/j.molcel.2008.06.002.

Begasse, Maria L. *et al.* (2015) 'Temperature dependence of cell division timing accounts for a shift in the thermal limits of C. elegans and C. briggsae', *Cell Reports*, 10(5), pp. 647–653. doi: 10.1016/j.celrep.2015.01.006.

Bellanger, J. M. *et al.* (2007) 'ZYG-9, TAC-1 and ZYG-8 together ensure correct microtubule function throughout the cell cycle of C. elegans embryos', *Journal of Cell Science*, 120(16), pp. 2963–2973. doi: 10.1242/jcs.004812.

Bettencourt-Dias, M. *et al.* (2005) 'SAK/PLK4 is required for centriole duplication and flagella development', *Current Biology*, 15(24), pp. 2199–2207. doi: 10.1016/j.cub.2005.11.042.

Blachon, S. *et al.* (2008) 'Drosophila asterless and vertebrate Cep152 are orthologs essential for centriole duplication', *Genetics*, 180(4), pp. 2081–2094. doi: 10.1534/genetics.108.095141.

Bloodgood, R. A. (2010) 'Sensory reception is an attribute of both primary cilia and motile cilia', *Journal of Cell Science*,123(Pt 4), pp. 505-509. doi: 10.1242/jcs.066308.

Bobinnec, Y., Fukuda, M. and Nishida, E. (2000) 'Identification and characterization of Caenorhabditis elegans γ -tubulin in dividing cells and differentiated tissues', *Journal of Cell Science*, 113(Pt 21), pp. 3747-3759.

Bonaccorsi, S., Giansanti, M. G. and Gatti, M. (1998) 'Spindle self-organization and cytokinesis during male meiosis in asterless mutants of Drosophila melanogaster', *Journal of Cell Biology*, 142(3), pp. 751–761. doi: 10.1083/jcb.142.3.751.

Bornens, M. and Gönczy, P. (2014) 'Centrosomes back in the limelight', *Philosophical Transactions of the Royal Society*, 369(1650), 20130452. doi: http://dx.doi.org/10.1098/rstb.2013.0452.

Le Bot, N. *et al.* (2003) 'TAC-1 , a Regulator of Microtubule Length in the C. elegans Embryo', *Current Biology*, 13(17), pp. 1499–1505. doi: 10.1016/s0960-9822(03)00577-3.

Boveri, T. (1887) 'Ueber den Antheil des Spermatozoon an der Theilung des Eies', *Sitzungsber, Ges. Morph. Physiol. München* 3, 151-164.

Boveri, T. (1914) 'Zur Frage der Entstehung maligner Tumoren', *G. Fischer:* Jena, Germany.

Boxem, M. *et al.* (2008) 'A Protein Domain-Based Interactome Network for C. elegans Early Embryogenesis', *Cell*, 134(3), pp. 534–545. doi: 10.1016/j.cell.2008.07.009.

Boxem, M., Srinivasan, D. G. and Van Den Heuvel, S. (1999) 'The Caenorhabditis elegans gene ncc-1 encodes a cdc2-related kinase required for M phase in meiotic and mitotic cell divisions, but not for S phase', *Development*, 126(10), pp. 2227-2239.

Brenner, S (1974) 'The genetics of Caenorhabditis elegans', *Genetics*, 77(1), pp. 71–94. Available at: http://www.ncbi.nlm.nih.gov/pmc/articles/PMC1213120/.

Byerly, L., Cassada, R. C. and Russel, R. L. (1976) 'The Life Cycle of the Nematode Caenorhabditis elegans', *Developmental Biology*, 51(1), pp. 23–33. doi: 10.1016/0012-1606(76)90119-6.

Cabral, G. *et al.* (2013) 'Multiple mechanisms contribute to centriole separation in C. elegans', *Current Biology*, 23(14), pp. 1380–1387. doi: 10.1016/j.cub.2013.06.043.

Carvalho-Santos, Z. *et al.* (2011) 'Tracing the origins of centrioles, cilia, and flagella', *Journal of Cell Biology*, 194(2), pp. 165–175. doi: 10.1083/jcb.201011152.

Castellanos, E. and Dominguez, P. (2008) 'Report Centrosome Dysfunction in Drosophila Neural Stem Cells Causes Tumors that Are Not Due to Genome Instability', *Current Biology*, 18(16), pp. 1209–1214. doi: 10.1016/j.cub.2008.07.029.

Chakraborty, S. *et al.* (2015) 'Engulfment pathways promote programmed cell death by enhancing the unequal segregation of apoptotic potential', *Nature Communications*, 6, 10126. doi: 10.1038/ncomms10126.

Chang, C. W. *et al.* (2016) 'CEP295 interacts with microtubules and is required for centriole elongation', *Journal of Cell Science*, 129(13), pp. 2501–2513. doi: 10.1242/jcs.186338.

Chase, D. *et al.* (2000) 'The Polo-Like Kinase PLK-1 Is Required for Nuclear Envelope Breakdown and the Completion of Meiosis in Caenorhabditis elegans', *Genesis*, 26(1), pp. 26–41. doi: 10.1002/(sici)1526-968x(200001)26:1<26::aid-gene6>3.0.co;2-o

Chavali, P. L. *et al.* (2014) 'Small organelle, big responsibility: the role of centrosomes in development and disease', *Phil. Trans. R. Soc. B.*, 369(1650), 10230468. doi: 10.1098/rstb.2013.0468.

Chen, C.-T. *et al.* (2014) 'A unique set of centrosome proteins requires pericentrin for spindle-pole localization and spindle orientation', *Current Biology*, 24(19), pp. 2327–2334. doi: 10.1016/j.cub.2014.08.029.

Chojnacki, S. *et al.* (2017) 'Programmatic access to bioinformatics tools from EMBL-EBI update: 2017', *Nucleic Acids Research*, 45(W1), pp. W550–W553. doi: 10.1093/nar/gkx273.

Clark-Maguire, S. and Mains, P. E. (1994) 'Localization of the mei-1 gene product of Caenorhabditis elegans, a meiotic-specific spindle component', *Journal of Cell Biology*, 126(1), pp. 199–209. doi: 10.1083/jcb.126.1.199.

Conduit, P. T. *et al.* (2010) 'Centrioles regulate centrosome size by controlling the rate of Cnn incorporation into the PCM', *Current Biology*, 20(24), pp. 2178–2186. doi: 10.1016/j.cub.2010.11.011.

Conduit, P. T. *et al.* (2014) 'A molecular mechanism of mitotic centrosome assembly in Drosophila', *eLife*, 3, e03399. doi: 10.7554/eLife.03399.

Conduit, P. T., Wainman, A. and Raff, J. W. (2015) 'Centrosome function and assembly in animal cells', *Nature Reviews Molecular Cell Biology*, 16(10), pp. 611–624. doi: 10.1038/nrm4062.

Corsi, A. K., Wightman, B. and Chalfie, M. (2015) 'A Transparent window into biology: A primer on Caenorhabditis elegans', *Genetics*, 200(2), pp. 387-407. doi: 10.1534/genetics.115.176099.

Costa, M. *et al.* (1998) 'A Putative Catenin-Cadherin System Mediates Morphogenesis of the Embryo', *International C. elegans Meeting*, 141(1), pp. 297–308. doi: 10.1083/jcb.141.1.297.

Cowan, C. R. and Hyman, A. A. (2006) 'Cyclin E-Cdk2 temporally regulates centrosome assembly and establishment of polarity in Caenorhabditis elegans embryos', *Nature Cell Biology*, 8(12), pp. 1441–1447. doi: 10.1038/ncb1511.

Cuenca, A. A. *et al*. (2003) 'Polarization of the C. elegans zygote proceeds via distinct establishment and maintenance phases', *Development*, 130(7), pp. 1255-1265. doi: 10.1242/dev.00284

Dammermann, A. *et al.* (2004) 'Centriole assembly requires both centriolar and pericentriolar material proteins', *Developmental Cell*, 7(6), pp. 815–829. doi: 10.1016/j.devcel.2004.10.015.

Davis, D. E. *et al.* (2009) 'The cation diffusion facilitator gene cdf-2 mediates zinc metabolism in Caenorhabditis elegans', *Genetics*, 182(4), pp. 1015–1033. doi: 10.1534/genetics.109.103614.

Decker, M. *et al.* (2011) 'Limiting amounts of centrosome material set centrosome size in C. elegans embryos', *Current Biology*, 21(15), pp. 1259–1267. doi: 10.1016/j.cub.2011.06.002.

Delattre, M. *et al.* (2004) 'Centriolar SAS-5 is required for centrosome duplication in C. elegans', *Nature Cell Biology*, 6(7), pp. 656–664. doi: 10.1038/ncb1146.

Dormoy, V., Tormanen, K. and Sütterlin, C. (2013) 'Par6γ is at the mother centriole and controls centrosomal protein composition through a Par6α-dependent pathway', *Journal of Cell Science*, 126(3), pp. 860–870. doi: 10.1242/jcs.121186.

Dougherty, E. C. and Grant Calhoun, H. (1948) 'Possible Significance of free-living Nematodes in Genetic Research', *Nature*, 161(4079), p. 29, doi: 10.1038/161029a0.

Doxsey, S. J. *et al.* (1994) 'Pericentrin, a highly conserved centrosome protein involved in microtubule organization', *Cell*, 76(4), pp. 639–650. doi: 10.1016/0092-8674(94)90504-5.

Dzhindzhev, N. S. *et al.* (2010) 'Asterless is a scaffold for the onset of centriole assembly', *Nature*, 467(7316), pp. 714–718. doi: 10.1038/nature09445.

Elia, A. E. H. *et al.* (2003) 'The Molecular Basis for Phosphodependent Substrate Targeting and Regulation of Plks by the Polo-Box Domain', *Cell,* 115(1), pp. 83–95. doi: 10.1016/s0092-8674(03)00725-6

Emmerich, J. *et al.* (2004) 'Cyclin D does not provide essential Cdk4-independent functions in drosophila', *Genetics*, 168(2), pp. 867–875. doi: 10.1534/genetics.104.027417.

Encalada, S. E. *et al.* (2005) 'A Spindle Checkpoint Functions during Mitosis in the Early Caenorhabditis elegans Embryo', *Molecular Biology of the Cell*, 16(3), pp. 1056–1070. doi: 10.1091/mbc.E04.

Enos, S. J. *et al.* (2018) 'Phosphatase PP2A and microtubule-mediated pulling forces disassemble centrosomes during mitotic exit', *Biology Open*, 7(1), bio029777. doi: 10.1242/bio.029777.

Equence, C. E. S. *et al.,* C. elegans Sequencing Consortium (1998) 'Genome Sequence of the Nematode C . elegans: A Platform for Investigating Biology', *Science*, 282(5396), pp. 2012–2018. doi: 10.1126/science.282.5396.2012

Erpf, A. C. *et al.* (2019) 'PCMD-1 OrganizesCentrosome Matrix Assembly in C. elegans', *Current Biology*, 29(8), pp. 1324-1336. doi: 10.1016/j.cub.2019.03.029.

Fan, L. *et al.* (2019) 'A multicellular rosette-mediated collective dendrite extension', *eLife*, 8, e38065. doi: 10.7554/elife.38065.

Fan, S. *et al.* (2004) 'Polarity Proteins Control Ciliogenesis via Kinesin Motor Interactions', *Current Biology*, 14(16), pp. 1451–1461. doi: 10.1016/j.cub.2004.08.025.

Feldman, J. L. and Priess, J. R. (2012) 'A Role for the Centrosome and PAR-3 in the Hand-Off of MTOC Function during Epithelial Polarization', *Current Biology*, 22(7), pp. 575–582. doi: 10.1016/j.cub.2012.02.044.

Ferguson, E. L. and Horvitz, H. R. (1985) 'Identification and characterization of 22 genes that affect the vulval cell lineages of the nematode Caenorhabditis elegans', *Genetics*, 110(1), pp. 17–72.

Flory, M. R. *et al.* (2002) 'Identification of a human centrosomal calmodulin-binding protein that shares homology with pericentrin', *Proceedings of the National Academy of Sciences*, 97(11), pp. 5919–5923. doi: 10.1073/pnas.97.11.5919.

Fong, K.-W. *et al.* (2008) 'CDK5RAP2 Is a Pericentriolar Protein That Functions in Centrosomal Attachment of the gamma-Tubulin Ring Complex', *Molecular Biology of the Cell*, 19(1), pp. 115–125. doi: 10.1091/mbc.e07-04-0371

Frøkjær-Jensen, C. *et al.* (2008) 'Single-copy insertion of transgenes in Caenorhabditis elegans', *Nature Genetics*, 40(11), pp. 1375–1383. doi: 10.1038/ng.248.

Frøkjær-Jensen, C. *et al.* (2014) 'Random and targeted transgene insertion in Caenorhabditis elegans using a modified Mos1 transposon', *Nature Methods*, 11(5), pp. 529–534. doi: 10.1038/nmeth.2889.

Fry, A. M. *et al.* (2017) 'Recent advances in pericentriolar material organization: ordered layers and scaffolding gels', *F1000Research*, 6, 1622. doi: 10.12688/f1000research.11652.1.

Fu, J. *et al*. (2016) 'Conserved molecular interactions in centriole-to-centrosome conversion', *Nature Cell Biology*, 18(1), pp. 87–99. doi: 10.1038/ncb3274.

Fu, J. and Glover, D. M. (2012) 'Structured illumination of the interface between centriole and peri-centriolar material', *Open Biology*, 2(8), 120104. doi: 10.1098/rsob.120104.

Galli, M. *et al.* (2016) 'Cell Size Determines the Strength of the Spindle Assembly Checkpoint during Embryonic Development', *Developmental Cell*, 36(3), pp. 344–352. doi: 10.1016/j.devcel.2016.01.003.

Geng, Y. *et al.* (2003) 'Cyclin E Ablation in the Mouse', *Cell*, 114(4), pp. 431–443. doi: 10.1016/S0092-8674(03)00645-7.

Godinho, S. A. and Pellman, D. (2014) 'Causes and consequences of centrosome abnormalities in cancer', *Phil. Trans. R. Soc. B.,* 369(1650), 20130467. doi: 10.1098/rst.2013.0467.

Golden, J. and Riddle, D. (1984) 'The Caenorhabditis elegans Dauer Larva: Developmental Effects of Pheromone, Food, and Temperature', *Developmental Biology*, 102(2), pp. 368–378. doi: 10.1016/0012-1606(84)90201-x.

Gomez-Ferreria, M. A. *et al.* (2012) 'Novel NEDD1 phosphorylation sites regulate γ-tubulin binding and mitotic spindle assembly', *Journal of Cell Science*, 125(16), pp. 3745–3751. doi: 10.1242/jcs.105130.

Gönczy, P. *et al.* (1999) 'Cytoplasmic Dynein is Required for Distinct Aspects of Mtoc Positioning, Including Centrosome Separation, in the One Cell Stage Caenorhabditis elegans Embryo', *The Journal of Cell Biology*, 147(1), pp. 135–150. doi: 10.1083/jcb.147.1.135.

Gönczy, P. (2012) 'Towards a molecular architecture of centriole assembly', *Nature Reviews Molecular Cell Biology*, 13(7), pp. 425–435. doi: 10.1038/nrm3373.

Gosti-Testu, F. *et al.* (1986) 'Identification of centrosomal proteins in a human lymphoblastic cell line', *The EMBO Journal*, 5(10), pp. 2545–2550. doi: 10.1002/j.1460-2075.1986.tb04533.x.

Gräf, R. (2018) 'Comparative Biology of Centrosomal Structures in Eukaryotes', *Cells*, 7(11), 202. doi: 10.3390/cells7110202.

Graser, S., Stierhof, Y. D. and Nigg, E. A. (2007) 'Cep68 and Cep215 (Cdk5rap2) are required for centrosome cohesion', *Journal of Cell Science*, 120(24), pp. 4321–4331. doi: 10.1242/jcs.020248.

Greenstein, D. (2005) 'Control of oocyte meiotic maturation and fertilization', *WormBook*, ed. The C. elegans Research Community, WormBook, doi: 10.1895/wormbook.1.53.1.

Habedanck, R. *et al.* (2005) 'The Polo kinase Plk4 functions in centriole duplication', *Nature Cell Biology*, 7(11), pp. 1140–1146. doi: 10.1038/ncb1320.

Hamill, D. R. *et al.* (2002) 'Centrosome maturation and mitotic spindle assembly in C. elegans require SPD-5, a protein with multiple coiled-coil domains', *Developmental Cell*, 3(5), pp. 673–684. doi: 10.1016/S1534-5807(02)00327-1.

Hannak, E. *et al.* (2001) 'Aurora-A kinase is required for centrosome maturation in Caenorhabditis elegans', *Journal of Cell Biology*, 155(7), pp. 1109–1115. doi: 10.1083/jcb.200108051.

Hannak, E. *et al.* (2002) 'The kinetically dominant assembly pathway for centrosomal asters in Caenorhabditis elegans is gamma-tubulin dependent', *Journal of Cell Biology*, 157(4), pp. 591–602. doi: 10.1083/jcb.200202047.

Haren, L., Stearns, T. and Lüders, J. (2009) 'Plk1-dependent recruitment of γ-tubulin complexes to mitotic centrosomes involves multiple PCM components', *PLoS ONE*, 4(6), e5976. doi: 10.1371/journal.pone.0005976.

Hayward, D. and Wakefield, J. G. (2014) 'Chromatin-mediated microtubule nucleation in Drosophila syncytial embryos', *Communicative and Integrative Biology*, 7(4), e28512. doi: 10.4161/cib.28512.

Heald, R. *et al.* (1996) 'Self-organization of microtubules into bipolar spindles around artificial chromosomes in Xenopus egg extracts', *Nature*, 382(6590), pp. 420–425. doi: 10.1038/382420a0.

Heiman, M. G. and Shaham, S. (2009) 'DEX-1 and DYF-7 Establish Sensory Dendrite Length by Anchoring Dendritic Tips during Cell Migration', *Cell*, 137(2), pp. 344–355. doi: 10.1016/j.cell.2009.01.057.

Hirase, S. (1894) 'Notes on the attraction-Spheres in the Pollen-Cells of Ginkgo bilob', *The Botanical Magazine*, 8(91), pp. 359–360.

Hodgkin, J. and Doniach, T. (1997) 'Natural variation and copulatory plug formation in Caenorhabditis elegans', *Genetics*, 146(1), pp. 149–164.

Hodgkin, J., Horvitz, H. R. and Brenner, S. (1979) 'Nondisjunction mutants of the nematode Caenorhabditis elegans', *Genetics*, 91(1), pp. 67–94.

Holway, A. H. *et al.* (2006) 'Checkpoint silencing during the DNA damage response in Caenorhabditis elegans embryos', *Journal of Cell Biology*, 172(7), pp. 999–1008. doi: 10.1083/jcb.200512136.

Hoyer-Fender, S. (2010) 'Centriole maturation and transformation to basal body', *Seminars in Cell and Developmental Biology*, 21(2), pp. 142–147. doi: 10.1016/j.semcdb.2009.07.002.

Hrus, A. *et al.* (2007) 'C. elegans agrin is expressed in pharynx, IL1 neurons and distal tip cells and does not genetically interact with genes involved in synaptogenesis or muscle function', *PLoS ONE*, 2(8), e731. doi: 10.1371/journal.pone.0000731.

Hu, Z. *et al.* (2015) 'Cilia disassembly with two distinct phases of regulation', *Cell Reports*, 10(11), pp. 1803–1810. doi: 10.1016/j.celrep.2015.02.044.

Hung, T. J. and Kemphues, K. J. (1999) 'PAR-6 is a conserved PDZ domain-containing protein that colocalizes with PAR-3 in Caenorhabditis elegans embryos', *Development (Cambridge, England)*, 126(1), pp. 127–135.

Inaba, M., Venkei, Z. G. and Yamashita, Y. M. (2015) 'The polarity protein Baz forms a platform for the centrosome orientation during asymmetric stem cell division in the Drosophila male germline', *eLife*, 4, e04960. doi: 10.7554/elife.04960.

Inglis, P. N. *et al.* (2007) 'The sensory cilia of Caenorhabditis elegans', *WormBook*, ed. The *C. elegans* Research Community, WormBook, doi: 10.1895/wormbook.1.126.2.

Inoue, D. and Sagata, N. (2005) 'The Polo-like kinase Plx1 interacts with and inhibits Myt1 after fertilization of Xenopus eggs', *The EMBO Journal*, 24(5), pp. 1057–1067. doi: 10.1038/sj.emboj.7600567.

Izquierdo, D. *et al.* (2014) 'Stabilization of cartwheel-less centrioles for duplication requires CEP295-mediated centriole-to-centrosome conversion', *Cell Reports*, 8(4), pp. 957–965. doi: 10.1016/j.celrep.2014.07.022.

Januschke, J. *et al.* (2011) 'Drosophila neuroblasts retain the daughter centrosome', *Nature Communications*, 2, 243. doi: 10.1038/ncomms1245.

Jaqaman, K., Loerke, D. and Mettlen, M. (2008) 'Robust single-particle tracking', *Nature Methods*, 5(8), pp. 695–702. doi: 10.1038/nmeth.1237.

Jeong, J.-Y. *et al.* (2012) 'One-Step Sequence- and Ligation-Independent Cloning as a Rapid and Versatile Cloning Method for Functional Genomics Studies', *Applied and Environmental Microbiology*, 78(15), pp. 5440–5443. doi: 10.1128/aem.00844-12.

Johnson, M. *et al*. (2008) 'NCBI BLAST: a better web interface', *Nucleic acids research*, 36(Issue_suppl_2), pp. W5–W9. doi: 10.1093/nar/gkn201.

Jordan, S. N. *et al*. (2016) 'Cortical PAR polarity proteins promote robust cytokinesis during asymmetric cell division', *Journal of Cell Biology*, 212(1), pp. 39–49. doi: 10.1083/jcb.201510063.

Joukov, V, Walter, J. and De Nicolo, A. (2014) 'The Cep192-organized Aurora A-Plk1 cascade is essential for centrosome cycle and bipolar spindle assembly', *Molecular Cell*, 55(4), pp. 578–591. doi: 10.1016/j.molcel.2014.06.016.

Kalaszczynska, I. *et al.* (2009) 'Cyclin A is Redundant in Fibroblasts but Essential in Hematopoietic and Embryonic Stem Cells', *Cell*, 138(2), pp. 352–365. doi: 10.1016/j.cell.2009.04.062.

Kaletta, T. and Hengartner, M. O. (2006) 'Finding function in novel targets: C . elegans as a model organism', *Nat Rev Drug Discov*, 5(5), pp. 387-398. doi: 10.1038/nrd2031.

Kamath, R. S. and Ahringer, J. (2003) 'Genome-wide RNAi screening in Caenorhabditis elegans', *Methods (San Diego, Calif.)*, 30(4), pp. 313–321. doi: 10.1016/S1046-2023(03)00050-1.

Katju, V. *et al.* (2008) 'Sex change by gene conversion in a Caenorhabditis elegans fog-2 mutant', *Genetics*, 180(1), pp. 669–672. doi: 10.1534/genetics.108.090035.

Kemp, C. A. *et al.* (2004) 'Centrosome maturation and duplication in C. elegans require the coiled-coil protein SPD-2', *Developmental Cell*, 6(4), pp. 511–523. doi: 10.1016/S1534-5807(04)00066-8.

Kemphues, K. J. *et al.* (1988) 'Identification of Genes Required for Cytoplasmic Localization in Early C. elegans Embryos', *Cell*, 52(3), pp. 311-320. doi: 10.1016/s0092-8674(88)80024-2.

Kim, J., Lee, K. and Rhee, K. (2015) 'PLK1 regulation of PCNT cleavage ensures fidelity of centriole separation during mitotic exit', *Nature Communications*, 6, 10076. doi: 10.1038/ncomms10076.

Kim, M. *et al.* (2016) 'Promotion and Suppression of Centriole Duplication Are Catalytically Coupled through PLK4 to Ensure Centriole Homeostasis', *Cell Reports*, 16(5), pp. 1195–1203. doi: 10.1016/j.celrep.2016.06.069.

Kim, S. and Rhee, K. (2014) 'Importance of the CEP215-pericentrin interaction for centrosome maturation during mitosis', *PLoS ONE*, 9(1), e87016. doi: 10.1371/journal.pone.0087016.

Kim, T. S. *et al.* (2013) 'Hierarchical recruitment of Plk4 and regulation of centriole biogenesis by two centrosomal scaffolds, Cep192 and Cep152', *PNAS*, 110(50), E4849-E4857. doi: 10.1073/pnas.1319656110.

Kipreos, E. T. and Pagano, M. (2000) 'The F-box protein family', *Genome Biology*, 1(5), REVIEWS3002. doi: 10.1186/gb-2000-1-5-reviews3002.

Kirkham, M. *et al.* (2003) 'SAS-4 is a C. elegans centriolar protein that controls centrosome size', *Cell*, 112(4), pp. 575–587. doi: 10.1016/S0092-8674(03)00117-X.

Kitagawa, D. *et al.* (2009) 'Phosphorylation of SAS-6 by ZYG-1 Is Critical for Centriole Formation in C. elegans Embryos', *Developmental Cell*, 17(6), pp. 900–907. doi: 10.1016/j.devcel.2009.11.002.

Klass, M. R. (1977) 'Aging in the Nematode Caenorhabditis elegans: Major biological and environmental factors influence life span', *Machanisms of Aging and Development*, 6(6), pp. 413–429. doi: 10.1016/0047-6374(77)90043-4

Klingseisen, A. and Jackson, A. P. (2011) 'Mechanisms and pathways of growth failure in primordial dwarfism', *Genes & Development*, 25(19), pp. 2011–2024. doi: 10.1101/gad.169037.

Knoblich, J. A. *et al.* (1994) 'Cyclin E controls S phase progression and its down-regulation during Drosophila embryogenesis is required for the arrest of cell proliferation', *Cell*, 77(1), pp. 107–120. doi: 10.1016/0092-8674(94)90239-9.

Knoblich, J. A. and Lehner, C. F. (1993) 'Synergistic action of Drosophila cyclins A and B during the G2-M transition', *The EMBO Journal*, 12(1), pp. 65–74. doi: 10.1002/j.1460-2075.1993.tb05632.x.

Kodani, A. *et al.* (2013) 'Kif3a interacts with Dynactin subunit p150 Glued to organize centriole subdistal appendages', *The EMBO Journal*, 32(4), pp. 597–607. doi: 10.1038/emboj.2013.3.

Kong, D. *et al.* (2014) 'Centriole maturation requires regulated Plk1 activity during two consecutive cell cycles', *Journal of Cell Biology*, 206(7), pp. 855–865. doi: 10.1083/jcb.201407087.

Kozar, K. *et al.* (2004) 'Mouse development and cell proliferation in the absence of D-cyclins', *Cell*, 118(4), pp. 477–491. doi: 10.1016/j.cell.2004.07.025.

Kratz, A. S. *et al*. (2015) 'Plk4-dependent phosphorylation of STIL is required for centriole duplication', *Biology Open*, 4(3), pp. 370–377. doi: 10.1242/bio.201411023.

Kuhn, M., Hyman, A. A. and Beyer, A. (2014) 'Coiled-Coil Proteins Facilitated the Functional Expansion of the Centrosome', *PLoS Computational Biology*, 10(6), e1003657. doi: 10.1371/journal.pcbi.1003657.

Kumagai, A. and Dunphy, W. G. (1996) 'Purification and molecular cloning of Plx1, a Cdc25-regulatory kinase from Xenopus egg extracts', *Science*, 273(5280), pp. 1377–1380. doi: 10.1126/science.273.5280.1377.

Lai, C. *et al.* (2000) 'Identification of Novel Human Genes Evolutionarily Conserved in Caenorhabditis elegans by Comparative Proteomics', *Genome Research*, 10(5), pp. 703–713. doi: 10.1101/gr.10.5.703

Laos, T., Cabral, G. and Dammermann, A. (2015) 'Isotropic incorporation of SPD-5 underlies centrosome assembly in C. Elegans', *Current Biology*, 25(15), pp. R648–R649. doi: 10.1016/j.cub.2015.05.060.

Lawo, S. *et al.* (2012) 'Subdiffraction imaging of centrosomes reveals higher-order organizational features of pericentriolar material', *Nature Cell Biology*, 14(11), pp. 1148–1158. doi: 10.1038/ncb2591.

Lee, J., Jongeward, G. D. and Sternberg, P. W. (1994) 'unc-l01, a gene required for many aspects of Caenorhabditis elegans development and behavior, encodes a clathrin-associated protein', *Genes & Development*, 8(1), pp. 60–73. doi: 10.1101/gad.8.1.60.

Lee, K. and Rhee, K. (2011) 'PLK1 phosphorylation of pericentrin initiates centrosome maturation at the onset of mitosis', *Journal of Cell Biology*, 195(7), pp. 1093–1101. doi: 10.1083/jcb.201106093.

Lee, K. and Rhee, K. (2012) 'Separase-dependent cleavage of pericentrin B is necessary and sufficient for centriole disengagement during mitosis', *Cell Cycle*, 11(13), pp. 2476–2485. doi: 10.4161/cc.20878.

Van Leeuwenhoek, A. (1677) 'Concerning little animals observed in rain-, well-, sea- and snow-water; as also in water wherein pepper had lain infused', *Philosophical Transactions of the Royal Society*, 12(133), pp. 821–831. doi:10.1098/rstl.1677.0003

Lehner, C. F. and O'Farrell, P. H. (1990) 'The Roles of Drosophila Cyclins A and B in Mitotic Control', *Cell*, 61(3), pp. 535–547. doi: 10.1016/0092-8674(90)90535-m

Leidel, S. *et al*. (2005) 'SAS-6 defines a protein family required for centrosome duplication in C. elegans and in human cells', *Nature Cell Biology*, 7(2), pp. 115-125. doi: 10.1038/ncb1220.

Leidel, S. and Gönczy, P. (2003) 'SAS-4 is essential for centrosome duplication in C. elegans and is recruited to daughter centrioles once per cell cycle', *Developmental Cell*, 4(3), pp. 431–439. doi: 10.1016/S1534-5807(03)00062-5.

Lettman, M. M. *et al.* (2013) 'Direct Binding of SAS-6 to ZYG-1 Recruits SAS-6 to the Mother Centriole for Cartwheel Assembly', *Developmental Cell*, 25(3), pp. 284–298. doi: 10.1016/j.devcel.2013.03.011.

Leung, B., Hermann, G. J. and Priess, J. R. (1999) 'Organogenesis of the C. elegans Intestine', *Developmental Biology*, 216(1), pp. 114–134. doi: 10.1006/dbio.1999.9471

Li, B. *et al.* (2010) 'Different Domains of C. elegans PAR-3 are required at different Times in Development', *Developmental Biology*, 344(2), pp. 745–757. doi: 10.1016/j.ydbio.2010.05.506.

Lin, Y. C. *et al.* (2013) 'Human microcephaly protein CEP135 binds to hSAS-6 and CPAP, and is required for centriole assembly', *The EMBO Journal*, 32(8), pp. 1141–1154. doi: 10.1038/emboj.2013.56.

Lingle, W. L. *et al.* (1998) 'Centrosome hypertrophy in human breast tumors: Implications for genomic stability and cell polarity', *PNAS*, 95(6), pp. 2950–2955. doi: 10.1073/pnas.95.6.2950.

Lingle, W. L. *et al.* (2001) 'Centrosome amplification drives chromosomal instability in breast tumor development', *PNAS*, 99(4), pp. 1978-1983. doi: 10.1073/pnas.032479999.

Loncarek, J. and Bettencourt-Dias, M. (2018) 'Building the right centriole for each cell type', *Journal of Cell Biology*, 217(3), pp. 823–835. doi: 10.1083/jcb.201704093.

Maiato, H. and Logarinho, E. (2014) 'Mitotic spindle multipolarity without centrosome amplification', *Nature Cell Biology*, 16(5), pp. 386–394. doi: 10.1038/ncb2958.

Mangal, S. *et al.* (2018) 'TPXL-1 activates Aurora A to clear contractile ring components from the polar cortex during cytokinesis', *Journal of Cell Biology*, 217(3), pp. 837–848. doi: 10.1083/jcb.201706021.

Martino, L. *et al.* (2017) 'Channel Nucleoporins Recruit PLK-1 to Nuclear Pore Complexes to Direct Nuclear Envelope Breakdown in C. elegans', *Developmental Cell*, 43(2), pp. 157-171.e7. doi: 10.1016/j.devcel.2017.09.019.

Matthews, L. R. *et al.* (1998) 'Zyg-9, A Caenorhabditis elegans Protein Required for Microtubule Organization and Function, Is a Component of Meiotic and Mitotic Spindle Poles', *The Journal of Cell Biology*, 141(5), pp. 1159–1168. doi: 10.1083/jcb.141.5.1159.

McKay, S. J. *et al.* (2003) 'Gene expression profiling of cells, tissues, and developmental stages of the nematode C. elegans', *Cold Spring Harbor Symposia on Quantitative Biology*, 68, pp. 159–169. doi: doi:10.1101/sqb.2003.68.159.

Megraw, T. L., Sharkey, J. T. and Nowakowski, R. S. (2011) 'Cdk5rap2 exposes the centrosomal root of microcephaly syndromes', *Trends in Cell Biology*, 21(8), pp. 470–480. doi: 10.1016/j.tcb.2011.04.007.

Mello, C. C. and Kramer, J. M. (1991) 'Efficient gene transfer in C. elegans: extrachromosomal maintenance and integration of transforming sequences', *The EMBO Journal*, 10(12), pp. 3959–3970.

Meng, L. *et al.* (2015) 'Bimodal Interaction of Mammalian Polo-Like Kinase 1 and a Centrosomal Scaffold, Cep192, in the Regulation of Bipolar Spindle Formation', *Molecular and Cellular Biology*, 35(15), pp. 2626–2640. doi: 10.1128/mcb.00068-15.

Mennella, V. *et al.* (2012) 'Subdiffraction-resolution fluorescence microscopy reveals a domain of the centrosome critical for pericentriolar material organization', *Nature Cell Biology*, 14(11), pp. 1159–1168. doi: 10.1038/ncb2597.

Mikeladze-Dvali, T. *et al.* (2012) 'Analysis of centriole elimination during C. elegans oogenesis', *Development*, 139(9), pp. 1670–1679. doi: 10.1242/dev.075440.

Morton, D. G. *et al.* (2002) 'The Caenorhabditis elegans par-5 gene encodes a 14-3-3 protein required for cellular asymmetry in the early embryo', *Developmental Biology*, 241(1), pp. 47–58. doi: 10.1006/dbio.2001.0489.

Motegi, F. *et al.* (2006) 'Two phases of astral microtubule activity during cytokinesis in C. elegans embryos', *Developmental Cell*, 10(4), pp. 509–520. doi: 10.1016/j.devcel.2006.03.001.

Moyer, T. C. *et al.* (2015) 'Binding of STIL to Plk4 activates kinase activity to promote centriole assembly', *Journal of Cell Biology*, 209(6), pp. 863–878. doi: 10.1083/jcb.201502088.

Munro, E., Nance, J. and Priess, J. R. (2004) 'Cortical flows powered by asymmetrical contraction transport PAR proteins to establish and maintain anterior-posterior polarity in the early C. elegans embryo', *Developmental Cell*, 7(3), pp. 413–424. doi: 10.1016/j.devcel.2004.08.001.

Murphy, M. *et al.* (1997) 'Delayed early embryonic lethality following disruption of the murine cyclin A2 gene', *Nature Genetics*, 15(1), pp. 83–86. doi: 10.1038/ng0197-83.

Nance, J., Munro, E. M. and Priess, J. R. (2003) 'C. elegans PAR-3 and PAR-6 are required for apicobasal asymmetries associated with cell adhesion and gastrulation', *Development (Cambridge, England)*, 130(22), pp. 5339–5350. doi: 10.1242/dev.00735.

Nechipurenko, I. V and Sengupta, P. (2017) 'The rise and fall of basal bodies in the nematode Caenorhabditis elegans', *Cilia*, 6, 9. doi: 10.1186/s13630-017-0053-9.

Nigg, E. A. and Raff, J. W. (2009) 'Centrioles, Centrosomes, and Cilia in Health and Disease', *Cell*, 139(4), pp. 663–678. doi: 10.1016/j.cell.2009.10.036.

Nigg, E. A. and Stearns, T. (2014) 'The centrosome cycle: Centriole biogenesis, duplication and inherent asymmetries', *Nature Cell Biology*, 13(10), pp. 1154–1160. doi: 10.1038/ncb2345.The.

Novak, Z. A. A. *et al.* (2016) 'Cdk1 Phosphorylates Drosophila Sas-4 to Recruit Polo to Daughter Centrioles and Convert Them to Centrosomes', *Developmental Cell*, 37(6), pp. 545–557. doi: 10.1016/j.devcel.2016.05.022.

O'Connell, K. F. *et al.* (2001) 'The C. elegans zyg-1 Gene Encodes a Regulator of Centrosome Duplication with Distinct Maternal and Paternal Roles in the Embryo', *Cell*, 105(4), pp. 547–558.

O'Neill, R. S. *et al.* (2018) 'Same but different: pleiotropy in centrosome-related microcephaly', *Molecular Biology of the Cell*, 29(3), pp. 241–246. doi: 10.1091/mbc.E17-03-0192.

O'Rourke, S. M. *et al.* (2011) 'A survey of new temperature-sensitive, embryonic-lethal mutations in C. elegans: 24 alleles of thirteen genes', *PLoS ONE*, 6(3), e16644. doi: 10.1371/journal.pone.0016644.

Oegema, K. (2006) 'Cell division', *WormBook*, ed. The *C. elegans* Research Community, WormBook, doi: 10.1895/wormbook.1.72.1.

Ohta, M. *et al.* (2014) 'Direct interaction of Plk4 with STIL ensures formation of a single procentriole per parental centriole', *Nature communications*, 5, 5267. doi: 10.1038/ncomms6267.

Özlü, N. *et al.* (2005) 'An essential function of the C. elegans ortholog of TPX2 is to localize activated Aurora A Kinase to Mitotic Spindles', *Developmental Cell*, 9(2), pp. 237–248. doi: 10.1016/j.devcel.2005.07.002.

Pagan, J. K. *et al.* (2015) 'Degradation of Cep68 and PCNT cleavage mediate Cep215 removal from the PCM to allow centriole separation, disengagement and licensing', *Nature Cell Biology*, 17(1), pp. 31–43. doi: 10.1038/ncb3076.

Peden, E. M. and Barr, M. M. (2005) 'The KLP-6 Kinesin Is Required for Male Mating Behaviors and Polycystin Localization in Caenorhabditis elegans', *Current Biology*, 15(5), pp. 394–404. doi: 10.1016/j.cub.2004.12.073.

Pelletier, L. *et al.* (2004) 'The Caenorhabditis elegans Centrosomal Protein SPD-2 Is Required for both Pericentriolar Material Recruitment and Centriole Duplication', *Current Biology,* 14(10), pp. 863–873. doi: 10.1016/j.cub.2004.04.012

Pelletier, L. *et al.* (2006) 'Centriole assembly in Caenorhabditis elegans', *Nature,* 444(7119), pp. 619–623. doi: 10.1038/nature05318.

Pereira, G. *et al.* (2001) 'Modes of spindle pole body inheritance and segregation of the Bfa1p - Bub2p checkpoint protein complex', *The EMBO Journal*, 20(22), pp. 6359–6370. doi: 10.1093/emboj/20.22.6359.

Perkins, L. A. *et al.* (1986) 'Mutant Sensory Cilia in the Nematode Caenorhabditis elegans', *Developmental Cell*, 117(2), pp. 456–487. doi: 10.1016/0012-1606(86)90314-3

Phillips, C. M. *et al.* (2005) 'HIM-8 binds to the X chromosome pairing center and mediates chromosome-specific meiotic synapsis', *Cell*, 123(6), pp. 1051–1063. doi: 10.1016/j.cell.2005.09.035.

Pihan, G. A. *et al.* (1998) 'Centrosome Defects and Genetic Instability in Malignant Tumors', *Cancer Research,* 58(17), pp. 3974-3985.

Piotrowska-Nitsche, K. and Caspary, T. (2012) 'Live imaging of individual cell divisions in mouse neuroepithelium shows asymmetry in cilium formation and Sonic hedgehog response', *Cilia*, 1(1), 6. doi: 10.1186/2046-2530-1-6.

Plotnikova, O. V., Pugacheva, E. N. and Golemis, E. A. (2009) 'Primary Cilia and the Cell Cycle', *Methods in Cell Biology*, 94, pp. 137–160. doi: doi:10.1016/S0091-679X(08)94007-3.

Rahman, M. M. *et al.* (2015) 'Caenorhabditis elegans polo-like kinase PLK-1 is required for merging parental genomes into a single nucleus', *Molecular Biology of the Cell*, 26(25), pp. 4718–4735. doi: 10.1091/mbc.e15-04-0244.

Raizen, D. M. *et al.* (2008) 'Lethargus is a Caenorhabditis elegans sleep-like state', 451(7178), pp. 569-572. doi: 10.1038/nature06535.

Renzaglia, K. S. and Garbary, D. J. (2001) 'Motile gametes of land plants: Diversity, development, and evolution', *Critical Reviews in Plant Sciences*, 20(2), pp. 107–213. doi: 10.1080/20013591099209.

Roque, H. *et al.* (2018) 'Drosophila PLP assembles pericentriolar clouds that promote centriole stability, cohesion and MT nucleation', *PLoS Genetics*, 14(2), e1007198. doi: 10.1371/journal.pgen.1007198.

Rose, L. and Gönczy, P. (2014) 'Polarity establishment, asymmetric division and segregation of fate determinants in early C. elegans', *WormBook*, ed. The *C. elegans* Research Community, WormBook, doi: 10.1895/wormbook.1.

Rose, L. S. and Kemphues, K. J. (1998) ' Early Patterning of the C. Elegans Embryo', *Annual Review of Genetics*, 32(1), pp. 521–545. doi: 10.1146/annurev.genet.32.1.521.

Salisbury, J. L. (2003) 'Centrosomes: Coiled-coils Organize the Cell Center', *Current Biology*, 13(03), pp. 88–90. doi: 10.1016/s0960-9822(03)00033-2.

Santamaría, D. *et al.* (2007) 'Cdk1 is sufficient to drive the mammalian cell cycle', *Nature*, 448(7155), pp. 811–815. doi: 10.1038/nature06046.

Saurya, S. *et al.* (2016) 'Drosophila Ana1 is required for centrosome assembly and centriole elongation', *Journal of Cell Science*, 129(13), pp. 2514–2525. doi: 10.1242/jcs.186460.

Scheer, U. (2014) 'Historical roots of centrosome research: Discovery of Boveri's microscope slides in Würzburg', *Phil. Trans. Roy. Soc. B.*, 369(1650), 20130469. doi: 10.1098/rstb.2013.0469.

Schindelin, J. *et al*. (2012) 'Fiji: an open-source platform for biological image analysis', *Nature Methods*, 9(7), pp. 676-682. doi: 10.1038/nmeth.2019.

Schlaitz, A. L. *et al.* (2007) 'The C. elegans RSA Complex Localizes Protein Phosphatase 2A to Centrosomes and Regulates Mitotic Spindle Assembly', *Cell*, 128(1), pp. 115–127. doi: 10.1016/j.cell.2006.10.050.

Schouteden, C. *et al.* (2015) 'The ciliary transition zone functions in cell adhesion but is dispensable for axoneme assembly in C. elegans', *Journal of Cell Biology*, 210(1), pp. 35–44. doi: 10.1083/jcb.201501013.

Schultz, J. *et al.* (2000) 'SMART: a web-based tool for the study of genetically mobile domains', *Nucleic acids research*, 28(1), pp. 231–4. doi: 10.1093/nar/28.1.231.

Schumacher, J. M. *et al.* (1998) 'A highly conserved centrosomal kinase, AIR-1 , is required for accurate cell cycle progression and segregation of developmental factors in Caenorhabditis elegans embryos', *Development*, 125(22), pp. 4391–4402.

Sdelci, S. *et al.* (2012) 'Nek9 phosphorylation of NEDD1/GCP-WD contributes to Plk1 control of γ-tubulin recruitment to the mitotic centrosome', *Current Biology*, 22(16), pp. 1516–1523. doi: 10.1016/j.cub.2012.06.027.

Serwas, D. *et al.* (2017) 'Centrioles initiate cilia assembly but are dispensable for maturation and maintenance in C. elegans', *Journal of Cell Biology*, 216(6), pp. 1659–1671. doi: 10.1083/jcb.201610070.

Sfakianos, J. *et al.* (2007) 'Par3 functions in the biogenesis of the primary cilium in polarized epithelial cells', *Journal of Cell Biology*, 179(6), pp. 1133–1140. doi: 10.1083/jcb.200709111.

Sharma, A. *et al.* (2016) 'Centriolar CPAP/SAS-4 Imparts Slow Processive Microtubule Growth', *Developmental Cell*, 37(4), pp. 362–376. doi: 10.1016/j.devcel.2016.04.024.

Shaye, D. D. and Greenwald, I. (2011) 'OrthoList: A Compendium of C. elegans Genes with Human Orthologs', *PLoS ONE*, 6(5), e20085. doi: 10.1371/journal.pone.0020085.

Sherrard, R. *et al.* (2017) 'miRNAs cooperate in apoptosis regulation during C. elegans development', *Genes Dev.*, 31(2), pp. 209–222. doi: 10.1101/gad.288555.116.

Simonis, N. *et al.* (2009) 'Empirically controlled mapping of the Caenorhabditis elegans protein-protein interactome network', *Nature Methods*, 6(1), pp. 47–54. doi: 10.1038/nmeth.1279.

Singson, A. (2001) 'Every sperm is sacred: Fertilization in Caenorhabditis elegans', *Developmental Biology*, 230(2), pp. 101–109. doi: 10.1006/dbio.2000.0118.

Sonnen, K. F. *et al.* (2012) '3D-structured illumination microscopy provides novel insight into architecture of human centrosomes', *Biology Open*, 1(10), pp. 965–976. doi: 10.1242/bio.20122337.

Sonnen, K. F. *et al.* (2013) 'Human Cep192 and Cep152 cooperate in Plk4 recruitment and centriole duplication', *Journal of Cell Science*, 126(14), pp. 3223–3233. doi: 10.1242/jcs.129502.

Srayko, M. *et al.* (2000) 'MEI-1/MEI-2 katanin-like microtubule severing activity is required for Caenorhabditis elegans meiosis', *Genes and Development*, 14(9), pp. 1072–1084.

Srayko, M. *et al.* (2003) 'Caenorhabditis elegans TAC-1 and ZYG-9 Form a Complex that Is Essential for Long Astral and Spindle Microtubules', *Current Biology*, 13(17), pp. 1506–1511. doi: 10.1016/s0960-9822(03)00597-9.

Srayko, M. *et al.* (2005) 'Identification and characterization of factors required for

microtubule growth and nucleation in the early C. elegans embryo', *Developmental Cell*, 9(2), pp. 223–236. doi: 10.1016/j.devcel.2005.07.003.

Strome, S. *et al.* (2001) 'Spindle Dynamics and the Role of gamma-Tubulin in Early Caenorhabditis elegans Embryos', *Molecular Biology of the Cell*, 12(6), pp. 1751–1764. doi: 10.1091/mbc.12.6.1751.

Sugioka, K. *et al.* (2017) 'Centriolar SAS-7 acts upstream of SPD-2 to regulate centriole assembly and pericentriolar material formation', *eLife*, 6, e20353. doi: 10.7554/eLife.20353.

Sulston, J. E., Albertson, D. G. and Thomson, J. N. (1980) 'The Caenorhabditis elegans Male: Postembryonic Development of Nongonadal Structures', *Developmental Biology*, 78(2), pp. 542–576. doi: 10.1016/0012-1606(80)90352-8.

Sulston, J. E. and Schierenberg, E. (1983) 'The Embryonic Cell Lineage of the Nematode Caenorhabditis elegans', *Developmental Biology*, 100(1), pp. 64–119. doi: 10.1016/0012-1606(83)90201-4.

Tabuse, Y. *et al.* (1998) 'Atypical protein kinase C cooperates with PAR-3 to establish embryonic polarity in Caenorhabditis elegans', *Development (Cambridge, England)*, 125(18), pp. 3607–3614.

Tang, C. J. C. *et al.* (2009) 'CPAP is a cell-cycle regulated protein that controls centriole length', *Nature Cell Biology*, 11(7), pp. 825–831. doi: 10.1038/ncb1889.

Thacker, C., Sheps, J. A. and Rose, A. M. (2006) 'Caenorhabditis elegans dpy-5 is a cuticle procollagen processed by a proprotein convertase', *Cellular and Molecular Life Sciences*, 63(10), pp. 1193–1204. doi: 10.1007/s00018-006-6012-z.

Thornton, G. K. and Woods, C. G. (2009) 'Primary microcephaly: do all roads lead to Rome?', *Trends in Genetics*, 25(11), pp. 501–510. doi: 10.1016/j.tig.2009.09.011.

Tinevez, J. Y. *et al.* (2017) 'TrackMate: An open and extensible platform for single-particle tracking', *Methods (San Diego, Calif.)*, 115, pp. 80–90. doi: 10.1016/j.ymeth.2016.09.016.

Toole, E. T. O. *et al.* (2003) 'Morphologically distinct microtubule ends in the mitotic centrosome of Caenorhabditis elegans', *Journal of Cell Biology*, 163(3), pp. 451–456. doi: 10.1083/jcb.200304035.

Tormanen, K. and Su, C. (2013) 'Par6γ is at the mother centriole and controls centrosomal protein composition through a Par-6α dependent pathway', *Journal of Cell Science*, 126(Pt3), pp. 860–870. doi: 10.1242/jcs.121186.

Tsou, M.-F. B. *et al.* (2009) 'Polo kinase and separase regulate the mitotic licensing of centriole duplication in human cells', *Developmental Cell*, 17(3), pp. 344–354. doi: 10.1016/j.devcel.2009.07.015.

Tsuchiya, Y. *et al.* (2016) 'Cep295 is a conserved scaffold protein required for generation of a bona fide mother centriole', *Nature Communications*, 7, 12567. doi: 10.1038/ncomms12567.

Vaizel-Ohayon, D. and Schejter, E. D. (1999) 'Mutations in centrosomin reveal requirements for centrosomal function during early Drosophila embryogenesis', *Current Biology*, 9(16), pp. 889–898. doi: 10.1016/s0960-9822(99)80393-5.

VanBeneden, E. (1887) 'Nouvelle recherches sur la fécondationet la division mitosique chez l'Ascaride mégalocéphale', *Bull. Acad. Royale Belgique*, 3(14), pp. 215–295.

Varmark, H. *et al.* (2007) 'Asterless Is a Centriolar Protein Required for Centrosome Function and Embryo Development in Drosophila', *Current Biology*, 17(20), pp. 1735–1745. doi: 10.1016/j.cub.2007.09.031.

Vaughn, K. C. and Harper, J. D. I. (1998) 'Microtubule-Organizing Centers and Nucleating Sites in Land Plants', *International Review of Cytology*, 181, pp. 75–149. doi: 10.1016/S0074-7696(08)60417-9.

Vaughn, K. C. and Renzaglia, K. S. (2006) 'Structural and immunocytochemical characterization of the Ginkgo biloba L. sperm motility apparatus', *Protoplasma*, 227(2–4), pp. 165–173. doi: 10.1007/s00709-005-0141-3.

Vitre, B. and Cleveland, D. (2012) 'Centrosomes, chromosome instability (CIN) and aneuploidy', *Current Opinion in Cell Biology*, 24(6), pp. 809–815. doi: 10.1016/j.ceb.2012.10.006.

Wang, S. *et al.* (2017) 'A toolkit for GFP-mediated tissue-specific protein degradation in C. elegans', *Development*, 144(14), pp. 2694-2701. doi: 10.1242/dev.150094.

Wang, W. J. *et al.* (2011) 'The conversion of centrioles to centrosomes: Essential coupling of duplication with segregation', *Journal of Cell Biology*, 193(4), pp. 727–739. doi: 10.1083/jcb.201101109.

Ward, S. *et al.* (1975) 'Electron Microscopical Reconstruction of the Anterior Sensory Anatomy of the Nematode Caenorhabditis elegans', *Journal of Comparative Neurology*, 160(3), pp. 313-337. doi: https://doi.org/10.1002/cne.901600305.

Watanabe, N . *et al.* (2004) 'M-phase kinases induce phospho-dependent ubiquitination of somatic Wee1 by SCFbeta-TrCP', *PNAS*, 101(13), pp. 4419–4424. doi: 10.1073/pnas.0307700101.

Watanabe, S. *et al*. (2011) 'Protein localization in electron micrographs using fluorescence nanoscopy', *Nature Methods*, 8(1), pp. 80-84. doi: 10.1038/nmeth.1537.

Waters, A. M. and Beales, P. L. (2011) 'Ciliopathies: an expanding disease spectrum', *Padiatric Nephrology,* 26(7), pp. 1039–1056. doi: 10.1007/s00467-010-1731-7.

Watts, J. L. *et al.* (2000) 'The C. elegans par-4 gene encodes a putative serine-threonine kinase required for establishing embryonic asymmetry', *Development*, 127(7), pp. 1467–1475.

Wicks, S. R. *et al.* (2001) 'Rapid gene mapping in Caenorhabditis elegans using a high density polymorphism map', *Nature Genetics*, 28(2), pp. 160–164. doi: 10.1038/88878.

Woodruff, J. B. *et al.* (2014) 'Pericentriolar material structure and dynamics', *Philos Trans R Soc B.*, 369(1650). doi: 10.1098/rstb.2013.0459.

Woodruff, J. B. *et al.* (2015) 'Regulated assembly of a supramolecular centrosome scaffold in vitro', *Sience*, 348(6236), pp. 808–812. doi: 10.1126/science.aaa3828.

Woodruff, J. B. *et al.* (2017) 'The Centrosome Is a Selective Condensate that Nucleates Microtubules by Concentrating Tubulin', *Cell*, 169(6), pp. 1066-1077.e10. doi: 10.1016/j.cell.2017.05.028.

Wueseke, O. *et al.* (2016) 'Polo-like kinase phosphorylation determines *Caenorhabditis elegans* centrosome size and density by biasing SPD-5 toward an assembly-competent conformation', *Biology Open*, 5(10), pp. 1431–1440. doi: 10.1242/bio.020990.

Yamashita, Y. M. *et al.* (2007) 'Asymmetric Inheritance of Mother Versus Daughter Centrosome in Stem Cell Division', *Science,* 315(5811), pp. 518–521. doi: 10.1126/science.1134910.

Zarkower, D. (2006) 'Somatic sex determination', *WormBook*, ed. The *C. elegans* Research Community, WormBook, doi: 10.1895/wormbook.1.84.1.

Zheng, X. *et al.* (2016) 'Molecular basis for CPAP-tubulin interaction in controlling centriolar and ciliary length', *Nature Communications*, 7, 11874. doi: 10.1038/ncomms11874.

Zimmerman, W. C. *et al.* (2004) 'Mitosis-specific anchoring of gamma-tubulin complexes by pericentrin controls spindle organization and mitotic entry', *Molecular Biology of the Cell*, 15(8), pp. 3642–3657. doi: 10.1091/mbc.e03-11-0796.